

Akademia Górniczo-Hutnicza
im. Stanisława Staszica w Krakowie

Wydział Informatyki, Elektroniki i Telekomunikacji
Katedra Informatyki



ROZPRAWA DOKTORSKA

**Zastosowania metody rzutu przypadkowego
w głębokich sieciach neuronowych**

PIOTR IWO WÓJCIK

Promotor:

prof. dr hab. inż. Witold Dzwinel

Promotor pomocniczy:

dr inż. Marcin Kurdziel

Kraków, 2018

AGH
University of Science and Technology in Kraków
Faculty of Computer Science, Electronics and Telecommunications
Department of Computer Science



DISSERTATION FOR THE DEGREE OF
DOCTOR OF PHILOSOPHY

Random Projection in Deep Neural Networks

PIOTR IWO WÓJCIK

Supervisor:

Witold Dzwiniel, Ph.D., Professor

Co-supervisor:

Marcin Kurdziel, Ph.D.

Kraków, 2018

STRESZCZENIE

Niniejsza praca prezentuje zastosowania metody rzutu przypadkowego (RP) w głębokich sieciach neuronowych. W pracy skupiono się na dwóch obszarach, w których użycie metody RP poprawia ich skuteczność: na efektywnym uczeniu głębokich sieci na danych wysokowymiarowych oraz na inicjalizacji parametrów sieci. Rozważono kilka klasycznych oraz niedawno zaproponowanych konstrukcji macierzy RP: macierze Gaussa, Achlioptasa i Li oraz metody subsampled randomized Hadamard transform (SRHT) i Count Sketch.

W pierwszym z rozważanych obszarów zastosowań metoda RP jest włączana do architektury sieci jako warstwa wejściowa (warstwa RP). Umożliwia to efektywne uczenie głębokich sieci neuronowych na danych pozbawionych struktury, reprezentowanych przez rzadkie, wysokowymiarowe wektory cech. Do tej pory analiza takich danych przy pomocy sieci neuronowych była trudna, lub wręcz niemożliwa, ze względu na wysoki koszt obliczeniowy wynikający z ogromnej liczby wag w pierwszej warstwie sieci. W pracy pokazano, że dzięki użyciu warstwy wejściowej której wagi zostały zainicjalizowane elementami macierzy RP możliwe jest efektywne trenowanie głębokich sieci na tego typu danych. Zostały rozważone dwa warianty zaproponowanej warstwy RP: z ustalonymi wagami oraz z wagami douczanymi w trakcie treningu. Przedstawiono również kilka modyfikacji architektury sieci oraz metod jej trenowania, dzięki którym możliwe jest uczenie sieci na danych zawierających dziesiątki milionów przykładów uczących o wymiarowości przekraczającej miliony cech. Pozwoliło to uzyskać wyniki porównywalne lub lepsze od najlepszych wyników publikowanych w literaturze dla kilku dużych problemów klasyfikacji danych wielowymiarowych. Eksperymenty z różnymi konstrukcjami RP pokazały również, że najlepsze wyniki osiągają sieci z douczaną warstwą RP typu Count Sketch.

W drugim obszarze zastosowań macierz RP wykorzystana jest do inicjalizacji wag sieci neuronowej. Inicjalizacja parametrów sieci przy pomocy elementów macierzy rzutu przypadkowego pozwoliła poprawić skuteczność residualnych sieci konwolucyjnych – modeli osiągających obecnie najlepsze wyniki w dziedzinie rozpoznawania obrazów. Eksperymenty wykazały, że najwyższą skuteczność osiągają sieci inicjalizowane gęstymi macierzami RP, których kolumny są bliskie ortogonalnym (np. konstrukcja SRHT).

ABSTRACT

This work investigates the ways in which deep learning methods can benefit from random projection (RP), a classic linear dimensionality reduction method. We focus on two areas where, as we have found, employing RP techniques can improve deep models: training neural networks on high-dimensional data and initialization of network parameters. We consider several recently proposed RP schemes: Gaussian, Achlioptas', Li's, subsampled randomized Hadamard transform (SRHT) and Count Sketch-based constructions.

Training deep neural networks (DNNs) on sparse, high-dimensional data with no exploitable structure poses a major computational challenge. It implies a network architecture with an input layer that has a huge number of weights, which often makes training infeasible. We show that this problem can be solved by prepending the network with an input layer whose weights are initialized with an RP matrix. We study cases where the weights of this RP layer are either fixed or learned during training. Furthermore, we propose several modifications to the network architecture and training regime that makes it possible to efficiently train DNNs with learnable RP layer on data with as many as tens of millions of input features and training examples. In comparison to the state-of-the-art methods, neural networks with RP layer achieve competitive performance or improve the results on several extremely high-dimensional real-world datasets. Our results also demonstrate that, out of the evaluated RP methods, Count Sketch is the overall best construction for DNNs with RP layer.

The second area where the application of RP techniques can be beneficial for training deep models is weight initialization. Specifically, we study setting the initial weights in DNNs to elements of various RP matrices instead of drawing them from a scaled normal distribution, as is done in current state-of-the-art initialization techniques. Such RP initialization enables us to train deep networks to higher levels of performance. In particular, our results show that dense orthogonal RP initialization schemes, such as SRHT, improve the performance of residual convolutional neural networks.

ACKNOWLEDGMENTS

I would like to express my deepest gratitude to Professor Witold Dzwinel for guiding and encouraging me during my research efforts. I also wish to thank Doctor Marcin Kurdziel for helpful discussion and invaluable advice that greatly improved this thesis.

I dedicate this thesis to my wife, Joanna. I know she will never read past this page, but still.

The research for this thesis was supported by:

- the Polish National Science Centre (NCN) grant No. DEC-2013/09/B/ST6/01549 “Interactive Visual Text Analytics (IVTA): Development of novel, user-driven text mining and visualization methods for large text corpora exploration.”
- the “HPC Infrastructure for Grand Challenges of Science and Engineering” Project, co-financed by the European Regional Development Fund under the Innovative Economy Operational Programme,
- the PL-Grid Infrastructure.

NOTATION

x	a scalar
\mathbf{x}	a vector
\mathbf{X}	a matrix
\mathbb{X}	a set
\mathbb{R}	the set of real number
$ \mathbb{X} $	the number of elements in \mathbb{X}
$[x, y]$	the real interval including x and y
\mathbf{X}^T	transpose of matrix \mathbf{X}
$\ \mathbf{x}\ _1$	L1 norm of vector \mathbf{x}
$\ \mathbf{x}\ _2$	L2 norm of vector \mathbf{x}
x_i	i -th element of vector \mathbf{x}
X_{ij}	element i, j of matrix \mathbf{X}
\mathbf{X}_i	i -th row of matrix \mathbf{X}
$\mathbf{X}_{\cdot j}$	j -th column of matrix \mathbf{X}
$\mathbf{x}^{(i)}$	i -th example from a dataset
$y^{(i)}$	label (target output) for i -th example
\mathbf{X}	design matrix of a dataset with example $\mathbf{x}^{(i)}$ in row \mathbf{X}_i .
$\frac{\partial y}{\partial x}$	partial derivative of y with respect to x
$\nabla_x y$	gradient of y with respect to x
$f(\mathbf{x}; \mathbf{y})$	a function of \mathbf{x} parametrized by \mathbf{y}
$a \sim P$	random variable a has distribution P
$\mathcal{N}(m, s^2)$	a Gaussian distribution with mean m and variance s^2

TABLE OF CONTENTS

Acknowledgments	v
Notation	vii
Table of contents	ix
1 Introduction	1
1.1 Thesis statement	2
1.2 Research contribution	2
1.3 Thesis structure	3
2 Background	5
2.1 Deep neural networks	5
2.1.1 Multilayer perceptron	6
2.1.2 Deep belief network	11
2.1.3 Autoencoder	12
2.1.4 Convolutional neural network	13
2.2 Challenges in training neural networks on sparse, high-dimensional data	14
2.2.1 Sparse, high-dimensional, unstructured data	14
2.2.2 Learning from sparse, high-dimensional data	17
2.2.3 Feature selection for sparse, high-dimensional data	19
2.2.4 Feature extraction for sparse, high-dimensional data	21
3 Random projection	25
3.1 Johnson-Lindenstrauss lemma and embedding quality	25
3.2 Construction of the projection matrix	27
3.2.1 Gaussian random matrix	27
3.2.2 Achlioptas' random matrix	28
3.2.3 Li's sparse matrix	28
3.2.4 Subsampled randomized Hadamard transform	28
3.2.5 Count Sketch-based projections	30
3.3 Summary	30
4 Training deep networks with random projection layer	33
4.1 Fixed-weight random projection layer	34
4.1.1 Experiments on large-scale synthetic data	37
4.1.2 Experiments on large-scale real-world data	48

4.1.3	Experiments on bag-of-words data	51
4.2	Learnable random projection layer	54
4.2.1	Experiments on large-scale data	56
4.3	Implementation notes	61
4.4	Conclusions	66
5	Initializing deep networks with random projection matrices	69
5.1	Weight initialization techniques	69
5.2	Random projection initialization	73
5.3	Experiments	75
5.3.1	Image classification with convolutional neural networks	75
5.3.2	Image classification with pretrained networks	78
5.3.3	Document retrieval with autoencoders	78
5.4	Conclusions	79
6	Conclusions	83
A	Datasets	85
	List of tables	89
	List of figures	91
	Acronyms	93
	Bibliography	97
	PhD candidate publications list	113

CHAPTER 1

INTRODUCTION

In this work we investigate the ways in which deep learning methods can benefit from random projection (RP), a classic linear dimensionality reduction method. In particular, we focus on two areas where, as we have found, employing RP techniques can enhance deep models.

In the first application of random projection, we make use of its original purpose, i.e., reducing the dimensionality of the input data. We show how this can be useful in the problem of learning from data that is represented by sparse, unstructured, high-dimensional feature vectors¹. This type of data often arises in areas such as social media, web crawling, gene sequencing or biomedical analysis. Currently, training deep neural networks (DNNs) or other complex nonlinear models is practically infeasible for similar applications. Therefore, simpler but faster linear approaches, such as support vector machine (SVM) or logistic regression (LR) classifiers [Yuan et al. 2012b] are usually employed. Importantly, these methods are capable of efficiently processing sparse, high-dimensional input data. With the assistance of RP, we hope to narrow this gap and enable deep networks to be trained on such problematic type of data.

The dimensionality of the input data in most modern neural network applications is relatively low. For example, networks trained for speech recognition tasks employ input vectors with the size on the order of hundreds of dimensions [Graves et al. 2013]. Learning with larger input dimensionality typically requires some structure in the input data. This is the case in convolutional neural networks (CNNs) trained on images, which can work with up to hundred thousand input pixels. This architecture takes advantage of the spatial structure of images by exploiting the local pixel connectivity and sharing the weights between spatial locations, which greatly reduces the number of learnable parameters. However, with no exploitable structure in the data, training DNNs on high-dimensional data poses a severe computational problem. The reason for this is the implied network architecture and in particular, a huge input layer, which may contain billions of weights. Even with recent advances in general-purpose computing on graphics processing units (GPGPU), training networks with that number of parameters is infeasible.

We show that this problem can be solved by incorporating random projection into

¹ While the term “high-dimensional” is sometimes used to refer to data described with at least four features, here we consider a feature vector high-dimensional when its dimensionality is on the order of millions.

the network architecture. In particular, we propose to prepend the network with an input layer whose weights are initialized to elements of an RP matrix. We study cases where the weights of this RP layer are either fixed during training or finetuned with error backpropagation. Our results demonstrate that, in comparison to the state-of-the-art methods, neural networks with RP layer achieve competitive performance on extremely high-dimensional real-world datasets.

The second, less conventional area, where we have found the application of RP techniques to be beneficial for training deep models is weight initialization. Specifically, we initialized the weights in deep networks with various RP matrices instead of drawing them from a scaled normal distribution, as is done in the current state-of-the-art initialization technique [He et al. 2015b]. Such random projection initialization enabled us to train deep networks to higher levels of performance: our experiments suggest that particularly deep CNNs can benefit from the introduced method.

1.1 Thesis statement

The goal of this dissertation is to show that random projection methods can be beneficial in training deep neural networks. The dissertation thesis is:

Random Projection enables training Deep Neural Networks on sparse, unstructured data with millions of dimensions. Furthermore, when used as a weight initialization method it improves the network performance.

Primarily, the dissertation presents how we can efficiently incorporate RP as an input layer in deep networks. This broadens their applicability to types of input data that currently can only be learned with fast linear classifiers. Additionally, the dissertation shows that RP can be successfully applied as a method for initializing weights in deep models.

1.2 Research contribution

The main contributions of this dissertation are:

- a review of the challenges and existing approaches to training DNNs on large-scale data that is sparse, high-dimensional and unstructured;
- the proposition of the fixed-weight random projection layer that enables efficiently training deep networks on sparse, high-dimensional, unstructured data;
- the proposition of network architectures and training regimes that make finetuning the weights in the RP layers feasible, even on large-scale datasets;
- the proposition of initializing weights in deep networks with RP matrices;
- an implementation of the proposed methods and their experimental evaluation on both synthetic and real-world large-scale datasets, including a comparison with the current state-of-the-art approaches.

1.3 Thesis structure

The dissertation is organized as follows.

Chapter 2 consists of two parts. In the first part, we introduce deep learning models and related training methods, which we extensively use in this work. In the second part, we present a particularly difficult type of data for neural network models – data that is sparse, high-dimensional and unstructured. We survey existing techniques that, by reducing the data dimensionality, can make training deep networks on such data possible.

In Chapter 3 we present in detail one of these methods, which is the core of the network architecture that we introduce in the following chapter – random projection. We review several important RP constructions: Gaussian, Achlioptas’, Li’s, subsampled randomized Hadamard transform and Count Sketch. We analyze their properties, focusing on the embedding quality and computational cost of performing the projection.

In Chapter 4 we show how to incorporate RP into the architecture of DNNs to enable them to learn from sparse, high-dimensional, unstructured data. We evaluate the performance of such networks on synthetic and real-world datasets. We compare the effectiveness and computational cost of our approach with competing state-of-the-art techniques. Finally, we discuss selected important implementation details.

In Chapter 5 we motivate and study initializing weights in DNNs with elements of RP matrices. We evaluate RP initialization in CNNs and in pretrained, fully-connected networks on several real-world datasets.

Finally, in Chapter 6 we conclude the dissertation and discuss further directions for research.

CHAPTER 2

BACKGROUND

In this chapter we first briefly introduce several important DNN models, algorithms and architectures. Specifically, we focus on models that we employ later in this work: multilayer perceptrons (MLPs), deep belief networks (DBNs), Autoencoders and CNNs. In the second part we focus on the problem of training deep networks on data that is simultaneously sparse, unstructured and high-dimensional. We show where data with these three properties may arise and why learning from it proves to be a challenging task. We explain how this can be leveraged by using fast dimensionality reduction techniques. Finally, we review existing dimensionality reduction approaches that are capable of efficiently processing sparse, high-dimensional data.

2.1 Deep neural networks

For years neural networks have been attracting the attention of researchers in both academia and industry. Unlike conventional machine learning techniques, they do not require handcrafted features, but instead discover features during learning. Yet, for a long time, training networks with a larger number of layers, called deep networks, was unsuccessful, and simpler machine learning algorithms, like support vector machines [Cortes and Vapnik 1995], were more useful in practical applications. However, advances from the last decade led to a resurgence of interest in neural networks. Since then, DNNs have demonstrated impressive results, significantly pushing the state of the art on many difficult tasks such as image recognition [Huang et al. 2016; Simonyan and Zisserman 2014], speech recognition [Hinton et al. 2012; Sercu et al. 2016] or sequence modeling [Graves et al. 2013; Mikolov et al. 2013; Sutskever et al. 2011, 2014].

During the recent years many types of artificial neural networks have been proposed, e.g., feedforward neural networks, recurrent neural networks, radial basis function networks or convolutional neural networks [Goodfellow et al. 2016]. Here we focus on networks that fall into the first, arguably most popular category, i.e., feedforward networks. Below we briefly introduce the most important feedforward models and architectures used in this work.

2.1.1 Multilayer perceptron

Deep feedforward networks are the backbone of modern deep learning methods. The most important architecture in this category is the multilayer perceptron. In fact, some authors consider the terms *multilayer perceptron* and *deep feedforward network* as synonyms [Goodfellow et al. 2016].

The aim of an MLP is to find the best approximation f^* of a function f that maps the information given to the network on input into the desired output. For example, in the image classification task, the input may correspond to pixel intensities of an image and the output may correspond to the category of the input image. In this case, by using observed data, MLP learns to map input images to the output categories in order to be able to predict the categories of previously unseen images.

The mapping from the input to the output is realized by feeding the input signal through multiple layers of computational nodes. Each node in one layer has weighted connections directed to the nodes of the subsequent layer (Fig. 2.1). Multilayer perceptron is called a feedforward network because of the flow of computations that are performed when processing information. Specifically, the input data is first fed into the input layer, where the inputs are multiplied by connection weights as they are passed to the first hidden layer. After the information is processed in the first hidden layer, it is again multiplied and passed to the subsequent layer. This process is repeated until the output layer is reached. Importantly, the information flows in one direction, forward, because there are no backward connections. In this aspect feedforward neural networks differ from recurrent neural networks.

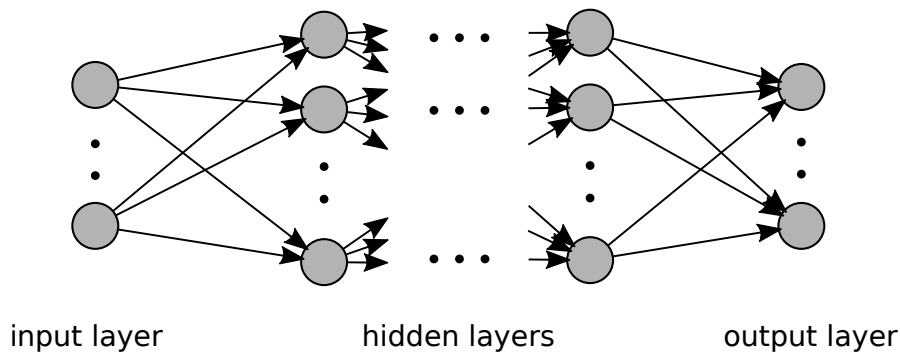


Figure 2.1: A schematic representation of a multilayer perceptron.

Activation function

Except for the input nodes, each node is a neuron that performs a simple computation:

$$y = \phi(z), \quad z = \sum_i w_i x_i + b, \quad (2.1)$$

where y is the output, x_i is the i -th input, w_i is its corresponding weight, b is the bias, and ϕ is the activation function. Historically, a popular choice for the activation

function, also called the transfer function, was the logistic sigmoid function:

$$\phi(z) = \frac{1}{1 + e^{-z}} \quad (2.2)$$

or the hyperbolic tangent function:

$$\phi(z) = \tanh(z) = \frac{e^z - e^{-z}}{e^z + e^{-z}}. \quad (2.3)$$

Nowadays the recommendation is to use the rectifier linear function [Nair and Hinton 2010], defined as:

$$\phi(z) = \max\{0, z\}. \quad (2.4)$$

Neurons employing this activation function are commonly called rectified linear units (ReLUs). There are also several variants of the rectifier linear function, e.g., the leaky rectifier linear function [Maas et al. 2013], defined as:

$$\phi(z) = \max\{az, z\}, \quad (2.5)$$

where a is usually small, e.g., $a = 0.01$. A leaky rectified linear unit (LReLU) works similarly to a rectified linear unit, but propagates a small, non-zero gradient when the unit is not active.

Training with stochastic gradient descent

In order for the MLP to accurately approximate the mapping function f , its parameters θ , i.e., weights \mathbf{w} and biases \mathbf{b} , have to be adjusted. This process of adjusting network parameters is called network training. Multilayer perceptron networks are usually trained in a supervised manner. That is, during training the network is presented with data examples $\mathbf{x}^{(i)}$ with known labels $y^{(i)}$. By knowing the desired output and the output computed by the network $f^*(\mathbf{x}^{(i)})$, the value of some per-example loss function $J_i(\mathbf{x}^{(i)}, y^{(i)}; \theta)$ can be calculated. This value indicates how well the model is approximating the mapping function f for the i -th example. The cost function, also called the objective function is the average loss over individual examples:

$$J(\mathbf{X}, \mathbf{y}; \theta) = \frac{1}{n} \sum_{i=1}^n J_i(\mathbf{x}^{(i)}, y^{(i)}; \theta), \quad (2.6)$$

where \mathbf{X} is the design matrix of the dataset¹, \mathbf{y} is the vector of labels, and n is the number of training examples. The goal of the training is to minimize the value of the objective function on the training examples \mathbf{X} by adjusting the values of parameters θ . Unfortunately, this cannot be done analytically. However, it is possible to compute the gradient of the objective function with respect to each parameter $\theta \in \theta$: $\frac{\partial J}{\partial \theta}$. This can be done starting from the output layer, by applying the chain rule for derivatives. The procedure for calculating the gradients is called **backpropagation** [Rumelhart et al. 1986]. When the gradients are known, we can use a gradient-based optimization algorithm to find a configuration of parameters θ that minimizes the objective function. In practice,

¹ A design matrix of a dataset is a matrix in which each row represents a training example.

the **stochastic gradient descent (SGD) algorithm**, a stochastic approximation of the gradient descent optimization method, works surprisingly well. In SGD the true gradient $\nabla_{\theta}J(\mathbf{X}, \mathbf{y}; \theta)$, i.e., the average gradient calculated over all training examples, is approximated by a gradient computed on a single training example. Pseudocode for SGD is presented in Algorithm 1.

Algorithm 1 Stochastic gradient descent pseudocode.

```

initialize network parameters  $\theta$ 
choose learning rate  $\gamma$ 
while not converged do
  shuffle training examples
  for each training example  $(\mathbf{x}^{(i)}, y^{(i)})$  do
    compute  $\nabla_{\theta}J_i(\mathbf{x}^{(i)}, y^{(i)}; \theta)$  with backpropagation
     $\theta \leftarrow \theta - \gamma \nabla_{\theta}J_i(\mathbf{x}^{(i)}, y^{(i)}; \theta)$ 
  end for
end while

```

However, performing the parameters update with a single training example is computationally inefficient. To speed up the training, most practitioners compute the average gradient over several training examples and then update the weights. This modification is called the mini-batch stochastic gradient descent [Bottou 1998]. Employing mini-batch SGD instead of the classic SGD is beneficial in two ways. First, mini-batch SGD can be parallelized more efficiently than SGD. This is because the majority of operations in mini-batch SGD involve matrix-matrix operations, while SGD utilizes mostly vector-matrix operations. Performing one matrix-matrix operation, e.g., matrix multiplication to compute activations for a mini-batch of 100 examples, is significantly faster than an equivalent number of vector-matrix multiplications. Second, mini-batch SGD leads to smoother convergence since the gradient estimates are less noisy than the gradients estimated using individual examples [Bousquet and Bottou 2008].

Momentum method

The momentum method [Polyak 1964] is a particularly important SGD extension, which usually improves the speed of convergence of DNNs. Stochastic gradient descent with momentum stores the values of the parameter updates at each iteration and uses them in the next update. The parameter update in SGD with momentum is given by:

$$\begin{aligned} \mathbf{v} &\leftarrow \mu \mathbf{v} - \gamma \nabla_{\theta}J(\mathbf{X}, \mathbf{y}; \theta) \\ \theta &\leftarrow \theta + \mathbf{v}, \end{aligned} \tag{2.7}$$

where \mathbf{v} is the velocity vector of the same size as the parameter vector θ and μ is an additional hyperparameter, usually referred to as *momentum*. In the physical interpretation μ is similar to the friction coefficient. Its value is usually set between 0.5 and 0.99. In practice, by taking into account gradients from the previous updates, the momentum method accelerates SGD learning, especially for gradients $\nabla_{\theta}J(\mathbf{X}, \mathbf{y}; \theta)$ that are noisy or small but consistent.

Output units and cost functions

In a supervised learning problem, the cost function quantifies the error a network makes by comparing the network prediction with the expected output. The way in which a network represents its output determines the type of the loss function. Therefore, we discuss output unit types together with corresponding loss functions. The most popular choices of the output units include linear units, sigmoid units and softmax units.

Linear units. Linear units do not employ a nonlinear transfer function and return real-valued outputs. This makes them suitable for regression tasks. Because linear units do not saturate, they can be used with any gradient-based optimization algorithm. Most often the mean square error (MSE) cost function, also known as the quadratic cost, is used along with linear outputs. The loss for a single example $(\mathbf{x}^{(i)}, y^{(i)})$ is then defined as:

$$J_i(\mathbf{x}^{(i)}, y^{(i)}; \boldsymbol{\theta}) = \frac{1}{2} \sum_j \left(a_j^{(i)} - y_j^{(i)} \right)^2, \quad (2.8)$$

where $a_j^{(i)}$ represents the activation value of the j -th neuron in the output layer when the network is presented with i -th example, and $y_j^{(i)}$ is the j -th component of the desired output for the i -th example.

Sigmoid units. Sigmoid units, on the other hand, are more suited for the classification task. Specifically, a single sigmoid unit in an output layer can be used for binary classification since its output $\sigma(z) = \frac{1}{1+e^{-z}} \in [0, 1]$ can be interpreted as class probability. In this context, rather than MSE, a more appropriate cost function is the cross entropy (CE) loss:

$$J_i(\mathbf{x}^{(i)}, y^{(i)}; \boldsymbol{\theta}) = - \left(a^{(i)} \ln y^{(i)} + (1 - a^{(i)}) \ln(1 - y^{(i)}) \right), \quad (2.9)$$

where $y^{(i)}$ is the desired output, and $a^{(i)}$ is the output produced by the sigmoid unit.

Softmax units. For the multi-class classification task, the network has to learn a categorical distribution over n possible categories. In these settings, the softmax function [Bridle 1990] is a perfect choice. To represent a valid probability distribution, each unit in a softmax layer is required to output a value in the $[0, 1]$ interval and the outputs must sum up to 1. A popular function that satisfies these conditions is softmax:

$$y(\mathbf{z})_i = \frac{e^{z_i}}{\sum_{j=1}^n e^{z_j}}, \quad (2.10)$$

where $\mathbf{z} = (z_1, \dots, z_n)$ is a vector of inputs to neurons in the softmax layer. For multiclass classification, the CE cost from Eq. 2.9 can be extended to:

$$J_i(\mathbf{x}^{(i)}, y^{(i)}; \boldsymbol{\theta}) = - \sum_{j=1}^C a_j^{(i)} \ln y_j^{(i)}, \quad (2.11)$$

where C is the total number of classes.

Regularization

The number of parameters in a neural network can be very high, which often makes the training process prone to overfitting. One way to avoid overfitting is to employ regularization. There are several means of regularizing neural networks. These include, for example, penalizing the magnitude of network parameters or employing more complex techniques, such as dropout.

Parameter penalty. Probably the simplest way to regularize a neural network model is to impose a penalty on the magnitudes of its parameters. This can be realized by adding a parameter norm penalty term $\omega(\boldsymbol{\theta})$ to the cost function:

$$\tilde{J}(\mathbf{X}, \mathbf{y}; \boldsymbol{\theta}) = J(\mathbf{X}, \mathbf{y}; \boldsymbol{\theta}) + \lambda\omega(\boldsymbol{\theta}), \quad (2.12)$$

where λ is a hyperparameter controlling the regularization strength. The most common parameter penalty norms are the L2 regularization $\omega(\boldsymbol{\theta}) = \frac{1}{2}\|\mathbf{w}\|_2^2$ and L1 regularization $\omega(\boldsymbol{\theta}) = \|\mathbf{w}\|_1$. Note that typically only the weights \mathbf{w} (and not the biases) are penalized [Goodfellow et al. 2016].

Dropout. Regularization techniques such as parameter norm penalties are not specific to neural networks. They have been used extensively, for example, in linear regression or logistic regression models, prior to the advent of deep learning. Dropout [Srivastava et al. 2014], however, is a recent regularization technique tailored specifically for reducing overfitting in DNNs.

Dropout can be applied during training with a mini-batch-based learning algorithm, such as mini-batch stochastic gradient descent. It amounts to disabling a randomly selected subset of units each time a mini-batch is processed. The neurons are kept alive with probability d , which is usually set to 0.5 for hidden units and 0.8 for input units.

Dropout can be viewed as an extreme form of bagging [Breiman 1996] – an ensemble learning technique in which each member of the ensemble is trained with a different subsample of the input data. For each mini-batch, dropout creates a different network that is trained on examples from just this single mini-batch. At test time, network with scaled weights is used and no units are dropped. Mathematically, this approximates ensemble averaging [Warde-Farley et al. 2013].

Batch normalization. Batch normalization (BN) [Ioffe and Szegedy 2015] is another recently introduced technique that acts as a regularizer. BN addresses the covariate shift problem, i.e., its goal is to assure that the distribution of layer inputs does not change during training. This is achieved by performing a zero-mean unit variance normalization for each mini-batch. Specifically, for a mini-batch containing m examples $(\mathbf{x}^{(1)}, \dots, \mathbf{x}^{(m)})$, where every example is a d -dimensional vector $\mathbf{x}^{(i)} = (x_1^{(i)}, \dots, x_d^{(i)})$, each dimension k is normalized separately:

$$\mu_k = \frac{1}{m} \sum_{i=1}^m x_k^{(i)}, \quad \sigma_k^2 = \frac{1}{m} \sum_{i=1}^m (x_k^{(i)} - \mu_k)^2, \quad \hat{x}_k^{(i)} = \frac{x_k^{(i)} - \mu_k}{\sqrt{\sigma_k^2 + \epsilon}}, \quad y_k^{(i)} = \gamma_k \hat{x}_k^{(i)} + \beta_k, \quad (2.13)$$

where μ_k and σ_k^2 are the mean and variance along k -th mini-batch dimension, respectively. Parameters γ_k and β_k are learned along with other network parameters and correspond to the scale and shift for the normalized \hat{x}_k . To avoid dividing by zero, a small constant $\epsilon > 0$ is introduced. The BN transformation is differentiable, and therefore it is possible to backpropagate the gradients through the normalization parameters. Batch normalization can significantly speed up the training and in some cases even replace dropout [Ioffe and Szegedy 2015].

Weight initialization

The question how the weights in a neural network should be initialized is not trivial and has prompted a vigorous research during the recent years [Glorot and Bengio 2010; Glorot et al. 2011; He et al. 2015b; Hinton and Salakhutdinov 2006; Martens 2010; Sutskever et al. 2013]. The spectrum of techniques attempting to solve this problem is wide and ranges from simply setting the weights to random numbers drawn from scaled distributions to more complex approaches, such as pretraining with DBNs or transfer learning. We elaborate on this topic in Section 5.1.

2.1.2 Deep belief network

The renaissance of deep learning in the 2000s began with the discovery that greedy layer-wise pretraining can be used to find a combination of initial parameters that make training deep networks possible. The first architecture that succeeded in this task was the deep belief network [Hinton and Salakhutdinov 2006]. Deep belief network is composed of stacked restricted Boltzmann machines (RBMs). Its training consists of first performing layer-by-layer unsupervised pretraining and then finetuning the network with error backpropagation.

Restricted Boltzmann machine

Restricted Boltzmann machine [Smolensky 1986] is a generative model that learns a probability distribution over a set of observations. It is composed of two groups of units, visible and hidden, that are arranged in a bipartite graph. The visible units correspond to features of the observations, and the hidden units represent latent factors that model the dependencies between these features. Each visible unit is connected to every hidden unit with a symmetrical weighted connection. In the simplest case, visible and hidden units are binary. That is: $v_i, h_j \in \{0, 1\}$, $i = 1 \dots n$, $j = 1 \dots m$, where n is the number of visible units, and m is the number of hidden units. Restricted Boltzmann machines work by simultaneously updating the states of all hidden units given the states of visible units and vice versa. The updates for binary visible and hidden units are stochastic:

$$p(v_i = 1 | \mathbf{h}) = \left(1 + e^{-(\mathbf{h}\mathbf{W}_{i\cdot}^T + a_i)}\right)^{-1}, \quad p(h_j = 1 | \mathbf{v}) = \left(1 + e^{-(\mathbf{v}\mathbf{W}_{\cdot j} + b_j)}\right)^{-1}, \quad (2.14)$$

where \mathbf{a} is a vector of visible unit biases, \mathbf{b} is a vector of hidden unit biases, and $\mathbf{W}_{i\cdot}$, $\mathbf{W}_{\cdot j}$ are the i -th row and the j -th column of the weight matrix \mathbf{W} , respectively. Note, however, that certain other activation functions can also be used with RBMs, e.g., to model non-binary vectors [Hinton 2012]. For example, to deal with real-valued

input, binary visible units can be replaced by linear units with independent Gaussian noise [Freund and Haussler 1992; Welling et al. 2005].

Contrastive divergence

In the RBM model the goal of training is to maximize the product of probabilities that the model assigns to observations from a training set. To do this, RBM training algorithms approximate the gradient of the log-likelihood of training vectors with respect to the weights and biases. This gradient is then used inside a gradient descent procedure to update the weights. One of the most commonly used gradient approximation methods is the contrastive divergence (CD) algorithm [Hinton 2002]. A training step in CD begins with taking a sample of visible and hidden units over the training data. The algorithm thus picks a random training example $\mathbf{v}^{(p)}$ and then takes a sample $\mathbf{h}^{(p)}$ of hidden units according to the activation probabilities $p(h_j^{(p)} = 1 | \mathbf{v}^{(p)})$. Next, CD takes an approximate sample $(\mathbf{v}^{(n)}, \mathbf{h}^{(n)})$ from the RBM model by performing alternating Gibbs sampling of the visible and hidden units, starting the chain from the hidden configuration $\mathbf{h}^{(p)}$. The gradient is then approximated as:

$$\begin{aligned} \frac{\partial \log p(\mathbf{v}^{(p)})}{\partial \mathbf{W}} &= \mathbf{v}^{(p)\top} \mathbf{h}^{(p)} - \mathbf{v}^{(n)\top} \mathbf{h}^{(n)} \\ \frac{\partial \log p(\mathbf{v}^{(p)})}{\partial \mathbf{a}} &= \mathbf{v}^{(p)} - \mathbf{v}^{(n)} \\ \frac{\partial \log p(\mathbf{v}^{(p)})}{\partial \mathbf{b}} &= \mathbf{h}^{(p)} - \mathbf{h}^{(n)}. \end{aligned} \tag{2.15}$$

In its fastest variant CD performs only one Gibbs step - the so-called CD₁ algorithm. CD₁ was used by Hinton and Salakhutdinov [2006] to train DBNs, i.e., stacked RBMs where the first RBM models the observed data and each subsequent RBM models outputs from the previous layer. This procedure was used to obtain initial weights for deep autoencoders and deep MLP networks. Networks initialized in this manner were then fine-tuned with error backpropagation, ultimately achieving state-of-the-art performance on several dimensionality reduction and classification tasks.

The pretraining procedure described in [Hinton and Salakhutdinov 2006] was further developed by Nair and Hinton [2010] with the introduction of noisy rectified linear units (NReLU), i.e., units with an activation function given by:

$$\text{NReLU}(x) = \max \left\{ 0, x + \mathcal{N} \left(0, (1 + e^{-x})^{-1} \right) \right\}. \tag{2.16}$$

Noisy rectified linear units replace binary hidden units during layer-wise pretraining. Afterwards, when the network is fine-tuned with error backpropagation, hidden layers employ a deterministic variant of the above activation function, i.e., the standard rectified linear function.

2.1.3 Autoencoder

The autoencoder is an MLP whose aim is to reconstruct at the output the same information that it was given as input. Therefore, autoencoders must have the same number of

input and output units. Autoencoder’s middle layer – called the coding layer – usually has the smallest number of units. This is the case in undercomplete autoencoders, whose task is to construct a compact representation of the data, for example for dimensionality reduction, data embedding or visualization.

The autoencoder is composed of two parts, the encoder and the decoder. For an observation \mathbf{x} presented to the network on the input, the encoder calculates its representation $\mathbf{c} = e(\mathbf{x})$, and the decoder calculates the reconstruction $d(\mathbf{c})$. Autoencoders are trained to minimize a loss function, whose aim is to penalize the dissimilarity between \mathbf{x} and $d(e(\mathbf{x}))$. By modifying the cost function, the training may also make the representation on the coding layer have various desired properties, such as sparsity [Ranzato et al. 2007] or being stable to small changes in the input [Rifai et al. 2011]. After training, the encoder part of the network can be used to extract codes for new inputs.

Autoencoders have been developed and studied for a long time before the advent of deep learning [Boulevard and Kamp 1988; LeCun 1987]. Originally these models were, however, composed of only three layers: the input layer, the coding layer and the output layer. The discovery of generative pretraining [Hinton and Salakhutdinov 2006] opened a possibility of training much deeper models.

2.1.4 Convolutional neural network

A CNN [LeCun et al. 1990, 1998a] can be thought of as an MLP-variant specialized for processing spatially structured data. The most important example of such data, on which CNNs perform exceptionally well, is the image data. By knowing that the input data is organized in a grid-like structure, CNNs can greatly reduce the number of learnable parameters, and thus speed up the training. This is achieved mostly by enforcing lower neuron connectivity, weights sharing and pooling.

Apart from the classical fully-connected layers, CNNs make use of two specific types of layers: convolutional layers and pooling layers. The purpose of a convolutional layer is to detect local features in the input volume. Neurons in convolutional layers are grouped into feature maps. However, instead of being connected to all units from the previous layer, each neuron is connected only to a small region of the input, called the receptive field. Weights of these connections form a filter and are shared among units from the same feature map. During the forward pass, filters from each feature map are convolved with the input to produce the activation maps. Convolutional layers are interleaved with pooling layers. Their function is to reduce the computation burden for subsequent layers, by down-sampling the data representation. Apart from controlling the overfitting, pooling layers additionally make the spatially reduced representation invariant to translation of the input. The most commonly used pooling method is max pooling [Zhou and Chellappa 1988], which amounts to partitioning the feature map from the previous layer into non-overlapping regions and returning maximum value for each region. Typically, a CNN employs a few stacks of convolutional layers with ReLU activations, followed by a pooling layer. This pattern can repeat itself several times before a transition to one or more fully-connected layers. Similarly to an MLP, a CNN can be trained with SGD and backpropagation, as all operations performed by its layers are differentiable.

CNNs were developed and used long before the advent of deep learning. One of

the first successful application of CNNs was the LeNet architecture employed for digit recognition [LeCun et al. 1998a]. However, the popularity of CNNs really skyrocketed after the ImageNet Large Scale Visual Recognition Challenge (ILSVRC) competition in 2012, where deep CNNs dominated its competitors on a large-scale image classification task [Krizhevsky et al. 2012]. Since then, deep convolutional networks are the model of choice for almost all image recognition tasks. Currently, the state-of-the-art results are achieved with a CNN variant called residual neural networks (ResNets) [He et al. 2015a]. These networks employ very deep architectures (e.g. 152-layer networks from [He et al. 2015a; Huang et al. 2016]) and introduce, so called, skip connections, which can bypass several layers.

2.2 Challenges in training neural networks on sparse, high-dimensional data

In this section, we focus on the problem of training DNNs on data that is unstructured, sparse and high-dimensional. We show why these three data properties, when occurring simultaneously, can make the training computationally challenging or, in some cases, even infeasible. We discuss how the above problem can be overcome by employing dimensionality reduction of the original data prior to network training. We survey existing dimensionality reduction approaches, focusing on methods that are capable of processing sparse, high-dimensional data.

2.2.1 Sparse, high-dimensional, unstructured data

We begin by describing the type of data we are interested in, along with the challenges it entails. We also look at domains and applications where such data may arise.

Data dimensionality. A common and intuitive way to represent a given dataset is by using the vector-space model [Salton 1979]. In the vector-space model, the observations are represented by an $n \times d$ matrix called the design matrix, in which each of the n rows corresponds to an observation that is described by d attributes (also called features or variables). The interpretation of the attributes depends, of course, on the nature of the dataset. For a set of images, an observation refers to an image that is defined by a list of pixel intensities or higher-level features, whereas text, for example, is often represented as a multiset of its words – the so-called bag-of-words (BOW) representation. Regardless of the feature interpretation, their number d , i.e., **the data dimensionality**, plays an important role in determining the applicability of machine learning and data mining methods.

High-dimensionality is a ubiquitous property of modern real-world datasets. Data having hundreds or even millions of features arise in various application domains, e.g., 2D/3D digital image processing, bioinformatics, e-commerce, web crawling, social media, mass spectrometry, text analysis or speech processing.

Data sparsity. Sparsity is a common property of many high-dimensional datasets. It is defined as the number of zero-valued elements in the $n \times d$ design matrix divided by

the total number of elements nd . However, when working with highly sparse datasets a more convenient term to use is **data density**, which is equal to one minus the sparsity [Herlocker et al. 2004].

Data can be sparse for two main reasons. Zeros in the design matrix may simply represent missing measurements, also denoted as null values or “NA” values. This is the case, for example, in recommender system data, where rows of the design matrix correspond to users and columns correspond to items. Each row of such data matrix contains user’s ratings of d items. As d is often extremely large, even the most active users are only able to rate just a small subset of all items. Therefore, most elements of the data matrix are missing and are often represented by zeros. The second reason for data sparsity stems from the type of data representation. For example, sparsity can be introduced as a result of binarization or discretization techniques. It may also result from converting categorical variables to a one-hot representation or when converting text data to BOW representation.

From the computational point of view processing sparse data has both advantages and disadvantages. On the one hand, sparsity is beneficial as it enables storing and manipulating large data in a compressed format. On the other hand, efficient manipulation of sparse matrices requires specialized algorithms and data structures that are capable of taking advantage of the sparse representation. Moreover, sparse data often entails using careful normalization during preprocessing.

Data structure. The third important property of datasets we are interested in is the lack of structure. The terms “structured data” and “unstructured data” are, however, imprecise and may have different meanings, depending on the area in which they are used. Here, we consider data as unstructured if its structure is not helpful for our task, i.e., training a neural network model. For example, images are a typical example of structured data, as their spatial structure, i.e., pixel adjacency, can be exploited when designing the network architecture (as convolutional networks do). On the other hand, text data in the BOW representation is unstructured: the context and word order do not matter and there is no apparent similarity between words, as they correspond to indices in a vocabulary.

Where does such data arise?

There are many kinds of data that exhibit the above properties. Millions or even billions of input features, high sparsity and lack of structure can be found in applications such as natural language processing, malware detection, recommendation and ranking systems, bioinformatics and high energy physics.

Text data. High dimensionality and sparsity of text data is usually the result of employing the BOW model. In this model, the text is represented as a multiset of its tokenized words. Therefore, a collection of text documents can be represented in the vector-space model as an $n \times d$ data matrix, with n equal to the number of documents and d equal to the size of the dictionary. The dictionary is the set of all unique words appearing at least once in the corpus. Since the great majority of documents typically use a tiny subset of the dictionary, the data matrix is often very sparse. Although being

simplistic, i.e., not taking grammar or word order into account, the BOW model is still a popular representation of text data. One extension of the BOW model capable of capturing phrases and multi-word expressions is the bag of n-grams representation. Instead of building a multiset of single words, it counts the occurrences of n-grams (usually bigrams or trigrams) of either words or characters. However, this greatly increases the dictionary size, especially when constructing representations of large text corpora.

Biological data. Certain types of biological data are also high-dimensional, sparse and unstructured. One example is thresholded microarray data. Microarray experiments measure expression levels of tens of thousands of genes (features) simultaneously. While these measurements are initially stored as dense real-valued matrices, it is not uncommon to preprocess them and only store the discretized values for genes that are significantly up- or down-regulated between different experimental conditions. In this representation, the microarray data becomes highly sparse, as usually, just a small fraction of all genes are up- or down-regulated.

Another example of sparse high-dimensional biological data is the single nucleotide polymorphism (SNP) data. A SNP is a variation of a single base-pair at a specific location in the DNA sequence among individuals of the same species. Dimensionality of SNP data can be very high, as the number of identified and mapped SNP sites often reaches hundreds of thousands or millions. Raw SNP data is mostly dense as the majority of SNPs occur at a frequency of more than 1%. Single nucleotide polymorphisms occurring less often are considered as low frequency variants or “mutations” [Barnes 2002]. Therefore, studies that focus on these low-frequency variants, such as cancer research, use sparse data (see, e.g., [Vural et al. 2016]).

A significant challenge in training neural networks on biological data stems from the disproportion between the number of available training examples and example dimensionality. In particular, for most biological datasets the number of features is up to several orders of magnitude greater than the number of examples. This is the result of treating samples or patients as observations (examples) and genes or proteins as variables. This perspective is common, e.g. in the identification of significantly expressed genes, cancer classification and other studies [Clarke et al. 2008].

Web data. The Internet is an important source of various types of large-scale data. In particular, huge amounts of data of different nature can be extracted from web pages using web crawlers. Many archives of web crawl data are publicly available for research and analysis. Such archives contain terabytes or even petabytes of raw web page data and metadata collected over several years of web crawling². However, because of storage and computational costs, these amounts of unprocessed data are usually unfit for research purposes. Fortunately, many projects, such as, e.g., Web Data Commons³, provide datasets extracted from raw web crawl data. Most often web crawl data is sparse and high-dimensional because of the use of the BOW model for text data or feature binarization and discretization techniques.

One interesting example of large-scale data closely related to web crawling is the uniform resource locator (URL) reputation data. Features in URL reputation datasets

² See, e.g., Common Crawl: <http://commoncrawl.org/>

³ <http://webdatacommons.org/>

are a combination of lexical features, such as BOW representation of tokens in the URL, with host-based features, such as DNS, WHOIS, AS and IP related information or blacklist membership [Ma et al. 2009]. Because of large amount of examples and dimensionality reaching millions of features, this type of data can be used for evaluating online learning methods.

Another example of sparse, high-dimensional web data is advertisement click-through rates prediction data. Here, the main cause of high dimensionality and sparsity is the use of one-hot-encoding representation for categorical features [Lee et al. 2012; Richardson et al. 2007].

Other types of data. Other, more exotic machine learning data include, for example, logs of student interactions with intelligent tutoring systems (KDD Cup 2010 data). The dimensionality of such datasets after preprocessing can reach tens of millions of features [Yu et al. 2010]. Another example of sparse, high-dimensional data is link data, i.e., graphs represented by adjacency matrices, where each feature corresponds to a weight or absence/presence of a link between nodes in a large network.

2.2.2 Learning from sparse, high-dimensional data

In many cases training neural networks on data characterized above can be computationally challenging or even infeasible. Note that this does not necessarily mean that neural networks cannot be trained on very-high-dimensional data. Often, when the data is structured the number of learnable parameters, i.e., weights, can be greatly reduced. CNNs, for example, reduce the number of parameters by exploiting local connectivity and sharing the weights between spatial locations. However, when the input data has no obvious structure it is difficult to constrain the network architecture. In such scenario, learning directly from unprocessed data ties the number of input units in the first layer to the data dimensionality. As a result, when the number of input dimensions exceeds tens of thousands, the number of weights in the first fully-connected layer is so large that the training becomes practically infeasible.

Fortunately, the above problem can be overcome by first **reducing the dimensionality** [Van Der Maaten et al. 2009]⁴ of the input space to a manageable size and then training a network on a representation with fewer dimensions. While in recent years a plethora of dimensionality reduction methods have been developed [Jović et al. 2015], few of them are suited for handling sparse, high-dimensional data. We focus on several such methods that can be applied as a preprocessing step before network training.

Note that even with the performance considerations put aside, performing dimensionality reduction prior to network training has its merits. In principle, the transformation realized by many dimensionality reduction techniques can as well be performed by one

⁴ The purpose of dimensionality reduction is to create a meaningful lower-dimensional representation of the original data. Dimensionality reduction limits the influence of the so-called, curse of dimensionality, which greatly facilitates or even enables, e.g., classification, clustering, visualization or compression of high-dimensional datasets. The term “curse of dimensionality”, originally coined in [Bellman 1961], broadly relates to problems that arise when the dimensionality of the analyzed data becomes high. In the context of machine learning, it refers to the difficulty of searching high-dimensional spaces and finding structure in data embedded in such spaces [Donoho 2000; Duda et al. 2012].

or more layers of the network (see for example principal component analysis (PCA) realized by a neural network layer [Oja 1982] or autoencoders [Hinton and Salakhutdinov 2006]). However, this approach results in larger network architectures that require more data to be trained and are more prone to overfitting. Therefore, we focus on performing the dimensionality reduction procedure separately, before the network training.

Dimensionality reduction methods can be divided into two categories: feature selection and feature extraction. The aim of feature selection is to limit the number of features by only keeping the most relevant ones and discarding the others. Feature extraction, on the other hand, constructs new derived features by transforming the original input variables. This transformation can be either linear or nonlinear. Feature selection is also employed in problems where the aim is not the dimensionality reduction itself but rather the identification of influential feature subsets: e.g., in bioinformatics for finding genes related to resistance to a pathogen [Guyon et al. 2002].

Feature selection methods. Feature selection is based on a premise that some features might be unnecessary by being either redundant or irrelevant, and thus can be removed from the feature set. Which features are considered relevant depends on the type of the feature selection algorithm. Traditionally, three approaches to feature selection were proposed: filter methods, wrapper methods and embedded methods [Guyon and Elisseeff 2003].

Filter methods try to assess feature relevancy only from the data, without evaluating the influence of the selected feature subset on the performance of the trained model. This approach is computationally much less expensive than the wrapper approach but produces feature subsets that are not tailored to a specific model. Most filter methods are univariate, i.e., they rank variables according to their individual predictive power, which was shown to yield inferior models compared to methods that rank subsets of features [Guyon and Elisseeff 2003]. In order to alleviate this problem a number of multivariate filter methods have also been proposed [Saeys et al. 2007].

In the wrapper approach selection of relevant features is performed with regard to the model performance. Wrapper methods view the feature selection process as a search problem, where the search space is defined by all possible feature subsets. Different feature combinations from the feature set \mathbb{F} are assigned scores that are based on the performance of models trained on these combinations. For practical applications, where $|\mathbb{F}|$ is large, evaluating all possible feature subsets is infeasible, as the number of subsets grows exponentially with $|\mathbb{F}|$. When an exhaustive search is impossible, a wide range of search strategies can be applied, including best-first, genetic algorithms, simulated annealing, particle swarm optimization or branch-and-bound [Kohavi and John 1997]. These methods may still be computationally prohibitive when training a single model on a particular feature subset is costly. In this case, greedy search strategies including, e.g., forward selection or backward elimination, may prove useful. Apart from being computationally expensive, these methods are also prone to overfitting, especially for large $|\mathbb{F}|$.

Similarly to wrapper methods, embedded methods [Guyon and Elisseeff 2003] rely on evaluating a classifier (or another model) on candidate feature subsets. However, they incorporate feature selection into the training method itself, i.e., they learn which features contribute to the model's performance while the model is being created. In this

way, they avoid expensive retraining of the whole model after every modification in the feature subset.

Feature extraction methods. Unlike feature selection methods, feature extraction approaches construct new features by performing a transformation of the original high-dimensional data into a lower-dimensional space [Van Der Maaten et al. 2009]. Based on the type of this transformation, feature extraction methods can be classified into linear and nonlinear methods. Linear feature extraction methods include, among others, PCA [Jolliffe 2002; Pearson 1901], random projection, linear discriminant analysis (LDA) [Friedman et al. 2001], multidimensional scaling (MDS) [Torgerson 1952] and maximum margin criterion [Li et al. 2006b]. Nonlinear methods include, for example, ISOMAP [Tenenbaum et al. 2000], locally linear embedding [Roweis and Saul 2000], autoencoders [Hinton and Salakhutdinov 2006], Sammon mapping [Sammon 1969] or t-SNE [Maaten and Hinton 2008]. In general, linear dimensionality reduction techniques are computationally more efficient than nonlinear methods, but often perform worse on complex, real-world data. For a comparative overview of popular feature extraction methods see [Storcheus et al. 2015; Van Der Maaten et al. 2009].

2.2.3 Feature selection for sparse, high-dimensional data

Many feature selection methods have been proposed throughout the years (for a comparative study see [Jović et al. 2015; Kumar and Minz 2014]). However, few of these methods are applicable to sparse, high-dimensional data. In particular, many state-of-the-art feature selection methods require calculating pairwise correlation coefficients between the features. This makes them infeasible for datasets with millions of features. Similarly, more complex wrapper methods, which require training the model multiple times, are not applicable in these settings due to their computational cost. Therefore, reducing data dimensionality using feature selection methods is viable mostly with the filter methods. Unfortunately, existing filter methods that are suitable for dense data cannot be easily modified to be applicable to sparse datasets [Liu and Yu 2005].

In an influential study, Forman [2003] evaluated several feature selection methods including Chi-square, information gain (IG), F1-measure, odds ration, bi-normal separation and others. However, Forman focused specifically on the problem of feature selection for the purpose of classification of BOW-represented text data. In a more recent study of feature selection methods for general big data, Bolón-Canedo et al. [2015] enumerate several popular algorithms suitable for processing high-dimensional datasets. These include mostly filter approaches and scalable embedded methods, i.e., Chi-square, F-score, IG, ReliefF, mRMR, SVM-RFE, CFS, FCBF, INTERACT and Consistency. Here, we are interested in processing datasets with the number of examples n and the number of features d both on the order $\geq 10^5$. Therefore, we only focus on the fastest feature selection methods, whose computational complexity is not worse than $\mathcal{O}(nd)$. These are: Chi-square [Liu and Setiono 1995], F-score [Duda et al. 2012] and IG [Quinlan 1986]. All these methods are univariate, i.e., each of them scores the features independently.

Chi-square

The Chi-square feature selection ranks features in a dataset represented by a design matrix \mathbf{X} by performing χ^2 tests between the feature vectors and the class vector \mathbf{y} . The method is applicable to continuous data after binning [Fayyad and Irani 1993], as the χ^2 test is only defined for categorical (nominal) data. The Chi-square statistic for a feature i is calculated as:

$$\chi^2(i; \mathbf{X}, \mathbf{y}) = \sum_{j \in \text{vals}(\mathbf{X}_{\cdot i})} \sum_{k=1}^N \frac{(O_{ijk} - E_{ijk})^2}{E_{ijk}}, \quad (2.17)$$

where $\text{vals}(\mathbf{v})$ is a function returning a set of unique values in \mathbf{v} , and N is the number of classes. O_{ijk} and E_{ijk} are the observed and expected numbers of examples belonging to class k whose i -th feature has value j . The value of O_{ijk} is calculated from the empirical data, and E_{ijk} is estimated assuming the independence of feature i from the predicted class. High scores of $\chi^2(i; \mathbf{X}, \mathbf{y})$ indicate that the null hypothesis of independence should be rejected and feature i and predicted class are correlated. Chi-square feature selection returns the highest ranked features, which are likely to be relevant during classification.

Importantly, Chi-square feature selection can be implemented in a way that leverages data sparsity, making it computationally efficient.

F-score

The Fisher score of the i -th feature can be defined as:

$$F_{\text{score}}(i; \mathbf{X}, \mathbf{y}) = \frac{\sum_{k=1}^N n_k (\mu_k^i - \mu^i)^2}{\sum_{k=1}^N n_k (\sigma_k^i)^2}, \quad (2.18)$$

where N is the number of classes, n_k is the number of examples in \mathbf{X} belonging to the k -th class, μ_k^i and σ_k^i are the average and standard deviation of feature i for examples belonging to class k , respectively, and μ^i is the average of feature i over all examples. Feature selection with Fisher score finds a set of features that are most discriminative between the classes, i.e., have the highest F_{score} values. Specifically, it seeks for features that maximize the distances between the means of the classes while minimizing the variance within each class. This criterion is also used in feature extraction, e.g., in linear discriminant analysis. Despite being simple, the F-score feature selection combined with random forest and SVM has been shown to work surprisingly well [Chen and Lin 2006].

Several more complex feature selection methods have been developed based on the Fisher score. For example, Gu et al. [2012] proposed a generalized multivariate F-score method, i.e., a method that selects a subset of features simultaneously. However, its computational cost makes it prohibitive in our settings. Although being suitable for sparse data, the method assumes that the data matrix has been centered. Unfortunately, centering each feature cannot be realized without making the data matrix dense.

Information gain

Information gain for a feature i is the amount of uncertainty about the predicted class that gets reduced when feature i is observed. Here we use the term *information gain*

as it was introduced in the context of decision trees [Quinlan 1986]. Therefore, it is equivalent to *mutual information*. Alternatively, some authors define information gain as the Kullback–Leibler divergence (also known as information divergence or relative entropy).

More formally, given a set of training examples \mathbb{X} , each of the form $(\mathbf{x}, y) = (x_1, \dots, x_k, y)$, information gain $\text{IG}(i; \mathbb{X})$ is the reduction of entropy that is achieved by observing feature i :

$$\begin{aligned} \text{IG}(i; \mathbb{X}) &= H(\mathbb{X}) - H(\mathbb{X}|i) \\ &= H(\mathbb{X}) - \sum_{v \in \text{vals}(\mathbb{X}_i)} \frac{|\{(\mathbf{x}, y) \in \mathbb{X} | x_i = v\}|}{|\mathbb{X}|} H(\{(\mathbf{x}, y) \in \mathbb{X} | x_i = v\}), \end{aligned}$$

where \mathbb{X}_i is a feature vector in the dataset that corresponds to feature i , and vals is defined as in the Chi-square method. Entropy H for a dataset \mathbb{S} is defined as:

$$H(\mathbb{S}) = - \sum_{c=1}^N p_c(\mathbb{S}) \log p_c(\mathbb{S}), \quad (2.19)$$

where N is the number of classes in \mathbb{S} and $p_c(\mathbb{S})$ is the probability of a training example in \mathbb{S} belonging to the class c . $\text{IG}(i; \mathbb{X})$ is equal to zero if variable represented with feature vector \mathbb{X}_i is independent from the predicted class vector. Similarly to F-score and Chi-square methods, information gain selects features with highest scores $\text{IG}(i; \mathbb{X})$, which suggest their high correlation with the predicted class.

Note that the above definition of information gain is suitable for datasets with a discrete set of feature values. For continuous data, several methods of discretization were developed, most notably the information theoretic binning [Fayyad and Irani 1993]. An alternative approach is to estimate the entropy with k -nearest neighbor distances [Kraskov et al. 2004].

2.2.4 Feature extraction for sparse, high-dimensional data

In general, most feature extraction methods are computationally more demanding than filter feature selection approaches. As performance is a key issue in our application, we focus on the most efficient linear feature extraction algorithms.

In a recent comprehensive study of commonly used linear feature extraction techniques Cunningham and Ghahramani [2015] discuss PCA, MDS, LDA, canonical correlations analysis (CCA), maximum autocorrelation factors (MAF), slow feature analysis (SFA), sufficient dimensionality reduction (SDR), locality preserving projections (LPP), independent component analysis (ICA), probabilistic PCA, factor analysis and distance metric learning. However, in their analysis Cunningham and Ghahramani focus on reducing the dimensionality of dense data. In particular, they assume that the original input data can be easily mean-centered. This step cannot be realized for large sparse datasets, without making them fully-dense and destroying the benefits of sparse representation. Moreover, most of the methods discussed in [Cunningham and Ghahramani 2015] were not developed for sparse data, and thus are unfit for such applications. These include MDS, LDA, SFA, SDR, LPP and ICA. James and Hastie [2001] presented a modified version of LDA, so called functional LDA and suggested that it can be extended

to be applicable to sparse data. However, they did not evaluate this modification on sparse datasets and did not specify its computational complexity. CCA and MAF both require performing eigendecomposition of the correlation or covariance matrix, which makes their computational complexity too high for our case. SFA also requires expensive estimation of the covariance matrix. To solve this problem, Kompella et al. [2012] propose an online version of SFA, called incremental SFA, which does not rely on computing a covariance matrix. However, similarly to previous methods, their approach is also not suited for sparse data. MDS, LPP, ICA and its numerous extensions also have prohibitive computational complexity – most often not lower than $\mathcal{O}(n^3)$ (assuming for simplicity that $n \approx d$) [He and Niyogi 2004; Van Der Maaten et al. 2009]. Distance metric learning methods like, e.g., neighbourhood components analysis are more suited for visualization purposes, as they learn low-dimensional embeddings [Goldberger et al. 2005].

Several scalable incremental feature extraction algorithms have also been proposed. These include incremental maximum margin criterion (IMMC) [Yan et al. 2004], online variants of LDA, incremental principal component analysis (IPCA) [Li et al. 2003] and candid covariance-free incremental principal component analysis (CCIPCA) [Weng et al. 2003]. These methods were developed in the context of online learning for problems associated with data streaming. However, their computational complexity is sometimes still too high for our purpose, i.e., for cases when both n and d are on the order of millions. For example, IMMC improves the complexity of batch maximum margin criterion (MMC) [Li et al. 2006b] from $\mathcal{O}(\min\{n^3, d^3\})$ to $\mathcal{O}(ndkc)$, where c is the number of classes. While much faster than the classical method, this is still significantly slower than, e.g., PCA realized via a randomized version of the block Lanczos method [Halko et al. 2011] (see the section about PCA below). Several variants of LDA offer faster computational time. Incremental dimension reduction via QR decomposition (IDR/QR) [Ye et al. 2005], for example, offers complexity of $\mathcal{O}(ndc)$. This is achieved by applying QR decomposition instead of singular value decomposition (SVD). Unfortunately, IDR/QR is not suited for sparse data. Another example of a fast LDA-based method is incremental linear discriminant analysis (ILDA) [Kim et al. 2007], which can be computed in $\mathcal{O}(dk^2)$ – time that is not dependent on the number of training examples. Similarly to ILDA, spectral regression discriminant analysis (SRDA) [Cai et al. 2008] is capable of processing sparse data and can be computed in just $\mathcal{O}(\min\{n, d\}s)$ operations, where s is the average number of non-zero features in each example. However, the application of LDA-based methods is limited due to the so-called *singularity problem* [Krzanowski et al. 1995], which occurs when the data dimensionality exceeds the number of examples. Several variants of PCA that construct an incremental representation of the covariance matrix have been proposed, e.g., IPCA and CCIPCA. However, these methods are also unable to efficiently process sparse datasets.

Principal component analysis

Principal component analysis, one of the most widely used tools in data analysis and data mining, is also one of the most popular linear dimensionality reduction methods. It attempts to find a feature subspace that preserves the most of the data variability. The basic approach to computing PCA of matrix $\mathbf{X} \in \mathbb{R}^{n \times d}$ involves calculating the covari-

ance matrix $\frac{1}{n-1} \mathbf{X}^T \mathbf{X}$ and performing its eigendecomposition. Then, k principal components with the highest eigenvalues are used to project the data into a lower-dimensional space. While efficient for datasets with $d < n$, this approach can be numerically inaccurate, as the condition number of the covariance matrix is the square of the condition number of \mathbf{X} (see, e.g., the Lauchli matrix [Lauchli 1961]). Instead, PCA is often realized by performing SVD of the normalized data matrix \mathbf{X} , which can be computed in $\mathcal{O}(\min\{nd^2, n^2d\})$. For dense datasets with $n \sim d$, this makes it prohibitive for values of n higher than several thousand. In practice, however, it is usually sufficient to compute a reduced version of SVD, i.e., a truncated SVD, to determine only the k largest singular values of \mathbf{X} [Friedman et al. 2001]. This can be achieved by using, e.g., iterative Lanczos’ methods and can speed up the computation to $\mathcal{O}(ndk)$ while also reducing the memory footprint of the algorithm. However, even calculating a partial SVD is computationally prohibitive when k is large and n and d are on the order of millions. A solution to this challenge arises from randomized matrix algorithms, which can reduce the computational complexity even further: from $\mathcal{O}(ndk)$ to $\mathcal{O}(nd \log k)$ [Mahoney 2011]. This can yield a significant speedup when we are interested in reducing the dimensionality of the data to k that is on the order of thousands. Such efficient algorithms for large-scale PCA have been presented in e.g., [Georgiev and Mukherjee 2012; Halko et al. 2011; Rokhlin et al. 2009].

Random projection

Random projection is a simple and computationally efficient linear dimensionality reduction technique. We present this method in detail and focus on its properties and applications in Chapter 3.

CHAPTER 3

RANDOM PROJECTION

Random projection is a computationally efficient and conceptually simple dimensionality reduction technique. The key idea behind RP stems from the Johnson-Lindenstrauss lemma, which states that a set of points in a high-dimensional space can be embedded into a lower-dimensional space, with distances between these points preserved up to a certain multiplicative factor. Surprisingly, the dimensionality of this lower-dimensional space is logarithmic in n and does not depend on the dimensionality of the original data. In other words, RP makes it possible to compactly approximate a dataset consisting of n examples using just $\mathcal{O}(n \log n)$ memory. This is a big advantage, especially when processing large-scale datasets whose dimensionality is on the order of, or even exceeds the number of examples. Most importantly, by reducing the number of features to $\mathcal{O}(\log n)$, RP can make many methods that strongly depend on data dimensionality viable. In the next chapter, for example, we report experiments in which we used RP to train neural networks on data whose dimensionality would otherwise be prohibitively high for such models.

The Johnson-Lindenstrauss lemma is at the core of many algorithms in signal processing, statistics and computer science. One notable example that greatly popularized RP is sparse signal reconstruction, also known as compressed sensing [Donoho 2006]. Random projection has also found use in various machine learning tasks, e.g., classification [Arriaga and Vempala 2006; Goel et al. 2005; Paul et al. 2014; Rahimi and Recht 2008], regression [Kabán 2014; Maillard and Munos 2012] or clustering [Boutsidis et al. 2010; Fern and Brodley 2003]. For an overview of applications of RP see [Indyk and Motwani 1998; Vempala 2005].

This chapter is organized as follows. In Section 3.1 we introduce the Johnson-Lindenstrauss lemma and the notion of oblivious subspace embeddings. Next, in Section 3.2 we present five important RP constructions: Gaussian, Achlioptas', Li's, subsampled randomized Hadamard transform and Count Sketch. We analyze their properties, focusing on the embedding quality, applicability to sparse data and computational cost of performing the projection.

3.1 Johnson-Lindenstrauss lemma and embedding quality

The most important theoretical result behind RP is the Johnson-Lindenstrauss lemma from [Johnson and Lindenstrauss 1984]. Formally it is the following fact:

Lemma 1 (JL-lemma [Johnson and Lindenstrauss 1984]) *Let $\epsilon \in (0, 1)$ and \mathbb{A} be a set of n points in \mathbb{R}^d . Let k be an integer and $k = \mathcal{O}(\epsilon^{-2} \log n)$. Then there exists a mapping $f : \mathbb{R}^d \mapsto \mathbb{R}^k$ such that for any $\mathbf{a}, \mathbf{b} \in \mathbb{A}$*

$$(1 - \epsilon)\|\mathbf{a} - \mathbf{b}\|_2 \leq \|f(\mathbf{a}) - f(\mathbf{b})\|_2 \leq (1 + \epsilon)\|\mathbf{a} - \mathbf{b}\|_2. \quad (3.1)$$

That is, every dataset with n examples, regardless of its dimensionality, can be represented in $k = \mathcal{O}(\epsilon^{-2} \log n)$ dimensions in a way that preserves the pairwise distances between any two examples up to a multiplicative factor $1 \pm \epsilon$, where ϵ is the distortion. This estimation is optimal both in n and ϵ , i.e., without a priori knowledge of the dataset, no linear dimensionality reduction technique can improve the JL-lemma guarantee on k [Alon 2003].

Note, however, that Lemma 1 is not constructive, i.e., it does not specify how to create the mapping f . In their proof, Johnson and Lindenstrauss chose f as an orthogonal transformation whose corresponding projection matrix is neither easy nor efficient to generate for practical applications. One approach is to initialize the projection matrix with random numbers drawn from a normal distribution and then apply an orthogonalization procedure, such as the Gram-Schmidt method, which runs in $\mathcal{O}(dk^2)$ [Golub and Van Loan 2012]. In recent years multiple more practical constructions that satisfy the JL-lemma have been proposed. Such mappings f that preserve pairwise distances between the observations are called random projection schemes or Johnson-Lindenstrauss transforms (JLTs). In Section 3.2, we present several important JLTs, from historically earliest to more recent. These schemes differ in two main aspects:

- the computational complexity of constructing the projection matrix (if it is explicitly needed) and projecting the data,
- the quality of embedding they provide.

To assess and compare the embedding quality of different JLTs, or more specifically, the distributions according to which their projection matrices are generated, we use two important concepts, first introduced in [Sarlos 2006]: the subspace embedding property and the oblivious subspace embedding (OSE) property. They are the main tools for analyzing recent RP schemes [Clarkson and Woodruff 2013; Nelson and Nguyễn 2013; Woodruff 2014].

Definition 1 (($1 \pm \epsilon$) ℓ_2 -subspace embedding [Woodruff 2014]) *Let \mathbf{A} denote an $n \times d$ matrix and \mathbf{S} denote a $d \times k$ matrix, where $k \ll d$. \mathbf{S} is a $(1 \pm \epsilon)$ ℓ_2 -subspace embedding for \mathbf{A} if $\forall \mathbf{x} \in \mathbb{R}^n$*

$$(1 - \epsilon)\|\mathbf{x}^T \mathbf{A}\|_2^2 \leq \|\mathbf{x}^T \mathbf{A} \mathbf{S}\|_2^2 \leq (1 + \epsilon)\|\mathbf{x}^T \mathbf{A}\|_2^2. \quad (3.2)$$

That is, matrix \mathbf{S} is a subspace embedding for \mathbf{A} if for any given vector $\mathbf{x} \in \mathbb{R}^n$ the length of vector $\mathbf{x}^T \mathbf{A}$ is similar to the length of its sketch $\mathbf{x}^T \mathbf{A} \mathbf{S}$. One particularly useful variant of subspace embeddings is the oblivious subspace embedding.

Definition 2 (Oblivious subspace embedding [Woodruff 2014]) *Let \mathbf{A} denote an $n \times d$ matrix and Π denote a distribution on $d \times k$ matrices \mathbf{S} , where k is a function of n, d, ϵ and δ . Π is an (ϵ, δ) oblivious ℓ_2 -subspace embedding if with probability at least $1 - \delta$ matrix \mathbf{S} drawn from distribution Π is a $(1 \pm \epsilon)$ ℓ_2 -subspace embedding for \mathbf{A} .*

That is, distribution $\mathbf{\Pi}$ is an OSE if a random matrix drawn according to $\mathbf{\Pi}$ is a subspace embedding with high probability. Nelson and Nguyễn [2014] proved that the optimal lower bound for k , in order for a distribution to be an OSE is $\mathcal{O}(\epsilon^{-2}n)$. Note that this does not mean that the lowest dimensional subspace into which RP can embed an n -example dataset is $\mathcal{O}(\epsilon^{-2}n)$. The OSE's lower bound for k is not a contradiction to the JL-lemma, because the subspace embedding property is not equivalent with the preservation of pairwise distances between examples. However, estimating OSE's lower bounds for k can be useful for comparing the embedding quality of different RP constructions.

3.2 Construction of the projection matrix

Let $\mathbf{A} \in \mathbb{R}^{n \times d}$ denote a data matrix consisting of n observations in \mathbb{R}^d . In RP, matrix \mathbf{A} is projected from a high-dimensional space \mathbb{R}^d into a lower-dimensional space \mathbb{R}^k ($k \ll d$) using a random matrix $\mathbf{P} \in \mathbb{R}^{d \times k}$:

$$\tilde{\mathbf{A}} = \mathbf{A}\mathbf{P}. \quad (3.3)$$

Of course, the projection matrix \mathbf{P} cannot be completely random. Recently, many constructions of \mathbf{P} that combine efficient projection with good embedding quality have been proposed. We can distinguish two main lines of research here: one focusing on fast embedding of potentially dense data [Ailon and Chazelle 2006; Ailon and Liberty 2009; Dasgupta et al. 2010] and one aiming at embedding data that is highly sparse [Clarkson and Woodruff 2013; Dasgupta et al. 2010; Kane and Nelson 2014; Nelson and Nguyễn 2013]. Below we present several important RP schemes from both of these groups, i.e., Gaussian, Achlioptas', Li's, subsampled randomized Hadamard transform and Count Sketch-based projections.

3.2.1 Gaussian random matrix

The original proof by Johnson and Lindenstrauss [Johnson and Lindenstrauss 1984] used a matrix composed of properly scaled dense orthogonal vectors. However, for practical applications generating a large matrix with dense orthogonal rows or columns is computationally too expensive. Luckily, as shown in [Dasgupta and Gupta 2003; Indyk and Motwani 1998] the orthogonality constraint can be dropped. This observation led to a simple RP matrix construction, i.e., a Gaussian random matrix, whose entries are i.i.d. samples drawn from $\mathcal{N}(0, \frac{1}{k})$. A justification for choosing random vectors was provided in [Hecht-Nielsen 1994]: the probability of random vectors being orthogonal or almost orthogonal grows quickly with the vector dimensionality.

The main disadvantage of the Gaussian projection, when compared to more recent RP constructions, is its computational cost – Gaussian projection matrix can be generated in $\mathcal{O}(dk)$ and requires $\mathcal{O}(ndk)$ operations to project a dense dataset. For sparse data, the projection time can be slightly improved (see Table 3.1). Despite being computationally demanding, the Gaussian projection scheme has two advantageous traits: its implementation is straightforward and, more importantly, it produces a high-quality sketch of the original data matrix. In fact, the Gaussian scheme achieves the optimal OSE lower bound for the projected dimensionality: $k = \mathcal{O}(\epsilon^{-2}n)$ [Nelson and Nguyễn 2014].

3.2.2 Achlioptas' random matrix

One of the historically earliest lines of research on RP matrices focused on improving the computational time of performing the projection. This was achieved mostly by sparsifying the projection matrix. The first construction was given in the seminal work by Achlioptas [2001], where he proposed two versions of the projection matrix with simple probability distributions for the matrix elements:

$$P_{ij} = \sqrt{\frac{1}{k}} \cdot \begin{cases} 1 & \text{with probability } 1/2 \\ -1 & \text{with probability } 1/2 \end{cases}, \quad (3.4)$$

$$P_{ij} = \sqrt{\frac{3}{k}} \cdot \begin{cases} 1 & \text{with probability } 1/6 \\ 0 & \text{with probability } 2/3 \\ -1 & \text{with probability } 1/6 \end{cases}. \quad (3.5)$$

Achlioptas argued that these matrices yield a quality of embedding comparable to the quality provided by the random Gaussian matrix. Practical applicability of Achlioptas' construction was later confirmed by experimental results [Bingham and Mannila 2001; Fradkin and Madigan 2003].

Similarly to the Gaussian RP, Achlioptas' distributions from Eq. 3.4 and Eq. 3.5 are easy to implement. Additionally, their sparsity can be leveraged to compute the projection faster. Furthermore, the form of Eq. 3.4 and Eq. 3.5 enables optimizations using integer arithmetics: scaling by the constant $\sqrt{\frac{1}{k}}$ can be performed after the matrix multiplication (this can also be done for the Li's construction presented in the next section). These properties make Achlioptas' RP scheme especially useful in database applications, which was in fact his main motivation. In this work, we use only the sparser construction (Eq. 3.5).

3.2.3 Li's sparse matrix

Achlioptas' work was continued by Li et al. [2006a], who introduced a sparser random matrix (in the literature often referred to as the *very sparse random projection*), by extending Achlioptas' constructions:

$$P_{ij} = \sqrt{\frac{s}{k}} \cdot \begin{cases} 1 & \text{with probability } \frac{1}{2s} \\ 0 & \text{with probability } 1 - \frac{1}{s} \\ -1 & \text{with probability } \frac{1}{2s} \end{cases}. \quad (3.6)$$

Note that setting $s = 1$ and $s = 3$ yields Achlioptas' matrices from Eq. 3.4 and Eq. 3.5, respectively. Li et al. showed, however, that one can use s as high as $\frac{d}{\log d}$, if the data follows a normal distribution. To maintain a robust embedding, they recommend using lower s : $s = \sqrt{d}$, which still significantly sparsifies the projection matrix and greatly speeds up the projection. Therefore, in this work we use $s = \sqrt{d}$ when performing Li's projection.

3.2.4 Subsampled randomized Hadamard transform

While the sparsification of \mathbf{P} introduced by Li et al. enables faster $\tilde{\mathbf{A}}$ computation, it severely distorts the distances between the observations when \mathbf{A} is also sparse. This

problem was noticed and tackled by Ailon and Chazelle [2006]. They proved that projection can be performed using a sparse matrix only if the input data vectors are “well-spread”. Data vector \mathbf{x} of length d is well-spread if $\max_{1 \leq i \leq d} x_i$ is close to $\frac{1}{\sqrt{d}}$, i.e., \mathbf{x} does not contain few non-zero components with large absolute values. In order to assure that the input data is well-spread, Ailon and Chazelle proposed to transform it with a generalized fast Fourier transform, called the Walsh-Hadamard transform. After the transformation, the data can be safely projected using a highly sparse matrix without introducing large distortions. This resulted in an efficient embedding scheme suitable for sparse input data, the so-called subsampled randomized Hadamard transform (SRHT) or alternatively the fast Johnson-Lindenstrauss transform.

Ailon and Chazelle defined their projection matrix \mathbf{P}_{SRHT} as a scaled product of three matrices:

$$\mathbf{P}_{\text{SRHT}} = \frac{1}{\sqrt{k}} \mathbf{DHS}, \quad (3.7)$$

where:

- \mathbf{D} is a $d \times d$ diagonal matrix with random entries drawn uniformly from $\{1, -1\}$,
- \mathbf{H} is a $d \times d$ normalized Hadamard-Walsh matrix: $\mathbf{H} = \sqrt{\frac{1}{d}} \mathbf{H}_d$. The Hadamard-Walsh matrix $\mathbf{H}_t \in \mathbb{R}^{t \times t}$ is defined recursively as:

$$\mathbf{H}_1 = 1, \quad \mathbf{H}_t = \begin{bmatrix} \mathbf{H}_{t/2} & \mathbf{H}_{t/2} \\ \mathbf{H}_{t/2} & -\mathbf{H}_{t/2} \end{bmatrix}, \quad (3.8)$$

for any t that is a power of two. If the dimensionality of the data d is not a power of two, \mathbf{A} can be padded with columns of zeros.

- \mathbf{S} is a sparse $d \times k$ random matrix, whose elements S_{ij} are:

$$S_{ij} = \begin{cases} 0 & \text{with probability } 1 - q \\ \text{value drawn from } \mathcal{N}(0, \frac{1}{q}) & \text{with probability } q \end{cases}, \quad (3.9)$$

where $q = \mathcal{O}(d^{-1} \log^2 n)$ is a sparsity parameter. Some authors, e.g., Matoušek [2008] also experimented with replacing the normal distribution with a distribution similar to the one proposed by Achlioptas’ to speed up the generation of \mathbf{S} .

The strength of SRHT lies in the fact that the product \mathbf{xH} for a d -dimensional input vector \mathbf{x} can be calculated in just $\mathcal{O}(d \log d)$ operations, by using the fast Fourier transform algorithm. Therefore, the product $\mathbf{AP}_{\text{SRHT}}$ can be computed in $\mathcal{O}(nd \log d)$, as opposed to $\mathcal{O}(ndk)$ if the projection was done by a naive matrix multiplication. Ailon and Liberty [2009] further improved the running time of SRHT to $\mathcal{O}(nd \log k)$.

Quality of the SRHT embedding is slightly worse than the quality provided by the Gaussian matrix – SRHT satisfies the OSE property for $k = \mathcal{O}(\epsilon^{-2}(n + d) \log n)$ with high probability [Woodruff 2014].

Very recently the Hadamard-Walsh matrix has received attention in the context of constructing dense structured random matrices whose columns are orthogonal. Such constructions, e.g., the orthogonal Johnson-Lindenstrauss transform proposed by Choromanski et al. [2017] provide promising theoretical guarantees on the embedding quality.

3.2.5 Count Sketch-based projections

An important recent family of RP methods stems from the Count Sketch algorithm. The Count Sketch algorithm was initially proposed by Charikar et al. [2004] as a method to estimate the frequency of items in a data stream. Weinberger et al. [2009] and Shi et al. [2009] applied it as a dimensionality reduction technique. The explicit form of the projection matrix was then presented by Dasgupta et al. [2010]. The Count Sketch projection matrix, also called the *sparse embedding matrix*, can be given as:

$$\mathbf{P}_{\text{CS}} = \mathbf{D}\mathbf{C}, \quad (3.10)$$

where \mathbf{D} is defined as in SRHT, and \mathbf{C} is a $d \times k$ sparse matrix with each row chosen randomly from the k standard basis vectors of \mathbb{R}^k . Such distribution, where a single element in each row is picked independently at random and randomly set to either 1 or -1 , while the other elements are set to zero, is also called the Rademacher distribution.

Projection using the Count Sketch scheme can be performed without a naive multiplication of the data matrix by \mathbf{P}_{CS} . Instead, the Count Sketch projection can be realized in linear time, i.e., $\mathcal{O}(nd)$. First, the result matrix $\tilde{\mathbf{A}}$ is initialized to zeros. Then each column of the data matrix \mathbf{A} is multiplied by -1 with probability 50% and is added to a randomly selected column of $\tilde{\mathbf{A}}$. When the input data is sparse, the time complexity of the Count Sketch projection can be decreased to $\mathcal{O}(\text{nnz}(\mathbf{A}))$ [Clarkson and Woodruff 2013], where $\text{nnz}(\mathbf{A})$ is the number of non-zero elements in the matrix \mathbf{A} . Because of its low computational cost, this projection method and its modifications have drawn considerable attention [Clarkson and Woodruff 2013; Meng and Mahoney 2013; Nelson and Nguyen 2013]. Random projections that are based on hash functions similar to Count Sketch have been employed in many practical machine learning applications, e.g., in Vowpal Wabbit developed by Microsoft [Langford et al. 2007]. For an overview of related hashing techniques see [Wang et al. 2018].

The only significant disadvantage of Count Sketch-based RP is its worse lower bound for k : the subspace embedding property is satisfied for $k = \mathcal{O}(\epsilon^{-2}n^2)$ [Meng and Mahoney 2013; Nelson and Nguyen 2013].

3.3 Summary

We summarize the important properties of the presented RP schemes in Table 3.1. Specifically, for each scheme, we focus on the time complexity of creating the projection matrix, the time complexity of the projection and the embedding quality. Regardless of the projection scheme, the time required to create the projection matrix is negligible when compared to the projection time. It can, however, be a factor if the projected dataset is very sparse, i.e., when $\text{nnz}(\mathbf{A}) \sim d$, which may be the case for some real-world datasets. For RP schemes that employ simple random number distributions, the construction time of \mathbf{P} is proportional to the number of non-zero matrix elements $\text{nnz}(\mathbf{P})$. Therefore, creating a Gaussian or Achlioptas' matrix requires $\mathcal{O}(dk)$ operations, while generating a sparser Li's matrix requires $\mathcal{O}(\sqrt{dk})$ operations. The construction cost of an SRHT matrix is $\mathcal{O}(dk + d \log d)$ – the sum of the cost of creating a sparse $d \times k$ matrix and the cost of computing its fast Walsh-Hadamard transform, which is

Table 3.1: Properties of random projection schemes. \mathbf{A} is a $n \times d$ dataset matrix and k is the projected dimensionality. For sparse matrices \mathbf{A} , $\text{nnz}(\mathbf{A})$ denotes the number of non-zero elements in \mathbf{A} . Embedding quality is the dimensionality for which the oblivious subspace embedding property is satisfied.

RP scheme	Matrix construction time	Projection time		Embedding quality
		Dense input	Sparse input	
Gaussian	$\mathcal{O}(dk)$	$\mathcal{O}(ndk)$	$\mathcal{O}(\text{nnz}(\mathbf{A})k)$	$\mathcal{O}(\epsilon^{-2}n)$
Achlioptas'	$\mathcal{O}(dk)$	$\mathcal{O}(ndk)$	$\mathcal{O}(\text{nnz}(\mathbf{A})k)$	$-^a$
Li's	$\mathcal{O}(\sqrt{d}k)$	$\mathcal{O}(n\sqrt{d}k)$	$\mathcal{O}(\text{nnz}(\mathbf{A})k)^b$	$-^a$
SRHT	$\mathcal{O}(dk + d \log d)$	$\mathcal{O}(nd \log k)$	$\mathcal{O}(nd \log k)$	$\mathcal{O}(\epsilon^{-2}(n + d) \log n)$
Count Sketch	$\mathcal{O}(d)$	$\mathcal{O}(nd)$	$\mathcal{O}(\text{nnz}(\mathbf{A}))$	$\mathcal{O}(\epsilon^{-2}n^2)$

^a For Achlioptas' and Li's projections, we did not find any estimates of k for which the OSE property holds.

^b For a standard sparse-dense matrix multiplication implementation.

loglinear in d . For Count Sketch, the cost is $\mathcal{O}(d)$, since we only need to generate the position of the non-zero element in each of d rows.

For simple projection schemes, i.e., Gaussian, Achlioptas' and Li's constructions the projection time depends only on the employed matrix multiplication algorithm, which in turn depends on the sparsity of the multiplied matrices. If both data and projection matrices are dense we assume the use of the schoolbook matrix multiplication algorithm, which runs in $\mathcal{O}(ndk)$ time. We are aware that there exist more elaborate and slightly faster techniques, such as the Coppersmith and Winograd-like algorithms [Greiner 2012; Le Gall 2014]. However, their use is beneficial mostly when computing a product of matrices that are square. In our case, i.e., when $n \sim d$ and $d \gg k$, these methods do not offer much improvement over the naive implementation. When \mathbf{A} is sparse we can improve the Gaussian, Achlioptas' and Li's projection time to $\mathcal{O}(\text{nnz}(\mathbf{A})k)$. Additionally, if non-zero elements in \mathbf{A} are evenly distributed among its columns, the cost of Li's projection can be further decreased to $\mathcal{O}(\text{nnz}(\mathbf{A})\text{nnz}(\mathbf{P})k^{-1})$, by using certain sparse-sparse matrix multiplication algorithms. For an overview of such methods see [Greiner 2012; Yuster and Zwick 2005]. Sparse-dense matrix multiplication can also be applied when projecting dense data with a sparse Li's matrix. Because the number of non-zero elements in Li's projection matrix is, on average, $\frac{dk}{\sqrt{d}} = \sqrt{d}k$, projecting dense data with Li's scheme is $\mathcal{O}(\text{nnz}(\mathbf{P})n) = \mathcal{O}(n\sqrt{d}k)$, where \mathbf{P} is a $d \times k$ Li's projection matrix.

In general, we can observe that more elaborate projection schemes, such as SRHT or Count Sketch offer much better computation time in exchange for embedding quality. However, this does not necessarily mean that these methods introduce too high distortions in the projected space to be useful for practical applications. On the contrary – recent experimental results with training linear classifiers on randomly projected data indicate that Count Sketch RP is an excellent choice, especially when the input data is

sparse [Paul et al. 2014].

CHAPTER 4

TRAINING DEEP NETWORKS WITH RANDOM PROJECTION LAYER

One factor that limits the number of learnable parameters in a neural network is the computational cost of the training. In certain applications, this number can be vastly reduced by exploiting the structure of the data. However, for unstructured data or data where the structure is not well defined, it might be impossible to constrain the network architecture and limit the number of parameters. In these cases learning directly from the input data requires employing a network architecture that uses input layer with as many units as the number of features in the input vectors. When the input dimensionality exceeds several thousand, such an input layer becomes too large to be trained in a reasonable time. One solution to this problem is reducing the dimensionality of the input space to a manageable size and then training a deep network on representation with fewer dimensions. Here, we focus on performing the dimensionality reduction step by randomly projecting the input data into a lower-dimensional space. Conceptually, this is equivalent to adding a layer, which we call **the random projection layer**, in front of the network. Several computationally efficient RP matrix constructions have been recently proposed (see Section 3.2), leading to simple dimensionality reduction methods that scale to even millions of dimensions while introducing a controlled amount of noise. These can, therefore, be used to efficiently train networks on input data with a huge number of dimensions.

We study two variants of RP layers: one where the parameters of the RP layer are fixed during training and one where they are finetuned with error backpropagation. The first variant, further called **fixed-weight RP layer**, can be interpreted as training a standard network architecture on data whose dimensionality has been reduced with random projection. A theoretical motivation for learning on such randomly projected data has been given in [Arriaga and Vempala 2006; Hegde et al. 2007]. Particularly, Arriaga and Vempala provided a clear motivation that can be summarized in two points: (i) learning from randomly projected data is possible since RP preserves a lot of the input structure in the lower-dimensional space, and (ii) learning in the lower-dimensional space should require fewer examples, and thus be faster. The second RP layer variant, which we call **the learnable RP layer**, or more precisely **the finetuned RP layer**, may improve the network performance, compared to fixed-weight RP layer. However, it has a significantly higher computational cost. Nevertheless, we show that with carefully

designed architecture and training regime it can be applied to real-world problems.

By incorporating RP into the network architecture we enable DNNs to be trained on a particularly challenging type of data – data whose representation is simultaneously sparse, unstructured and high-dimensional. This opens an opportunity for applying DNNs in tasks where learning has previously been restricted to simple linear methods, such as support vector machine (SVM) or logistic regression (LR) classifiers. For a short survey of application areas where sparse, unstructured, high-dimensional data can be found see Section 2.2.1.

This chapter is organized as follows. In Section 4.1, we start by presenting the concept of the fixed-weight RP layer, its motivation and related approaches. In Section 4.1.1, we evaluate the performance of the fixed-weight RP layer on large synthetic data. In particular, we investigate how the layer dimensionality and properties of the learned data, such as its sparsity or the fraction of significant features influence the training process. Additionally, we compare the performance and computational cost of our approach with different baseline techniques. Then, in Section 4.1.2, we conduct large-scale experiments on several real-world datasets and show the effectiveness of neural networks with RP layers in comparison to the state-of-the-art methods. In Section 4.1.3, we explore the prospects of employing DNNs with fixed-weight RP layers for learning from BOW data. In Section 4.2, we discuss in detail how the weights in the RP layer can be learned. We focus on techniques that enable us to reduce the training cost and make this task feasible. Then, in Section 4.2.1 we experimentally evaluate the performance of deep networks with finetuned RP layers on large synthetic and real-world datasets. In particular, we investigate the influence of different normalization schemes on their performance and the prospects of applying a nonlinear activation after the RP layer. Finally, in Section 4.3, we discuss the important implementation decisions and details.

Selected results from this chapter were presented in [Wójcik and Kurdziel 2018].

4.1 Fixed-weight random projection layer

We begin with the analysis and evaluation of DNNs with fixed-weight RP layers. By fixed-weight RP layer we mean a layer in which the weights are not updated during training, but instead, are fixed to an RP matrix (Fig. 4.1). There are two main reasons for using fixed weights in the RP layer. First, this enables us to perform the projection and normalization of the whole dataset only once prior to the network training. Such optimization is especially beneficial when the lower-dimensional projection fits in the operating memory, while the original input data requires out-of-core processing. Second, for dense RP constructions, such as Gaussian, Achlioptas’ or SRHT, an update of the weights in the RP layer may have a prohibitively high computational cost: for example, dense RP matrices for some of the tasks reported in Section 4.1.2 have up to tens of billions of weights – several times more than the number of weights in the largest currently used networks [Coates et al. 2013]¹. Finetuning weights of the RP layer is

¹ Note that the approach presented by Coates et al. [2013] was designed specifically to train the largest networks (with up to 11 billion parameters) and requires a cluster of GPU servers with Infiniband connections and MPI. Deep networks that recently achieved the state-of-the-art results on popular benchmarks are typically at least an order of magnitude smaller in terms of the parameter count. For example, the VGGNet network [Simonyan and Zisserman 2014] contains “just” 140 million learnable

more practical for sparse RP constructions, especially if we restrict the updates to the weights that are initially non-zero. We further investigate this approach in Section 4.2.

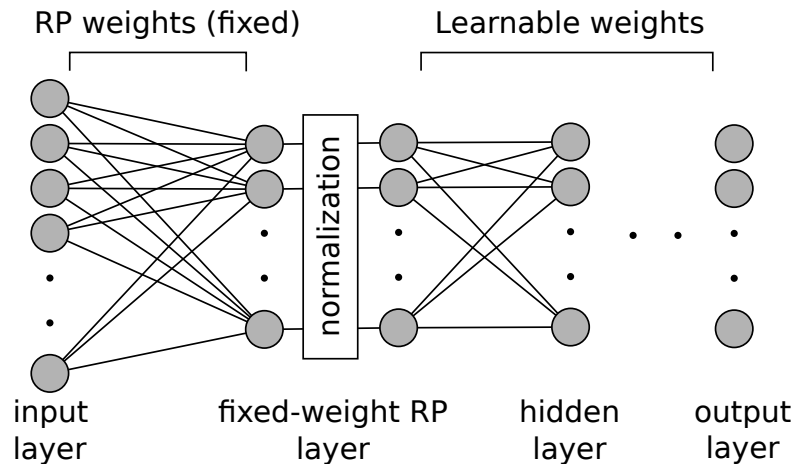


Figure 4.1: Neural network with fixed-weight random projection layer.

Layers that follow the fixed-weight random projection can be trained from scratch using error backpropagation. However, we found that the performance can be improved by pretraining these layers with DBNs and then finetuning them with error backpropagation. Before the projected data is used to train the “learnable” part of the network, we normalize each dimension to zero mean and unit variance. Initial evaluation showed that this is necessary: pretraining on unnormalized data was unstable, especially for highly sparse datasets. One particular advantage of pretraining a DBN on normalized data is that, regardless of the input data type, we can use Gaussian units [Welling et al. 2005] in the first layer of the “learnable” part of the network.

The choice of the projection matrix in the RP layer is not trivial and depends on the dimensionality and sparsity of the input data. In particular, these two factors have a significant impact on the computational cost of training. While the projection time is usually negligible in comparison to the training time, this may not be the case when the data dimensionality is very high. Fortunately, especially for large unstructured datasets, high dimensionality often goes hand in hand with high sparsity. This is beneficial from the computational point of view since sparse representation enables us to perform the projection faster. In particular, the performance of RP schemes that involve matrix multiplication can be improved by fast algorithms for sparse matrix multiplication [Bank and Douglas 1993; Greiner 2012]. Some other RP schemes can also be optimized to take advantage of the data sparsity [Clarkson and Woodruff 2013].

Another aspect to consider is the sparsity of the projection matrix itself. Random projection matrices that provide the best quality of embedding are typically dense [Nelson and Nguyen 2014]. Unfortunately, applying dense projection schemes to huge datasets can be computationally prohibitive. In this case, one needs to resort to more efficient projection schemes. One possibility is to employ a projection scheme that does not require naive matrix multiplication. A good example of such projection scheme

weights and takes 2–3 weeks to be trained on four NVIDIA Titan Black GPUs.

is SRHT. Another approach is to use a sparse projection matrix, as in, e.g., Li’s construction. Moreover, these two approaches can be combined into a projection scheme, where the RP matrix is sparse and the projection does not require an explicit matrix multiplication. This results in very efficient projection methods, such as the Count Sketch projection. However, projecting sparse data with sparse RP matrices, regardless if they are explicitly or implicitly constructed, can introduce significant distortions in the embedding [Ailon and Chazelle 2006]. These distortions may, in turn, affect the network accuracy. Therefore, for large datasets, the choice of the RP layer type is a trade-off between the network accuracy and the computational complexity of the RP embedding. Investigating this trade-off, apart from enabling training of neural networks on high-dimensional data is one of the goals of this work.

Related approaches. The idea of using fixed random weights in neural networks is not new and has been incorporated into different models proposed throughout the years. Note, however, that not every layer with random weights realizes a random projection (see Chapter 3). One important family of shallow networks employing random weights are the random weight feedforward neural networks (RW-FNNs). These models differ from our approach in two important aspects. First, instead of lowering the data dimensionality, they transform the input data into a higher-dimensional space in which learning should, theoretically, be easier. Importantly, this transformation is most often nonlinear and, in general, does not preserve the distances between the training examples. Additionally, after randomly transforming the input, RW-FNNs do not employ any feature normalization. Second, RW-FNNs cast the weight optimization problem as a standard regularized least-squares problem, which can be solved analytically in a single step. While this approach offers a computational advantage compared to stochastic gradient descent, it is suitable only for networks with a single hidden layer. For a more comprehensive overview of RW-FNNs see [Scardapane and Wang 2017]. Predecessors of these models were proposed in a number of early works on feedforward architectures, e.g. in [Gallant and Smith 1987; Schmidt et al. 1992]. A more mature version of RW-FNNs, called random vector functional-link networks was introduced in [Pao et al. 1994; Pao and Takefuji 1992].

In an interesting work Arriaga and Vempala [2006] suggest that the human brain may reduce the amount of information generated by visual stimuli in a process that resembles random projection. They show that RP can be realized by a shallow neural network with weights drawn from a Gaussian distribution or just set randomly to -1 or 1 (note that this is the denser variant of the Achlioptas’ construction [Achlioptas 2001], which we described in Section 3.2). Arriaga and Vempala use this so-called neuron-friendly RP to show that efficient learning is possible in the projected space. However, similarly to RW-FNNs, they do not train deeper models on the projected data and use a simple learning algorithm instead of error backpropagation.

To the best of our knowledge the only attempt at training DNNs on randomly projected large-scale data, and therefore the approach that is most relevant to our fixed-weight RP layers, is presented in [Dahl et al. 2013]. Therein, Dahl et al. use randomly projected data as input to networks trained for the malware classification task. Specifically, they project the original 179,000-dimensional data (trigrams of system API calls) to 4000 dimensions and use the projected data to train a neural network with two hid-

den layers. With this approach, they achieve 43% relative improvement in classification performance, compared to logistic regression trained on the unprojected data. However, their classification task is fairly simple, with the classes being nearly linearly separable. Unfortunately, Dahl et al. only evaluate Li’s matrix construction [Li et al. 2006a], which is extremely sparse and, from our experience, is unsuited for projecting sparse n-gram data (see Section 4.1.3). It is also worth mentioning that in their experiments unsupervised pretraining does not improve network performance, unlike in experiments reported in our work. Additionally, Dahl et al. do not employ data normalization after the projection, whereas our experiments show that scaling each feature to zero mean and unit variance greatly helps, especially when training networks on sparse data. Finally, Dahl et al. evaluate only networks with the sigmoid activation function and do not report results for the current state-of-the-art ReLU activation [Nair and Hinton 2010].

Another recent work by Choromanska et al. [2016] explore a similar approach to our networks with fixed-weight RP layer. Specifically, the authors consider networks in which the first layer uses untrained pseudo-random weights and a nonlinear activation function. However, their approach differs from ours in two ways. First, Choromanska et al. mostly focus on using structured pseudo-random matrices, such as various modifications of the circulant or Toeplitz matrices and not classic RP matrices. Second, since they consider layers that realize binary embeddings of the input data, they only employ the sign activation function. Importantly, the results presented in [Choromanska et al. 2016] show that using fully-random matrices, such as the Gaussian RP matrix, for projecting the input data yields better performing networks than using pseudo-random structured matrices.

Random weight matrices were also used in certain convolutional neural network architectures [Saxe et al. 2011]. In particular, Saxe et al. report convolutional networks with random weights that perform only slightly worse than networks with learned parameters. This inspired us to investigate the prospects of using RP schemes to initialize weights in deep networks. We elaborate on this topic in Chapter 5.

Apart from neural networks other models also have been successfully trained on randomly projected data. In particular, Paul et al. [2014] evaluated SVM classifiers and regression models on data projected with several RP schemes and achieved promising results on small- and medium-size datasets. Similarly to our results, they also found Count Sketch to be one of the best performing RP methods.

4.1.1 Experiments on large-scale synthetic data

To evaluate the performance of the fixed-weight RP layer we begin with experiments on the synthetic datasets described in Appendix A. Each synthetic dataset variant consists of one million training examples represented by one-million-dimensional feature vectors. First, we investigate the influence of the RP layer dimensionality on the network performance. We also analyze the computational cost of employing different types of RP layers. We then explore how the properties of the input data affect the training process. In particular, we study the effects of the data sparsity and the effect of the fraction of features that are informative for learning. We evaluate five RP constructions presented in Section 3.2, i.e., Gaussian, Achlioptas’, Li’s, SRHT and Count Sketch. We compare the effectiveness of DNNs that employ fixed-weight RP layers with other

baseline approaches to learning from sparse, high-dimensional data. Specifically, we experiment with replacing the random projection with other fast dimensionality reduction methods, such as F-score, Chi-square, IG and principal component analysis. We also evaluate another baseline approach – training efficient linear models directly on the high-dimensional feature space. We discuss both the performance and the computational cost of the presented baseline approaches.

Effects of the size of random projection layer

We begin the evaluation with experiments in which we investigate the impact of the size of the RP layer on the network performance. These experiments were carried out on a synthetic dataset variant with density $\rho = 10^{-5}$ and fraction of significant features $\psi = 0.2$ (Appendix A).

We first generated the low-dimensional representations of the dataset using five evaluated RP schemes. We reduced the dataset dimensionality from one million to k dimensions, where k ranged between 10 and 1000. We then normalized every feature in each projected dataset to zero mean and unit variance. We also experimented with scaling each feature by its maximum absolute value or not applying any normalization of the projected data. However, these approaches resulted in poorly performing models. For the details on RP implementation and other implementation notes see Section 4.3.

We trained deep networks on the projected datasets in two phases: unsupervised pretraining with CD followed by finetuning with error backpropagation. The networks were trained using mini-batch SGD with momentum. Amplitudes of the weights were limited with the L2 cost. During finetuning the learning rate was decreased according to a slow exponential decay, while the momentum was slowly increased. We also used dropout to prevent overfitting. We employed ReLUs in the hidden layers and Gaussian units in the input layer. Validation sets constructed from the training data were used to select the learning hyperparameters. For all input layer sizes, we used a network architecture with two hidden layers, each consisting of 1000 neurons. After pretraining, we added a logistic regression unit on top and finetuned the networks to minimize the binary CE cost.

In Fig. 4.2 we report the early stopping errors for different sizes of the RP layer. Early stopping error is the test error in the training epoch with the best performance on the validation set. In general, increasing the value of k improved the network performance. This agrees with the intuition derived from the Johnson-Lindenstrauss lemma [Johnson and Lindenstrauss 1984] (see Section 3.1). If we assume that the network classification error is correlated with the embedding error ϵ , then for a constant number of examples n , the network classification error should be correlated with $\frac{1}{\sqrt{k}}$. Therefore, the network error should decrease when k increases, as, in fact, can be seen in Fig. 4.2. For dense RP schemes, i.e., Gaussian, Achlioptas' and SRHT, the best and almost equal results were achieved for the highest values of k . Interestingly, Count Sketch performed slightly better than dense RPs, especially for lower values of k . For larger sizes of the RP layer, its performance became comparable to dense RP schemes. Li's projection was significantly outperformed by the other four RP schemes. This outcome cannot be attributed only to the high sparsity of the projection matrix – the Count Sketch projection matrix, which performed much better, had the same number of non-zero elements as Li's projection

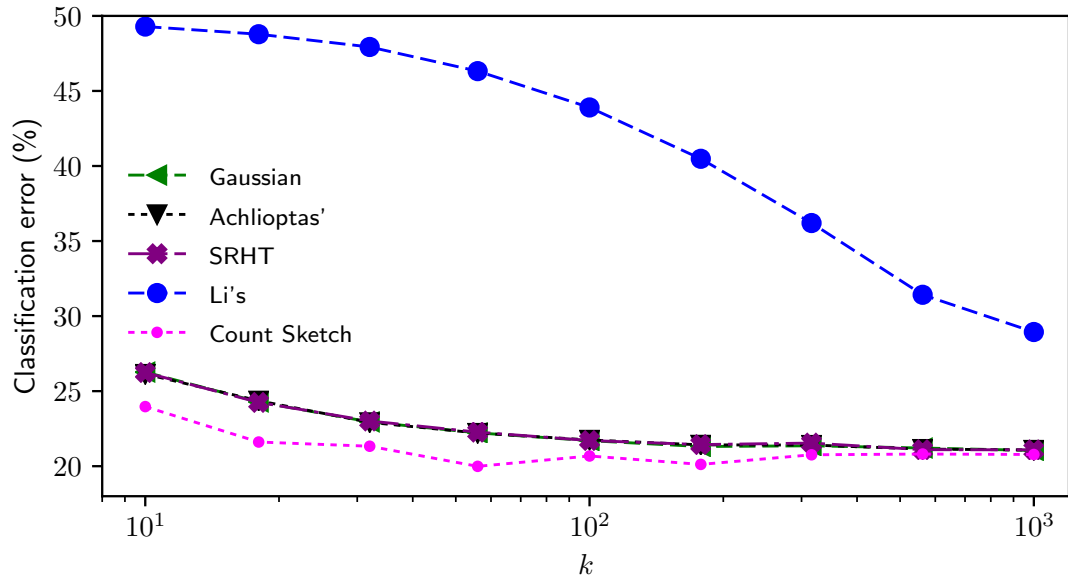


Figure 4.2: Classification error for different sizes of the random projection input layer (k). Gaussian, Achlioptas' and SRHT yielded almost equal results.

matrix. While it has been argued that sparse projection matrices are not suited for sparse data [Ailon and Chazelle 2006], these results demonstrate that matrix construction also plays an important role. Note that, unlike Li's construction, columns in the Count Sketch projection matrix are fully orthogonal. Moreover, orthogonal weight initialization has been shown to improve the performance of deep networks [Mishkin and Matas 2015]. We believe that this may be the reason behind the very good performance of the Count Sketch RP layer.

In addition to network performance, we also investigated the computational cost of performing RP for different values of k . The experiments in this and the subsequent sections were carried out on a 64-bit machine with Intel Xeon 2.50GHz CPU (E5-2680 v3), 30MB cache and 128GB main memory. For every value of k , we ran the projection procedure five times. The average RP execution times are presented in Figure 4.3. For larger values of k , sparse RP schemes were significantly more efficient than dense schemes: for $k > 100$ they sped up the projection more than ten-fold. The execution time of both Gaussian and Achlioptas' RPs scaled linearly with the RP layer size. For the Count Sketch scheme the projection time was approximately constant in k , and for Li's and SRHT the dependence was more complex.

To further explore these results, we separately measured the RP matrix generation time and the projection time. The results are presented in Figure 4.4. For most of the evaluated schemes, the computational cost of creating the RP matrix increases linearly with the size of the RP layer. For Gaussian, Achlioptas' and Li's matrices, this dependence is linear because the number of random numbers that need to be generated is proportional to k . The computational time of generating the SRHT projection matrix is also linear in k – this relation is, however, significantly offset by the high cost of performing the fast Walsh–Hadamard transform on a matrix with, in our case, one million

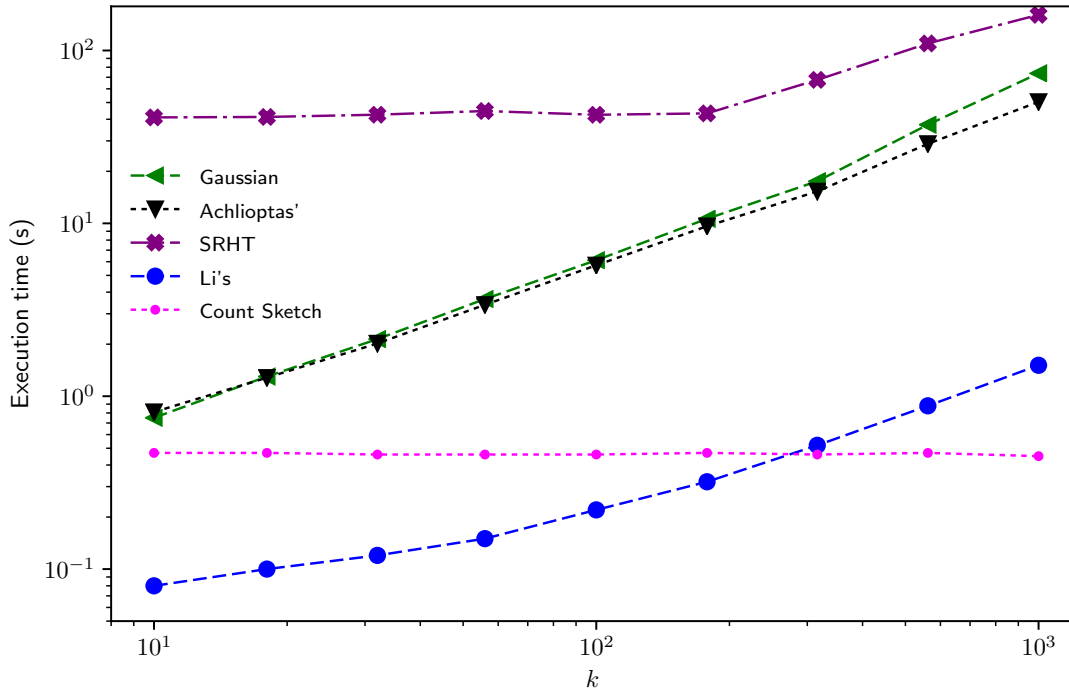


Figure 4.3: Average time of performing random projection on the million-dimensional synthetic dataset ($\rho = 10^{-5}$, $\psi = 0.2$) for different RP layer size k .

rows. The Count Sketch matrix, on the other hand, can be created in a constant time. This is because the number of non-zero elements in the Count Sketch projection matrix is equal to the constant data dimensionality d and not to the projection dimensionality k . For Gaussian, Achlioptas' and SRHT, the projection time depended linearly on k . For Count Sketch RP the dependence was approximately constant and for Li's RP it was nearly linear for higher values of k . This is a consequence of the type of the employed matrix multiplication algorithm. For dense RP schemes, the projection was realized with sparse-dense matrix multiplication, which is linear in k . For sparse RP matrices, we used a matrix multiplication procedure that exploits the matrix sparsity. Specifically, we employed an implementation of the sparse matrix multiplication package (SMMP) algorithm [Bank and Douglas 1993]. For a more detailed time complexity analysis see Section 4.3.

Note that we intentionally test RP layers with sizes $k \leq 1000$. There are several reasons why we do not consider larger values of k . First of all, we observe that one thousand features extracted from the original multi-million-dimensional feature space often captures most of the information that is useful for learning. This hypothesis is supported by the good performance of deep networks with $k = 1000$ on several different real-world datasets (see Section 4.1.2). Second, restricting the RP layer size limits the number of weights in the DNN which, in turn, decreases the training time. In our experiments on the synthetic datasets, network training could be performed moderately fast, i.e., between 1 and 3 hours, depending on the RP scheme. However, for larger

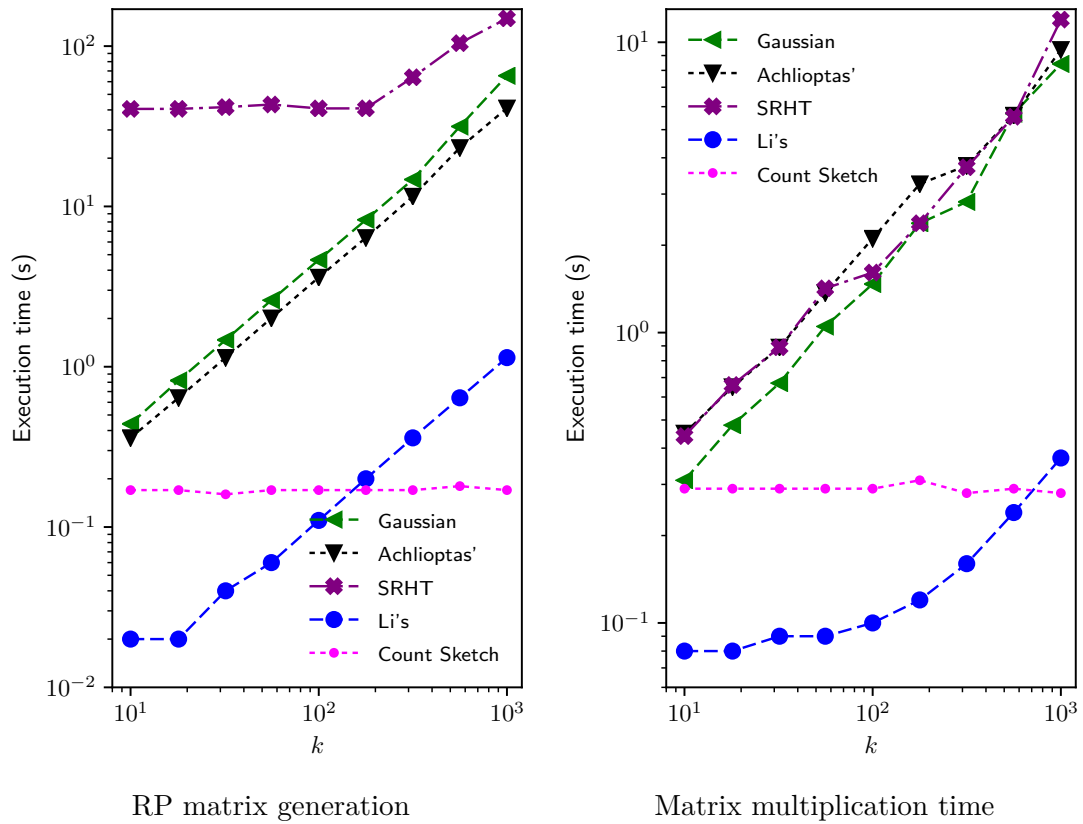


Figure 4.4: Average time of generating an RP matrix and performing the projection by matrix multiplication for the synthetic dataset.

and more difficult real-world datasets, the network convergence may be significantly slower. In such cases, the training may take several days. Finally, for large values of k , the available memory may become a limiting factor. Randomly projecting even very high-dimensional data is computationally efficient, provided that the whole projection matrix can be stored in the operating memory. However, for some datasets, this may be impossible, especially if the projection matrix is dense. For example, projecting the 20-million-dimensional KDD2010-a dataset to $k = 2000$ dimensions requires nearly 160GB of RAM for the projection matrix alone, which exceeds the available memory on most modern machines. In such cases, the projection matrix has to be divided columnwise into smaller slices, which can be stored and fetched on demand from the disk. Unfortunately, such out-of-core processing greatly increases the projection time.

Effects of data sparsity

To evaluate the influence of the data sparsity on the performance of DNNs with RP layer we carried out experiments on multiple synthetic dataset variants with density ρ ranging from 10^{-6} to $1.7 \cdot 10^{-4}$ and constant fraction of significant features $\psi = 0.2$. We chose these density values because they are representative of typical high-dimensional real-world datasets, such as `ur1`, `KDD2010-a` or `webspam` (see Table A.1 in Appendix A).

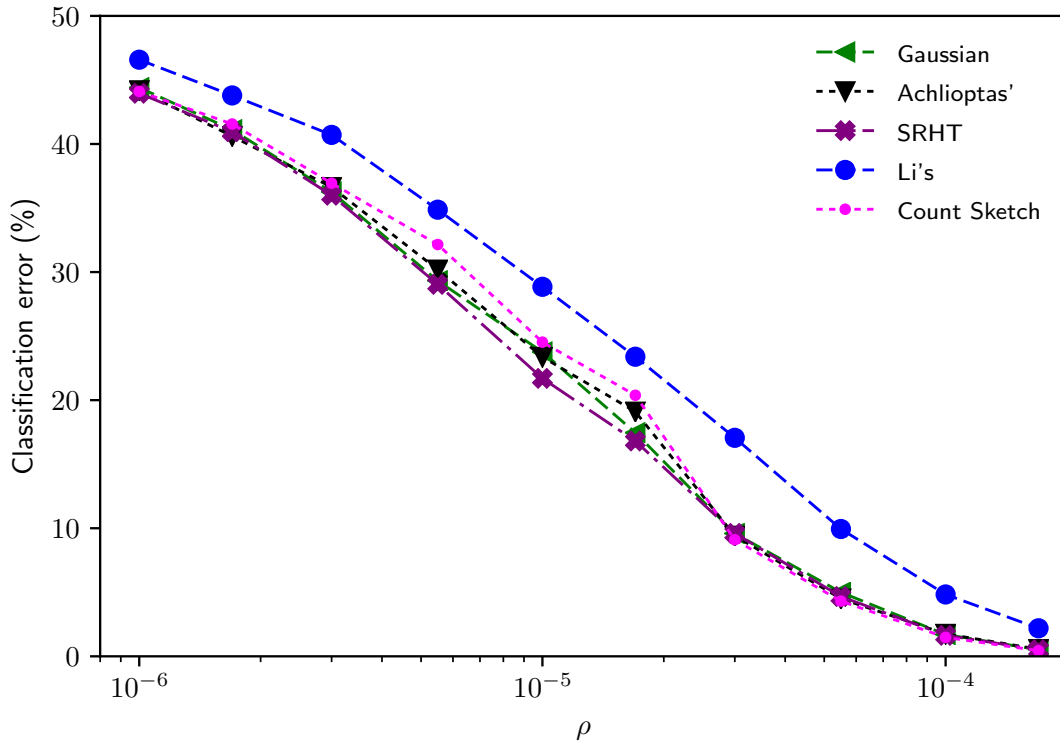


Figure 4.5: Classification error on the synthetic datasets with fixed significant feature fraction $\psi = 0.2$ and varying density level ρ .

We generated 1000-dimensional representations of the synthetic datasets and normalized each feature to zero mean and unit variance. We then trained DNNs on the lower-dimensional datasets following the training regime described in the previous section. We used a network architecture with two hidden layers, each consisting of 3000 neurons. In Fig. 4.5 we report the early stopping errors for different density levels ρ . For all evaluated RP schemes, the accuracy of DNNs depends nearly linearly on the logarithm of the dataset density. For most density levels Gaussian, SRHT and Achlioptas' projections yielded the best and quite similar results. The Count Sketch projections performed slightly worse, especially for dataset variants with $\rho < 10^{-5}$. Similarly to the previous experiments, for all evaluated density levels Li's projection was significantly outperformed by the other four RP schemes.

Effects of the percentage of significant features

Next, we carried out experiments to investigate the influence of the fraction of significant features on the network performance. For these experiments, we employed synthetic dataset variants with fractions of significant features ψ ranging from 0.01 to 0.2 and a constant density level $\rho = 10^{-4}$.

As in the previous section, we generated the 1000-dimensional dataset representations and used them to train the networks. We employed the same network architecture, i.e., two hidden layers with 3000 units each. Early stopping errors for different fractions

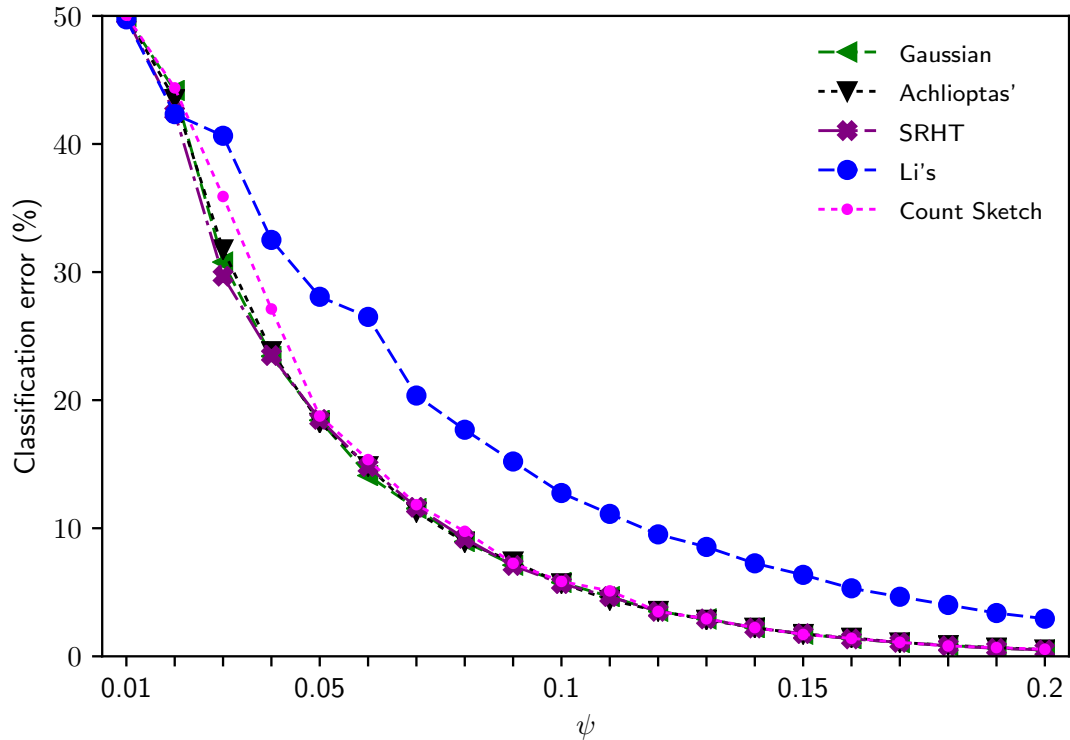


Figure 4.6: Classification error on the synthetic datasets with fixed density $\rho = 10^{-4}$ and varying fraction of significant features ψ .

of significant features are presented in Fig. 4.6. The fraction of significant features in the projected dataset had a strong impact on the performance of neural networks: networks trained on dataset variants with larger ψ performed much better, especially for lower values of ψ . For example, for all RP schemes except Li's, doubling the number of significant features from 5% to 10% reduced the test error from approximately 18% to less than 6%. For $\psi > 0.1$, all RP schemes apart from Li's yielded almost equal performance. For $\psi \leq 0.1$, i.e., for dataset variants where each example contains on average only 1 – 10 significant features, dense RP schemes performed better than sparse projections.

Comparison with baseline approaches

Training DNNs on data whose dimensionality has been reduced with RP is not the only viable approach to learning models on sparse high-dimensional data. As we discussed in Section 2.2, the dimensionality reduction prior to network training can be performed with other efficient feature selection or feature extraction techniques. Another even simpler approach is to train fast linear models directly on the high-dimensional feature space. In this section we compare the performance and computational cost of such approaches.

For our tests we employ three synthetic dataset variants with density $\rho \in \{3 \cdot 10^{-6}, 10^{-5}, 3 \cdot 10^{-5}\}$ and constant fraction of significant features $\psi = 0.2$. Addi-

tionally, we use the permutation invariant version of the popular MNIST benchmark [LeCun et al. 1998a]. While it is a relatively dense (density $\approx 19\%$) and low-dimensional dataset, it is frequently used to evaluate neural networks and has well-established reference results.

Dimensionality reduction methods for training DNNs. First, we explore the prospects of training DNNs on sparse, unstructured, high-dimensional data whose dimensionality has been reduced with techniques discussed in Section 2.2.3 and Section 2.2.4. Specifically, we evaluate three feature selection methods: IG, Chi-square and F-score and PCA-based feature extraction. We compare these methods to random projection. Similarly to previous experiments, we test five RP constructions, i.e., Gaussian, Achlioptas’, Li’s, SRHT and Count Sketch.

To compare the performance of deep networks trained on data with reduced dimensionality we first generated the low-dimensional representations of the datasets using all evaluated methods. Similarly to the previous experiments, we reduced the dimensionality of the synthetic datasets from one million to 1000. For MNIST we reduced the dimensionality from 784 to 400. For the experiments on the synthetic datasets, we used the same network architecture and training regime as described in the previous sections. We followed a similar procedure for the MNIST experiments. However, we used hidden layers with just 1000 units each, and, after pretraining, we added a 10-way softmax layer instead of a sigmoid unit. This is the same network architecture as reported in [Sutskever et al. 2013], except it has a smaller input layer (400 units instead of 784). We finetuned this network to minimize multinomial CE cost.

Table 4.1: Early stopping errors (%) for different dimensionality reduction methods. For each dataset we highlight the best performing dimensionality reduction technique.

Dimensionality reduction method	Dataset			
	synthetic, $\psi = 0.2$			MNIST
	$\rho = 3 \cdot 10^{-6}$	$\rho = 10^{-5}$	$\rho = 3 \cdot 10^{-5}$	
IG	50.04	49.67	50.05	0.98
F-score	50.00	49.63	48.82	1.04
Chi2	49.98	49.61	48.86	1.03
PCA	45.24	22.80	4.28	2.59
Gaussian RP	35.66	21.10	7.94	1.06
Achlioptas’ RP	35.64	21.49	7.62	0.94
SRHT RP	35.64	21.42	7.84	1.04
Li’s RP	39.47	29.42	15.37	1.11
Count Sketch RP	35.14	22.19	7.59	1.34

In Table 4.1 we report early stopping errors for all evaluated datasets and dimensionality reduction methods. All feature selection methods, i.e., IG, F-score and Chi-square

performed very similarly on the test datasets. On dense MNIST, they yielded results only slightly worse than networks trained on the original 784-dimensional data. Srivastava et al. [2014] achieved a test error of 0.92% by employing a training regime similar to ours, i.e., pretraining with DBNs followed by finetuning with dropout. Intuitively, removing almost half of the input dimensions (we discard 384 features from the original 784-dimensional data) should significantly impede the network classification performance. In fact, the task of selecting meaningful features is quite simple for the MNIST dataset – the most informative features are located in the central area of the 28-by-28-pixel images. A large portion of features corresponding to pixels near the image edges is equal to zero for all train and test examples. Therefore, all evaluated feature selection techniques had no difficulty identifying the most informative features. In Fig. 4.7 we present a visualization of the 400 features selected with IG, F-score and Chi-square.

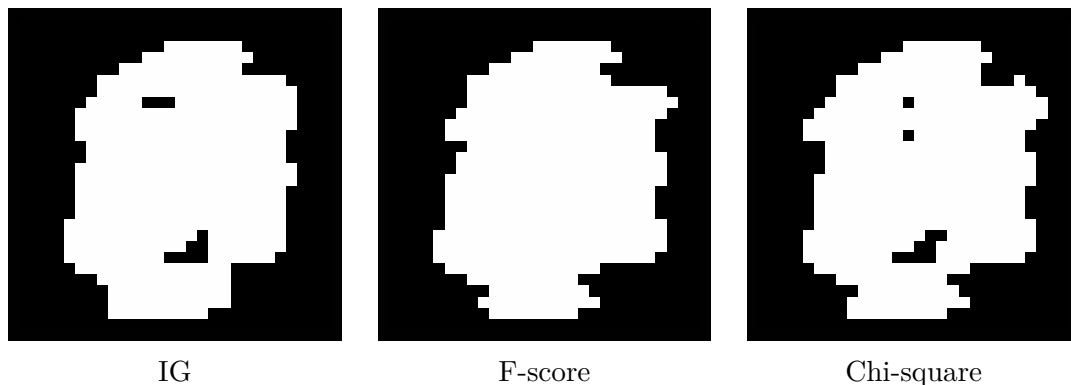


Figure 4.7: Visualization of features that were chosen by different feature selection methods on the MNIST dataset. Selected and discarded features are represented by white and black pixels, respectively.

Evaluated feature selection methods did not perform well on the synthetic datasets. In fact, networks trained on features chosen by these techniques performed not much better than a random binary classifier. The main reason for this poor performance is the sparsity of the synthetic datasets. Let us consider the densest evaluated variant, i.e., $\rho = 3 \cdot 10^{-5}$. It has approximately $3 \cdot 10^{-5} \cdot 10^6 \cdot 10^6 = 3 \cdot 10^7$ non-zero values in the training set. The reduced dataset is built from 1000 selected features, and therefore contains on average $\frac{10^3}{10^6} \cdot 3 \cdot 10^7 = 3 \cdot 10^4$ non-zero elements. This results in a situation where at least 97% of the training examples contains only zeros. More importantly, even by selecting only the significant features, the feature selection methods inevitably discard $199,000/200,000 = 99.5\%$ of all significant features. This puts them at a substantial disadvantage, compared to feature extraction techniques, which are able to combine information from a bigger number of the original features.

On dense MNIST, all RP techniques yielded comparable performance to the feature selection methods. The only exceptions were the Count Sketch and Li's RPs, which achieved slightly worse results. Their poorer performance can be attributed to the low density of the projection matrices: $\frac{1}{\sqrt{784}} \approx 3.57\%$ for Li's matrix and $\frac{1}{400} = 0.25\%$ for Count Sketch matrix. Projecting the data by multiplying the data matrix by such sparse matrices can result in many informative features from the original space being lost in

the transformed feature space. PCA performed worse than the evaluated RP schemes.

On sparse synthetic datasets, feature extraction methods outperformed feature selection techniques. In particular, RP methods achieved the best results on the two most sparse variants, i.e., with $\rho = 3 \cdot 10^{-6}$ and $\rho = 10^{-5}$. While Gaussian, Achlioptas', SRHT and Count Sketch RP yielded comparable results, Li's construction performed significantly worse on all synthetic dataset variants. The Count Sketch-based RP yielded the best results out of the evaluated RP schemes on all synthetic datasets beating dense projections, such as Gaussian or SRHT. Principal component analysis's performance strongly depended on the sparsity of the original dataset: for the sparsest variant ($\rho = 3 \cdot 10^{-6}$) it yielded classification error nearly 10% worse than most of the random projection schemes, and for the densest variant with $\rho = 3 \cdot 10^{-5}$ it outperformed other competing dimensionality reduction techniques.

Training linear models on unprojected feature space. As a reference to DNNs trained on lower-dimensional data, we conducted experiments with linear classifiers trained on the original data. Specifically, we evaluated LR and SVMs, implemented in the LIBLINEAR package [Fan et al. 2008].

LR and SVM models were trained on the original feature space, with each feature normalized to $[-1, 1]$ (synthetic datasets) or $[0, 1]$ (MNIST) as recommended by Hsu et al. [2003]. Following Yuan et al. [2010], we used solvers with L2 regularization, namely L2-regularized logistic regression and L2-regularized L2-loss support vector machine. For each solver and dataset, we carried out cross-validation experiments to find the best value of the hyperparameter C^2 . We report LR and SVM test errors in Table 4.2. For a comparison with the previous approach, we also include the test errors of DNNs trained on feature space reduced with Gaussian RP.

Table 4.2: Test errors (%) for linear classifiers trained on the unprojected data. For a comparison, we also report the test errors for deep networks trained on data projected with Gaussian random projection.

Classifier	Dataset			
	synthetic, $\psi = 0.2$			MNIST
	$\rho = 3 \cdot 10^{-6}$	$\rho = 10^{-5}$	$\rho = 3 \cdot 10^{-5}$	
LR	44.90	33.73	25.72	8.10
SVM	44.90	33.73	25.72	8.39
Gaussian RP + DNN	35.66	21.10	7.94	1.06

In our experiments, LR and SVM models yielded almost identical performance. The test error on the MNIST dataset was similar to the 12.0% error achieved by a linear classifier (1-layer neural network) reported in [LeCun et al. 1998a]. However, on all evaluated datasets, the accuracy of the linear models was significantly lower than the accuracy of DNNs with RP layer. We believe that this is a result of model underfitting that stems from training a linear model on highly nonlinear data.

² C is the penalty parameter of the error term.

Computational cost comparison. The time T_{total} required to train a neural network on a high-dimensional dataset is the sum of the dimensionality reduction time T_{DR} and the time needed to train the network on the reduced feature space T_{train} . Here we are interested in comparing the computational efficiency of the evaluated dimensionality reduction techniques, and thus we mostly focus on the dimensionality reduction time T_{DR} and the relation of this time to the total training time T_{total} .

To compare the dimensionality reduction execution times T_{DR} , we ran each procedure five times on every dataset. The averages of these times are presented in Table 4.3. In our measurements of T_{DR} , we did not include the data loading time nor the time required to normalize the reduced features. The total training time T_{total} includes the time of loading the data, reducing its dimensionality, data normalization and training the network for e epochs, where e is the epoch with the best error on the validation set. In Table 4.3, we also report the percentage of the total training time spent for reducing the data dimensionality $T_{\text{DR}}/T_{\text{total}}$.

Table 4.3: Average time T_{DR} of performing dimensionality reduction. In parenthesis we report $T_{\text{DR}}/T_{\text{total}} = T_{\text{DR}}/(T_{\text{DR}} + T_{\text{train}})$ – the fraction of time required to reduce the data dimensionality over the total time of training the network.

Dimensionality reduction method	Dataset							
	synthetic, $\psi = 0.2$						MNIST	
	$\rho = 3 \cdot 10^{-6}$		$\rho = 10^{-5}$		$\rho = 3 \cdot 10^{-5}$			
IG	1.0s	(0.1%)	1.3s	(0.1%)	2.1s	(0.1%)	0.4s	(0.3%)
F-score	3.6s	(0.1%)	3.8s	(0.1%)	4.7s	(0.1%)	0.4s	(0.2%)
Chi2	1.0s	(0.1%)	1.4s	(0.1%)	2.2s	(0.1%)	0.4s	(0.4%)
PCA	3912.4s	(33.1%)	3865.4s	(26.4%)	4013.6s	(39.8%)	150.1s	(35.6%)
Gaussian RP	57.3s	(0.5%)	63.3s	(1.6%)	75.2s	(2.7%)	0.6s	(0.3%)
Achlioptas' RP	33.7s	(1.2%)	40.5s	(1.0%)	49.7s	(1.3%)	0.6s	(0.4%)
SRHT RP	112.1s	(3.9%)	109.9s	(3.4%)	128.5s	(3.9%)	1.3s	(0.4%)
Li's RP	3.9s	(0.2%)	4.4s	(0.1%)	5.6s	(0.2%)	1.0s	(0.6%)
Count Sketch RP	1.9s	(0.1%)	2.5s	(0.1%)	3.9s	(0.2%)	0.3s	(0.1%)

For most of the evaluated dimensionality reduction methods, their execution time T_{DR} was much lower than the total training time T_{total} . This is especially true for sparse RP methods and fast feature selection techniques that, even for the densest synthetic dataset variants could be computed in less than several seconds. Random projection schemes that employ dense projection matrices were approximately ten times slower compared to sparse RP schemes. However, dense RP methods are still a viable option – performing dimensionality reduction with these schemes takes little time in relation to T_{total} . Principal component analysis proved to be the least efficient method in our evaluation. Dimensionality reduction with PCA was almost 40 times more expensive

than dimensionality reduction with the slowest dense RP schemes – depending on the dataset calculating PCA took up to 40% of T_{total} .

Note that the relative cost of performing the dimensionality reduction $T_{\text{DR}}/T_{\text{total}}$ can vary significantly depending on the difficulty of the dataset. Our synthetic datasets are easier to learn than some real-world datasets, and thus require shorter training (i.e., a smaller number of epochs). For harder datasets, the networks may converge much slower, making the relative cost $T_{\text{DR}}/T_{\text{total}}$ less significant.

Finally, we compare the time of training DNNs on reduced feature space with the time required to train linear models on the original data. In Table 4.4, we report the average times of training linear classifiers. Due to the model simplicity and much lower number of learnable parameters, linear classifiers can be trained several orders of magnitude faster than DNNs.

Table 4.4: Average time of training linear classifiers on the original data. For a comparison, we also report training times for deep networks trained on data projected with Gaussian random projection.

Classifier	Dataset			
	synthetic, $\psi = 0.2$			MNIST
	$\rho = 3 \cdot 10^{-6}$	$\rho = 10^{-5}$	$\rho = 3 \cdot 10^{-5}$	
LR	2.3s	4.2s	10.1s	23.9s
SVM	2.0s	4.0s	10.0s	9.8s
Gaussian RP + DNN	$\sim 12000.0\text{s}$	$\sim 4000.0\text{s}$	$\sim 2000.0\text{s}$	$\sim 200.0\text{s}$

Conclusion. Our experiments show that the best approach to learning models on sparse, high-dimensional data is to train DNNs on data whose dimensionality has been reduced with random projection. Specifically, in our evaluation, networks with Count Sketch, Gaussian, SRHT and Achlioptas’ RP layers achieved the highest accuracy. Gaussian, SRHT and particularly Count Sketch RP combined the best network performance with reasonable execution time. Replacing RP with feature selection techniques did not improve the network performance. Training DNNs on data reduced with PCA yielded good results only on one relatively dense dataset variant. Unfortunately, computing PCA for large-scale datasets was computationally much more expensive than performing random projection. Linear classifiers trained on the original data were computationally very efficient but produced models that performed poorly on nonlinear tasks.

4.1.2 Experiments on large-scale real-world data

To demonstrate the practical effectiveness of networks with RP input we performed experiments on four real-world classification datasets: `webspam`, `url`, `KDD2010-a` and `KDD2010-b`. The datasets are described in Appendix A. All four datasets are large binary classification tasks. For all datasets, we randomly projected the data to 1000

dimensions and employed a network with two hidden layers, each one with 3000 neurons. Each network was pretrained and then finetuned to minimize the binary CE cost.

Baseline algorithms. The state-of-the-art results in the classification of high-dimensional, unstructured, sparse data are currently achieved with linear classifiers. In particular, the need to learn high-dimensional data with millions of examples has recently led to a surge of interest in fast linear classifiers, such as support vector machines. Many algorithms have been proposed to speed up the SVM training. One of the first methods that could efficiently handle large-scale optimization problems in SVMs were LIBLINEAR and Pegasos. LIBLINEAR [Fan et al. 2008] implements dual coordinate descent method and focuses mainly on solving the dual problem, while Pegasos [Shalev-Shwartz et al. 2011] uses SGD to solve the primal problem.

One line of research on large-scale SVM classification focuses on the so-called *out-of-core learning*, i.e., being able to work with data that does not fit in the operating memory. For example, Yu et al. [2012], authors of the LIBLINEAR library propose the block minimization (BM) algorithm – a simple approach that involves splitting the data into smaller blocks, compressing and storing them on disk and then sequentially loading and processing each block. However, despite being faster than LIBLINEAR, BM does not produce models that perform significantly better. Chang and Roth [2011] propose a modification to the BM method, in which the set of informative examples from the previous blocks persists in memory when a subsequent block is loaded. This approach, called selective block minimization (SBM) outperforms BM both in speed and classification performance. Vowpal Wabbit [Langford et al. 2007] is another out-of-core learning implementation that uses a similar compression strategy to [Yu et al. 2012]. Unlike BM, it employs a variant of online gradient descent as the learning algorithm. Another line of research on out-of-core methods focuses on parallelizing the training process. Zhang et al. [2012] employ the alternating direction method of multipliers (ADMM) for training linear classifiers in a distributed environment. They use the L2-regularized L2-loss (squared hinge loss) SVM as the classification model. However, as pointed out by Yuan et al. [2012b], their approach may suffer from slow convergence and the difficulty of choosing the hyperparameters. Other works, in addition to ensuring good parallelization properties of the developed algorithms, concentrate on encouraging the sparsity of trained models. For example, Yuan and Ma [2012] propose dual alternating direction method (DADM) for L1-regularized L1-/L2-loss SVMs. Dual alternating direction method can train sparse linear models and offers competitive prediction performance. Based on the GLMNET method proposed by Friedman et al. [2010], Yuan et al. [2012a] introduce a computationally efficient method called newGLMNET that solves the primal L1-regularized L2-loss SVM problem.

For more complex datasets, where examples of different classes cannot be separated with a linear decision boundary, nonlinear kernel SVMs offer superior performance. Unfortunately, standard kernelized SVMs do not scale well to larger datasets and are computationally prohibitive for datasets with millions of examples and features. Recently, the gap between linear and nonlinear SVMs has been narrowed by novel approaches that employ additive kernels. Specifically, Wu [2012] proposed the power mean support vector machine (PmSVM) algorithm that employs a polynomial approximation of the gradient to speed up the training with coordinate descent. Yang and Wu [2012] further

improved the running time of PmSVM by introducing look-up tables. This modification, called power mean support vector machine with look-up tables (PmSVM-LUT), although several-fold slower than the state-of-the-art linear SVM solvers improved the classification performance on several large-scale datasets. Another method that attempts to bridge the scalability gap between linear and kernel SVMs is the adaptive multi-hyperplane machine (AMM). Introduced in [Wang et al. 2011], AMM uses online learning with stochastic gradient descent to solve a modified SVM problem.

Results. In Table 4.5 we compare the performance of DNNs with RP layer with the performance of the baseline algorithms. Error rates of the baseline algorithms were taken from: [Yang and Wu 2012] for LIBLINEAR, [Wang et al. 2011] for Pegasos, [Yuan and Ma 2012] and Vowpal Wabbit (VW) documentation³ for VW, [Chang and Roth 2011] for SBM, [Yang and Wu 2012] for PmSVM-LUT, [Yuan and Ma 2012] for DADM, [Yuan et al. 2012a] for newGLMNET, [Zhang et al. 2012] for ADMM and [Wang et al. 2011] for AMM.

Table 4.5: Classification errors (%) on large-scale real-world datasets. For each dataset we highlight the result of the best performing method.

Method	Dataset			
	webspam	url	KDD2010-a	KDD2010-b
Gaussian RP	0.38	1.03	10.86	10.51
Achlioptas' RP	0.40	1.12	10.88	10.49
Li's RP	0.36	3.75	11.95	10.98
SRHT RP	0.40	1.01	10.86	10.49
Count Sketch RP	0.32	0.96	11.49	10.54
LIBLINEAR	7.31	1.55	11.44	11.06
Pegasos	7.28	1.50	-	-
SBM	0.45	-	-	10.33
VW	1.52	1.64	-	11.09
ADMM	0.42	-	-	10.01
DADM	0.40	-	-	10.43
newGLMNET	0.36	-	-	13.40
PmSVM-LUT	5.72	1.23	10.39	9.99
AMM	4.50	1.34	-	-

Gaussian, Achlioptas', SRHT and Count Sketch projections performed similarly well on the real-world datasets, while Li's method generally performed worse. This agrees with the results from the previous tests on synthetic datasets. Overall, networks with randomly projected input significantly improved the current state-of-the-art results on the url dataset and achieved competitive performance on webspam and KDD2010 datasets. Specifically, on webspam, DNNs with Count Sketch RP layer slightly

³ https://github.com/JohnLangford/vowpal_wabbit/wiki/Malicious-URL-example

outperformed the state-of-the-art results obtained by DADM and newGLMNET. The nonlinear PmSVM-LUT achieved better results on the KDD2010 datasets but was significantly outperformed by DNNs with RP layer on the two denser benchmarks.

4.1.3 Experiments on bag-of-words data

In addition to the experiments described in the previous sections, we also conducted experiments with networks trained on randomly projected BOW data. Note that some of the datasets evaluated in the previous section also contain BOW features. For instance, in the `url` dataset the lexical features that constitute over half of the 3.2 million features are BOW representations of tokenized URL addresses [Ma et al. 2009]. However, in this section, we focus on training DNNs on purely BOW representation. For the evaluation we employ deep autoencoder networks trained on two text datasets: 20-newsgroups (TNG) and RCV1 (for details on the dataset construction see Appendix A). Unlike previous experiments, in which all models were trained for the classification task, here we train the networks for document retrieval.

When training autoencoders, text data is often represented by BOW vectors over a dictionary of D most frequent words in the training set. The dictionary size D is commonly on the order of a few thousand words [Salakhutdinov 2009; Salakhutdinov and Hinton 2009]. Our aim, therefore, is to employ RP to train networks on much larger dictionaries. By extending the vocabulary with rarely occurring words we hope to allow the network to learn a more informative representation of the original text data.

Reference networks. As a baseline we use deep autoencoders trained on 2000-word BOW representations of TNG and RCV1. We employ network architectures similar to [Grzegorzczak et al. 2016a; Salakhutdinov 2009; Salakhutdinov and Hinton 2009]. Specifically, for TNG we started by pretraining 2000-500-250-125-32 DBNs with binary units in the hidden layers and Gaussian units in the output layer. For RCV1 we used a similar network with 2000-500-500-128 architecture. For the input layer in both networks we used the constrained Poisson model [Salakhutdinov and Hinton 2009], i.e., an RBM variant suitable for modeling word count data. Deep belief networks were pre-trained with CD_1 and used to initialize deep autoencoders. The autoencoders were then finetuned with error backpropagation to minimize the CE cost. The hyperparameters were selected with experiments on the validation sets.

We use the 32-dimensional (for TNG) and 128-dimensional (for RCV1) codes inferred with the trained autoencoders for the document retrieval task. Following Salakhutdinov and Hinton [2009], we perform document retrieval by choosing a query from the test set and ranking the remaining test documents according to the cosine similarity between their codes and the code of the query document. We do this for every document from the test set. Then, after averaging the results, we calculate the precision-recall curve. To determine the relevance of a retrieved document to a given query document we either directly compare their class labels (TNG) or use the fraction of equal labels (RCV1).

Deep autoencoders with random projection layer. To evaluate the performance of deep autoencoders with RP layer we first generated several BOW representations of TNG and RCV1 using larger dictionary sizes: $D \in \{4000, 6000, 8000, 10000\}$. We then

randomly projected these representations to 2000 dimensions and normalized each feature to zero mean and unit variance. However, we did not use the raw BOW data, i.e., word-counts for the words from the dictionary. Instead, we first converted the BOW representation to term frequency–inverse document frequency (TF-IDF) representation. Initially, we also experimented with training autoencoders with an RP layer on raw BOW data. However, using TF-IDF values yielded significantly better-performing networks.

TF-IDF is one of the most widely used measure of word importance in information retrieval [Salton 1991; Salton and Buckley 1988]. Suppose we have a corpus $\mathbb{C} = \{d_1, \dots, d_N\}$ of N documents. We denote $f(t, d)$ as the number of occurrences of term t in document d . The TF-IDF score is then defined for term t in document d as a product of two statistics, term frequency $\text{TF}(t, d)$ and inverse document frequency $\text{IDF}(t; \mathbb{C})$:

$$\text{TF-IDF}(t, d; \mathbb{C}) = \text{TF}(t, d) \cdot \text{IDF}(t; \mathbb{C}). \quad (4.1)$$

The term frequency can be defined in various ways, with the simplest: $\text{TF}(t, d) = f(t, d)$. Here, however, we use logarithmically scaled word frequency:

$$\text{TF}(t, d) = 1 + \log(1 + f(t, d)), \quad (4.2)$$

as in our experiments it produced the best performing networks. The inverse document frequency of a term measures its rarity in the corpus \mathbb{C} :

$$\text{IDF}(t; \mathbb{C}) = \log \left(\frac{N}{|\{d \in \mathbb{C} : f(t, d) > 0\}|} \right). \quad (4.3)$$

We trained deep autoencoder networks on the projected TF-IDF data using a network architecture and training settings similar to those in the baseline network. However, we employed Gaussian units instead of constrained Poisson units in the first layer. For the hidden layers, instead of binary units, we used rectifier linear units since they yielded significantly better performing models. We used similar training regime as in the reference network, that is, we pretrained the DBNs with CD_1 and unfolded them to initialize the autoencoders. The autoencoders were then finetuned with error back-propagation to minimize the mean square error cost. For each dataset representation, we selected the learning hyperparameters with experiments on the validation sets. We used the area under the precision-recall curve (AUC) to compare the performance of the trained models.

Results. In Table 4.6 and Table 4.7 we report the AUC values for autoencoders trained on different dataset representations. The baseline autoencoders trained on unprojected 2000-dimensional BOW data achieves AUC of 0.373 and 0.315, for **TNG** and **RCV1**, respectively. Even the best performing autoencoders with RP input layer yield results worse than these reference networks. In general, increasing the dictionary size D does not lead to higher AUC of the trained models. For most RP schemes, the best document retrieval performance is achieved with $D = 4000$ or $D = 6000$. This result suggests that broadening the input dictionary to include rarely occurring words and then projecting this representation to 2000 dimensions does not produce a more informative data representation. In Figure 4.8 we present the precision-recall curves for autoencoders trained on randomly projected BOW representations constructed over 6000 and 4000

Table 4.6: Area under the precision-recall curve for deep autoencoders with RP layer trained on different TNG representations. The baseline network trained on 2000-dimensional bag-of-words data achieves AUC of 0.373.

RP layer type	Dictionary size D			
	4000	6000	8000	10,000
Gaussian	0.341	0.366	0.336	0.333
Achlioptas'	0.321	0.348	0.326	0.337
Li's	0.307	0.356	0.321	0.350
SRHT	0.344	0.326	0.352	0.327
Count Sketch	0.327	0.314	0.311	0.313

Table 4.7: Area under the precision-recall curve for deep autoencoders with RP layer trained on different RCV1 representations. The baseline network trained on 2000-dimensional bag-of-words data achieves AUC of 0.315.

RP layer type	Dictionary size D			
	4000	6000	8000	10,000
Gaussian	0.306	0.300	0.296	0.295
Achlioptas'	0.312	0.299	0.296	0.290
Li's	0.304	0.299	0.292	0.289
SRHT	0.305	0.303	0.294	0.293
Count Sketch	0.254	0.260	0.280	0.278

most common words, for TNG and RCV1, respectively. The best results are achieved by autoencoders with Gaussian and Achlioptas' RP layers. However, they are significantly worse than the baseline, especially for lower recall values.

We believe that the poor performance of networks trained on randomly projected BOW data is a consequence of two facts. First, as the autoencoders were trained on projected, real-valued data, their input units were Gaussian. The reference networks, on the other hand, used the constrained Poisson model, which is tailored specifically for word count data. Importantly, employing the constrained Poisson model makes the learning much more stable, by properly dealing with documents of different lengths [Salakhutdinov and Hinton 2009]. Second, the 2000-word dictionary used by the reference autoencoders already captured most of the useful information from the text. This is especially significant for the smaller TNG dataset and to a lesser degree for RCV1. Extending the vocabulary with rarely occurring words added little information to the network. In fact, using too large dictionary size resulted in decreased network performance, as can be seen in Table 4.6 and Table 4.7: for most RP schemes increasing D above 6000 did not improve the network performance. To further investigate the influence of enriching the input data representation we also experimented with concatenating the basic 2000-word BOW representation with bigram and trigram features. While such concatenated

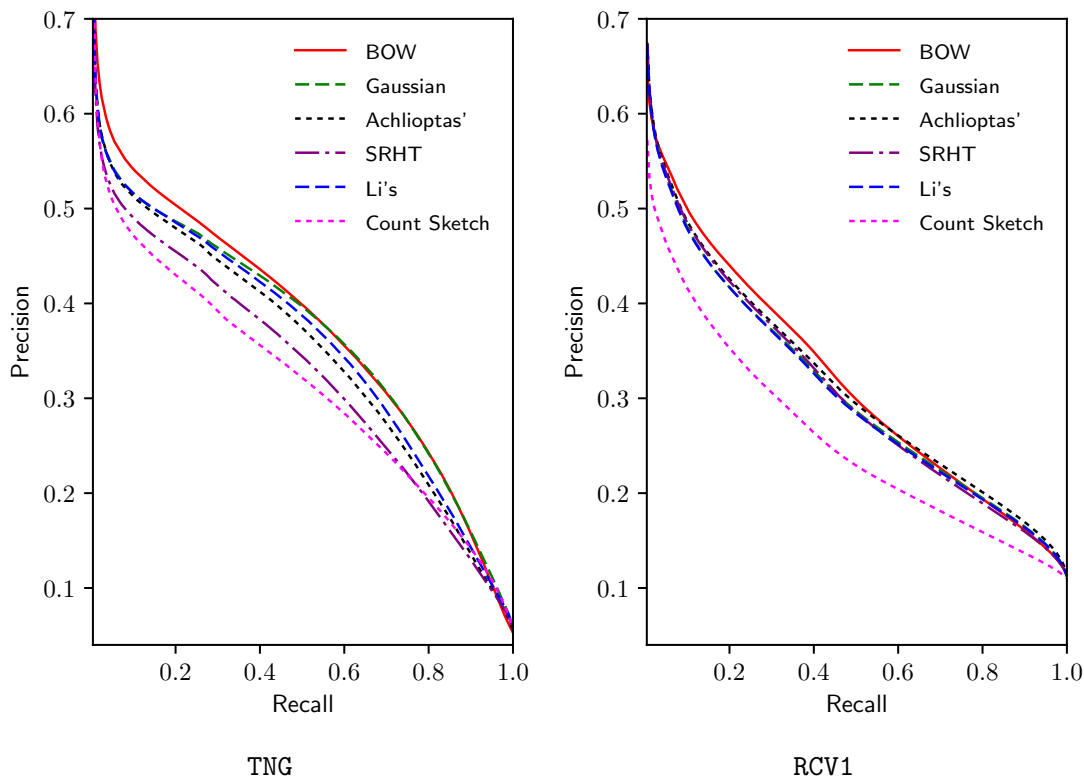


Figure 4.8: Precision-recall curves for deep autoencoders trained on unprojected BOW data (solid red line) and randomly projected BOW representations (dashed lines).

representations (reaching more than 10^5 features) carried more information from the input text, they yielded much worse performing networks. We believe that adding more features to the input representation did not improve the network performance because in all tests the RP layer projected the data to a fixed number of dimensions (2000). We hypothesize that with a fixed projection dimensionality adding less and less informative features to the input representation causes the projected features to become increasingly noisy. This is because each feature in the projected space is a linear combination of all input features, including less informative ones.

4.2 Learnable random projection layer

In the previous section, we employed RP to enable training deep networks on sparse, high-dimensional, unstructured datasets. We showed that training a network on randomly projected input can be viewed as prepending the network with a linear layer, whose weights are initialized to elements of an RP matrix. However, in order to reduce the computational cost of the training, we did not adjust the weights in such fixed-weight RP layers. In this section, we show that finetuning the weights in RP layers is feasible in practical applications and can improve the network performance. This holds under two conditions: (i) the RP scheme that is used to initialize the weights in the RP

layer is sparse, and (ii) only the non-zero weights are updated. We discuss important network architecture considerations as well as training regime settings that enable us to efficiently train networks with the finetuned RP layer.

While the idea of finetuning weights in the RP layer may seem straightforward, there are several technical difficulties that make its implementation challenging. They stem primarily from the high computational cost of performing the weight updates and normalizing the layer outputs. As we discussed in the previous section, for high-dimensional datasets performing even a single update of a dense RP layer is computationally prohibitive. Fortunately, we can reduce the number of weights to a manageable size by choosing a sparse variant of the RP layer. In this work, we propose to construct finetuned RP layers using two sparse random projection schemes discussed in Chapter 3, i.e., Li’s and Count Sketch-based projections. Compared to dense RP matrices, Li’s and Count Sketch constructions reduce the total number of weights by a factor of \sqrt{d} and k , respectively, where d is the number of input units, and k is the number of output units. This is usually sufficient to make the training feasible.

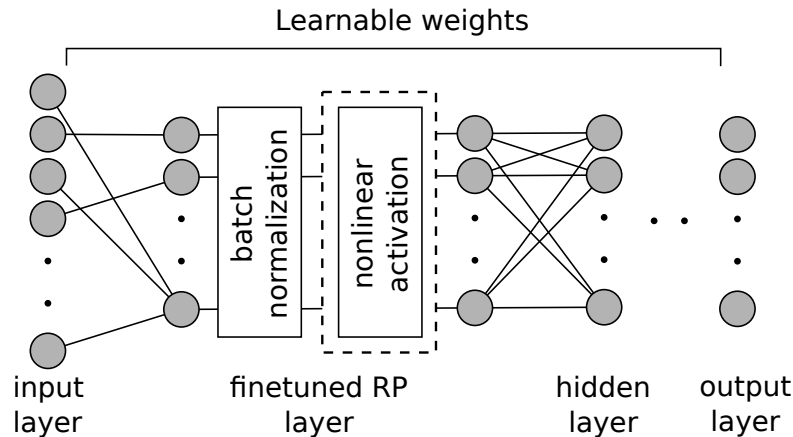


Figure 4.9: Neural network with finetuned random projection layer. Weights in the finetuned random projection layer are initialized to a sparse RP matrix. Only the weights that are initially non-zero are part of the model. The output of the projection is batch normalized and optionally transformed with a nonlinear activation function.

To ensure that the number of model parameters does not increase during training, we update only these elements in the finetuned RP matrix that are initially non-zero. However, since the number of output units in an RP layer is relatively small, we do learn the biases for these units. This construction can be interpreted as an input layer with sparse connectivity (Fig. 4.9). To further improve the training performance we can restrict the weight updates in the RP layer to a fraction of the training mini-batches. We found that even with the sparse RP layers this approximation is necessary for our largest benchmark datasets. Importantly, to reduce the bias introduced by skipping some of the weight updates, the updates are performed for randomly selected mini-batches. Since for large datasets SGD typically uses incremental gradient [Bertsekas 2010]⁴, this can be realized by simply performing the update with a fixed probability for each mini-batch.

⁴ In the incremental gradient method the mini-batches are processed in the same order during every epoch.

We denote this probability as η . Equivalently, η can be interpreted as the expected fraction of mini-batches on which the RP layer is finetuned.

When training networks with fixed-weight RP layers, we normalize the RP layer activations to zero mean and unit variance using moments calculated on the training set. Since the weights in this RP layer variant do not change during training, this operation can be performed only once before the training. This is no longer true in networks with finetuned random projection where the RP weights change over time. In this case, to ensure proper normalization of the RP layer outputs we propose to either normalize the input data (and thus indirectly the RP layer outputs) or to insert a batch normalization layer [Ioffe and Szegedy 2015] between the random projection and the activation function. Note, however, that in the first approach the feature-wise normalization of the input data is limited to scaling (e.g., by the reciprocal of the maximum absolute value for each feature), since shifting the mean would destroy the sparsity of the data. Compared to the one-time normalization in the fixed-weight RP layer, batch normalization is computationally more expensive, since the normalization has to be performed for each training mini-batch. Furthermore, BN introduces additional $2k$ learnable parameters needed for the scaling and shifting of the k normalized activations.

We found that networks with finetuned RP layer are best trained end-to-end, starting from randomly initialized weights in the layers succeeding the RP layer. Initially, we also considered different training regimes. For example, we experimented with networks that were first trained without changing the RP layer and then finetuned end-to-end with backpropagation. However, this training regime yielded inferior results.

4.2.1 Experiments on large-scale data

We evaluated the performance of finetuned RP layers on several large-scale datasets: a variant of the synthetic dataset with the density $\rho = 10^{-5}$ and the fraction of significant features $\psi = 0.2$, `webspam` dataset and `url` dataset. Additionally, we report results on a toy benchmark – MNIST.

We begin by evaluating the influence of different normalization schemes on the performance of networks with finetuned RP layers. We follow up by looking into the problem of choosing the optimal fraction of RP layer updates η . This gives us an insight into the balance between the RP layer quality and the network training time. Finally, we study whether adding a nonlinear activation to the RP layer improves the network performance.

Effects of normalization

We experimented with two normalization schemes:

- scaling each feature in the input dataset by the reciprocal of its maximum absolute value over the training set (further called MaxAbs scaling),
- batch normalization of the projected data.

In the comparison, we also include results obtained without any normalization of the input data or the RP layer outputs.

We trained MLPs with the same network architectures and using the same training settings as in Section 4.1. Specifically, we employed a 784-400-1000-1000-10 architecture for MNIST and a d -1000-3000-3000-1 architecture for the large-scale datasets, where d is the dataset dimensionality. We used linear activation function in the finetuned RP layer and ReLUs in the subsequent hidden layers. We trained the networks using mini-batch SGD with momentum. To prevent overfitting we used dropout, and we additionally limited the magnitudes of the weights with L2 cost. During training, we gradually decreased the learning rate following an exponential decay, while simultaneously increasing the momentum. We chose the hyperparameter values with experiments on the validation sets. In the experiments on MNIST and synthetic dataset, we performed the weight update in the RP layer for all mini-batches. For `webspam` and `url` we used $\eta = 0.5$, which made training our models feasible.

Table 4.8: Test errors (%) for networks with Li’s finetuned random projection layer trained using different normalization schemes.

Network architecture	Dataset			
	MNIST	synthetic $\rho = 10^{-5}$ $\psi = 0.2$	<code>webspam</code>	<code>url</code>
No normalization	1.04	26.25	0.46	3.39
MaxAbs scaling	0.97	38.21	0.88	3.41
Batch Normalization	1.10	26.55	0.35	3.30
Fixed-weight RP layer	1.11	29.42	0.36	3.75

Table 4.9: Test errors (%) for networks with Count Sketch finetuned random projection layer trained using different normalization schemes.

Network architecture	Dataset			
	MNIST	synthetic $\rho = 10^{-5}$ $\psi = 0.2$	<code>webspam</code>	<code>url</code>
No normalization	0.97	20.36	0.47	0.87
MaxAbs Scaling	1.10	40.87	0.99	0.90
Batch Normalization	1.22	20.16	0.25	0.75
Fixed-weight RP layer	1.34	22.19	0.32	0.96

We report the early stopping errors for different normalization schemes in Table 4.8 and Table 4.9. Training networks with the finetuned RP layer on unnormalized data yielded surprisingly good results: compared to the reference networks with fixed-weight RP layers, these networks performed better on all datasets except `webspam`. Our ini-

tial experiments also showed that training networks with the finetuned RP layer on unnormalized data is greatly facilitated by learning the biases. Interestingly, scaling the features by reciprocal of their maximum absolute values yielded the worst results, especially for large-scale datasets. For `webspam` and synthetic dataset, networks trained on data scaled in this way performed even worse than the reference networks with fixed-weight RP layer. Only networks that used BN consistently outperformed the reference networks. Importantly, in experiments on the real-world datasets, i.e., `webspam` and `url`, networks with BN performed best. Therefore, in our subsequent experiments, we focus only on networks with batch normalized RP layer.

Adjusting the fraction of RP layer updates

The fraction of mini-batches that are used for learning the weights in the RP layer, η , lets us control the computational cost of its training. For smaller datasets, where performing the weight update for every mini-batch is possible, $\eta = 1$ should yield the best performing network. However, for large-scale datasets, training the RP layer on every input mini-batch may be too costly. Therefore, when the available training time is limited, choosing the η value becomes an important training decision. While increasing the η value makes the RP layer learn faster, it also increases the computational time.

To shed light on the balance between the RP layer quality and the training time, we conducted a series of experiments with varying η . Importantly, we limited each network training time to 24 hours. Consequently, using larger η values resulted in lower number of training epochs. We experimented on three large-scale datasets: synthetic dataset with $\rho = 10^{-5}$ and $\psi = 0.2$, `webspam` and `url`. We used the same network architectures and training settings as described in the previous section. In Figure 4.10 we present how the performance of networks with finetuned RP layer depended on η . For each dataset and η value, we report the network’s early stopping error.

The balance between the RP layer quality and the training time varied between the datasets. For the synthetic dataset, the best performing networks were trained with $\eta \in \{0.25, 0.5\}$, while for the real-world datasets η values close to 1 yielded the best results. Importantly, all experiments with small η values show that networks can significantly benefit from finetuning the RP layer weights, even if these weights are rarely updated. Nevertheless, the optimal η depends on factors, such as the properties of the dataset, its dimensionality, the network architecture and the available training time. Therefore, for practical applications we recommend starting with relatively small η and, if the training time is acceptable, test higher η values. Assuming that the number of training epochs is sufficient and that the network is properly regularized, the performance should improve with increasing η .

Activation function in finetuned random projection layer

So far we only experimented with RP layers without an activation function (or, equivalently, with the linear activation function). In this section, we investigate the prospects of applying the sigmoid, LReLU and ReLU nonlinearities after batch normalization of the RP layer output. Note that if we disregard the large computational cost stemming from high data dimensionality d and the additional BN layer, our previously used network architectures could technically be simplified from `d-1000-3000(ReLU)-3000(ReLU)-1` to

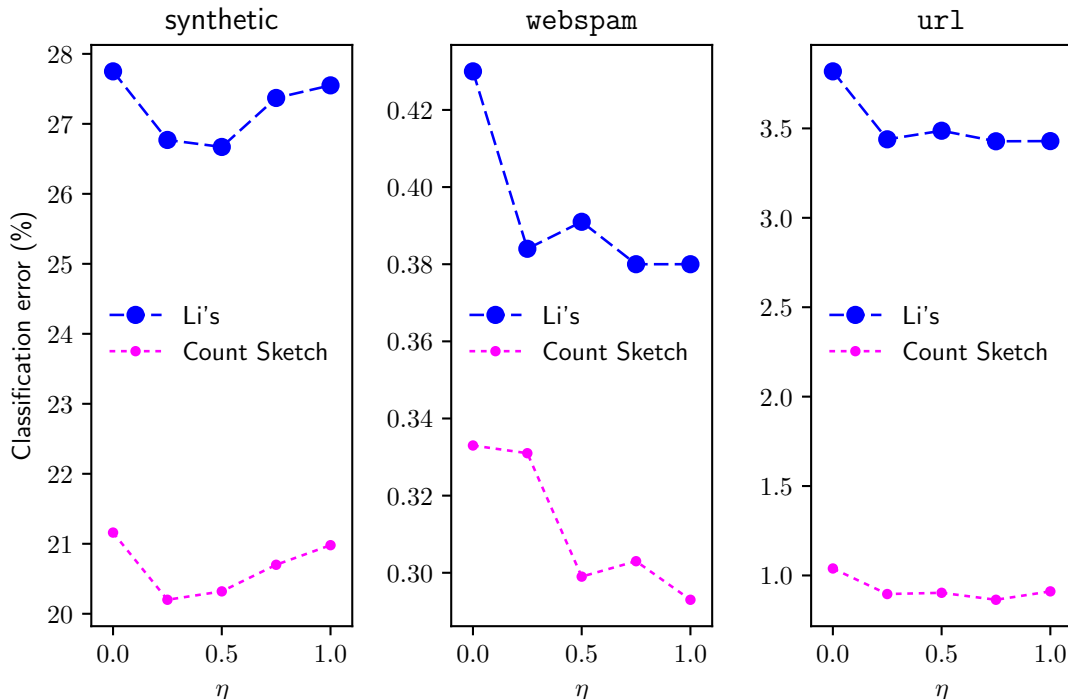


Figure 4.10: Influence of η on the performance of networks with finetuned random projection layer. η is the fraction of mini-batches used to train the random projection layer.

d-3000(ReLU)-3000(ReLU)-1. This is because the first two layers effectively realize two consecutive linear transformations of the input data and can be replaced with just one linear layer. Therefore, inserting a nonlinear activation function after the RP layer should increase the network ability to represent complex nonlinear data.

For our experiments, we used the same network architecture as in the previous experiments. We report the early stopping errors for different activation functions in Table 4.10 and Table 4.11. Compared to networks with the fixed-weight RP layer, networks with linear finetuned RP layer performed better on all datasets. Importantly, linear finetuned RP layer further improved the state-of-the-art results on **webspam** and **url** datasets. Surprisingly, introducing a nonlinearity after the RP layer decreased the network performance. In fact, networks with a nonlinearity after the finetuned RP layer performed very similarly to, or were outperformed by, networks with the fixed-weight RP layer. We hypothesize that this poor performance is a consequence of the small size of the RP layer output⁵ and the sparse connectivity in the RP layer. Particularly, when a sparse RP layer processes a sparse training example, the total input to the nonlinearity is also sparse. If we now apply an element-wise nonlinear transformation, we lose some information about the projected example. Specifically, in the case of ReLU activation, we effectively zero-out, on average, half of the non-zero elements in the sparse input.

⁵ Because of the computational cost, in our main experiments we limited the output of the finetuned RP layer to 1000 dimensions.

Table 4.10: Test errors (%) for networks with Li’s finetuned random projection layer using different activation functions.

Activation function	Dataset			
	MNIST	synthetic $\rho = 10^{-5}$ $\psi = 0.2$	webspam	url
Linear	1.10	26.55	0.35	3.30
Sigmoid	1.12	50.05	0.50	5.80
LReLU	1.28	30.57	0.48	3.86
ReLU	1.25	30.59	0.38	3.78
Reference RP layer	1.11	27.49	0.36	3.75

Table 4.11: Test errors (%) for networks with Count Sketch finetuned random projection layer using different activation functions.

Activation function	Dataset			
	MNIST	synthetic $\rho = 10^{-5}$ $\psi = 0.2$	webspam	url
Linear	1.22	20.16	0.25	0.75
Sigmoid	1.23	28.11	0.36	1.05
LReLU	1.51	27.15	0.34	0.82
ReLU	1.41	27.16	0.33	0.81
Reference RP layer	1.34	20.42	0.32	0.96

We believe that this loss of information causes the decrease in network performance. If our hypothesis is correct, random projection followed by a nonlinear activation function should perform better with larger output dimensionality.

To verify this hypothesis, we performed additional experiments with larger RP layers. In particular, we experimented with Li’s RP layer on MNIST and the synthetic dataset. Training large RP layers on **webspam** and **url** was not possible due to the computational cost. To reduce the training time, we employed smaller network architectures compared to the previous experiments. Specifically, in experiments on MNIST we trained networks with 784- k -300-10 architecture, for $k \in \{100, 300, 500, 700\}$, and in experiments on the synthetic datasets we used 10^6 - k -3000-1 architecture, for $k \in \{1000, 2000, 3000, 4000\}$. We experimented with linear and ReLU activation function after RP. We employed the same training settings as in the previous experiments. For each k and each activation function we selected the learning hyperparameters with experiments on the validation sets. Figure 4.11 presents the early stopping errors for networks with different activation functions in the RP layer and varying RP layer size.

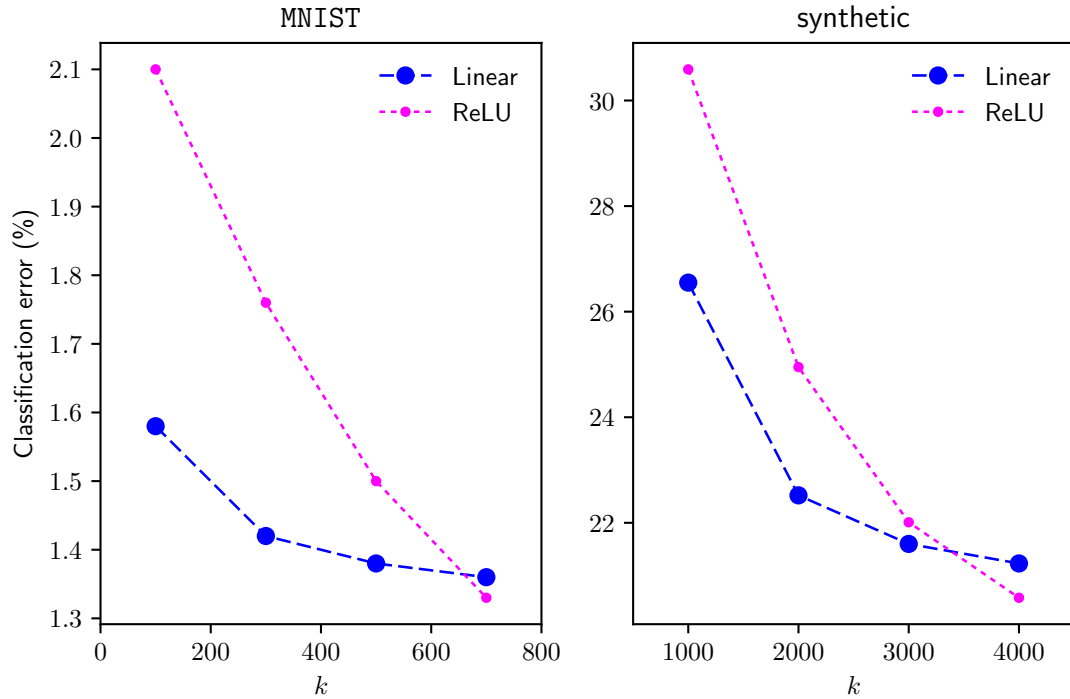


Figure 4.11: Performance of networks with different activation functions in the finetuned random projection layer for varying number of outputs, k , in the RP layer.

Our results suggest that introducing the ReLU activation function after the RP layer can improve the network performance, provided that the dimensionality of the RP layer k is sufficiently high. In our experiments on the synthetic dataset, it was necessary to use 4000 units in the RP layer to make ReLU viable. However, such a large RP layer greatly increases the overall computational cost of training. Therefore, for practical applications involving large, high-dimensional data we recommend using networks with linear finetuned RP layers.

4.3 Implementation notes

In this section, we present important implementation details of algorithms used in this chapter. In particular, we focus on the technicalities of implementing efficient random projection of sparse large-scale data.

Deep neural networks

We implemented a library with all essential deep learning algorithms and models that we use in this chapter. The implementation is designed to run on GPGPU and is written in C++ and CUDA⁶. It supports RBMs, DBNs, MLPs and deep autoencoders along with their training algorithms: error backpropagation for feedforward networks and

⁶ http://www.nvidia.com/object/cuda_home_new.html

CD for energy-based models. As most deep learning algorithms map well to the level 3 BLAS (Basic Linear Algebra Subprograms) operations, we implemented them with NVIDIA CUDA BLAS library (cuBLAS)⁷. To efficiently produce pseudo-random numbers from various distributions we use the NVIDIA CUDA Random Number Generation library (cuRAND)⁸. Our library functionality is exposed in Python via bindings based on Boost Python⁹. The bindings make the library easy to use and hide the low-level memory management of the underlying objects. For a more elaborate description of our GPU-accelerated library and its features see [Grzegorzczuk et al. 2016b]. As shown in [Grzegorzczuk et al. 2016b], our implementation offers a significant speedup compared to NumPy/OpenBLAS and MATLAB implementations running on a multi-core system.

All of our experiments with DNNs were conducted on NVIDIA Tesla K40 XL GPUs, which are based on the Kepler microarchitecture.

Random projection methods

We implemented the five RP methods from Section 3.2 in Python with extensive use of NumPy¹⁰. NumPy is a Python library for scientific computing that provides us with simple handling of large multidimensional arrays, an abundance of useful linear algebra procedures and random number generation capabilities. For sparse matrix construction and manipulation and efficient sparse matrix multiplication procedures we use the `scipy.sparse` module, which is a part of the SciPy library¹¹.

Data projection. To randomly project an $n \times d$ data matrix \mathbf{A} with a given RP scheme we first explicitly construct its $d \times k$ projection matrix \mathbf{P} and then compute the matrix product $\mathbf{A}\mathbf{P}$. This lets us implement all projection schemes in a uniform framework. Note that by enforcing the explicit construction of \mathbf{P} we only slightly hinder the SRHT projection – during construction of $\mathbf{P}_{SRHT} = \frac{1}{\sqrt{k}}\mathbf{DHS}$ we are still able to benefit from the speedup provided by the fast Fourier transform when computing \mathbf{HS} (see Section 3.2.4). Because all datasets in our evaluations are represented by sparse matrices in the compressed sparse row (CSR) format, we use either sparse-dense or sparse-sparse matrix multiplication algorithm, depending on the format of the projection matrix. When the projection matrix is dense, i.e., for Gaussian, Achlioptas’ and SRHT schemes we use the `csr_matvec` function¹², which runs in $\mathcal{O}(k(\text{nnz}(\mathbf{A}) + n))$ operations. When \mathbf{P} is sparse, i.e., for Li’s and Count Sketch schemes, we employ the SMMP algorithm [Bank and Douglas 1993], which has the computational complexity of $\mathcal{O}(nK^2 + \max\{n, d\})$, where K is the maximum number of non-zero elements in rows of \mathbf{A} and columns of \mathbf{P} . Despite the quadratic dependence on K , in practice, SMMP is much more efficient than `csr_matvec`. While in the worst case the multiplication may require $\mathcal{O}(nd^2)$ operations, K is typically much lower than d and grows very slowly with k . Of course, for higher densities of \mathbf{A} the maximum number of non-zero elements in rows of \mathbf{A} may decide the value of K . However, for most sparse real-world datasets

⁷ <http://docs.nvidia.com/cuda/cublas/index.html>

⁸ <http://docs.nvidia.com/cuda/curand/host-api-overview.html>

⁹ http://www.boost.org/doc/libs/1_64_0/libs/python/doc/html/index.html

¹⁰ <http://www.numpy.org/>

¹¹ <https://www.scipy.org/>

¹² <https://github.com/scipy/scipy/blob/v0.19.1/scipy/sparse/sparsetools/csr.h>

this value does not exceed several hundreds (see Table 4.12). Even for `webspam`, where

Table 4.12: Maximum and average number of non-zero elements in rows of the training data matrix for large-scale datasets.

Dataset	Number of non-zero elements per example	
	Average	Maximum
<code>url</code>	71	414
<code>webspam</code>	63	46,947
<code>KDD2010-a</code>	15	85
<code>KDD2010-b</code>	19	75
synthetic, $\rho = 10^{-4}$	100	148

the maximum number of non-zero elements in rows is high (and therefore determines K), the multiplication time of SMMP is low (~ 20 seconds for Count Sketch and ~ 4 minutes for Li’s matrix; projection to $k = 1000$ dimensions) compared to `csr_matvec` (~ 30 minutes for the Gaussian matrix). For most datasets, however, the value of K is determined by the maximum number of non-zero elements in columns of \mathbf{P} . For Count Sketch, the value of K can be estimated using the analogy of the Count Sketch matrix construction to the balls-into-bins problem [Raab and Steger 1998]. If we treat columns of \mathbf{P} as bins and the non-zero elements as balls, we can calculate with high probability (defined as probability that tends to 1 when the number of columns grows) the maximum bin load, which is equivalent to K . Specifically, when $d \geq k \log k$ the maximum load of any bin is $\Theta(\frac{d}{k})$, i.e., on the order of the mean value. Therefore, the time of multiplying the data matrix by the Count Sketch projection matrix decreases with the growth of k and for higher values of k is lower-bounded by the maximum non-zero element count in the rows of the data matrix. For Li’s scheme, the value of K grows with d and k , however, this dependence is not linear. Obviously, K depends on d as each column of \mathbf{P} contains, on average, \sqrt{d} non-zero elements. K ’s dependence on k is a consequence of the fact that increasing the number of columns also increases the probability of adding a column with a higher number of non-zero elements.

In Table 4.13 we report a summary of the time complexity of constructing different projection matrices and using them to perform random projection.

Matrix slicing. With high data and projection dimensionality, even the projection matrix alone may not fit into the available memory. For example, in our experiments on the real-world datasets projecting the `KDD2010-b` data matrix to 1000 dimensions using a dense RP scheme requires constructing a projection matrix that needs nearly 120GB of memory, assuming a 4-byte floating point representation. To perform the projection efficiently, additional space is also needed for the input data and the projected result. To alleviate the memory consumption problem we employed two types of data matrix slicing: horizontal slicing of the input data and vertical slicing of the projection matrix. With these two techniques, we can control the amount of memory that is needed to perform the projection. Of course, these techniques come with an additional cost of disk IO operations.

Table 4.13: Time complexity of constructing a random projection matrix and performing the projection via matrix multiplication $\mathbf{A}\mathbf{P}$, where \mathbf{A} is a $n \times d$ data matrix and \mathbf{P} is a $d \times k$ projection matrix. $\text{nnz}(\mathbf{A})$ denotes the number of non-zero elements in matrix \mathbf{A} . K is the maximum number of non-zero elements in rows of \mathbf{A} and columns of \mathbf{P} .

Random projection scheme	Matrix construction	Matrix multiplication
Gaussian	$\mathcal{O}(dk)$	$\mathcal{O}(k(\text{nnz}(\mathbf{A}) + n))$
Achlioptas'	$\mathcal{O}(dk)$	$\mathcal{O}(k(\text{nnz}(\mathbf{A}) + n))$
Li's	$\mathcal{O}(d^{\frac{1}{2}}k)$	$\mathcal{O}(nK^2 + \max\{n, d\})$
SRHT	$\mathcal{O}(d(k + \log d))$	$\mathcal{O}(k(\text{nnz}(\mathbf{A}) + n))$
Count Sketch	$\mathcal{O}(d)$	$\mathcal{O}(nK^2 + \max\{n, d\})$

To randomly project a data matrix \mathbf{A} using an RP matrix \mathbf{P} we do not need to create the whole projection matrix at once. Instead, we can generate v vertical slices \mathbf{P}_i of the projection matrix \mathbf{P} one by one and use them to calculate slices \mathbf{R}_i of the result matrix \mathbf{R} . This procedure is illustrated in Figure 4.12. Importantly, at any point during the projection, we only need to store \mathbf{A} , \mathbf{P}_i and \mathbf{R}_i in memory.

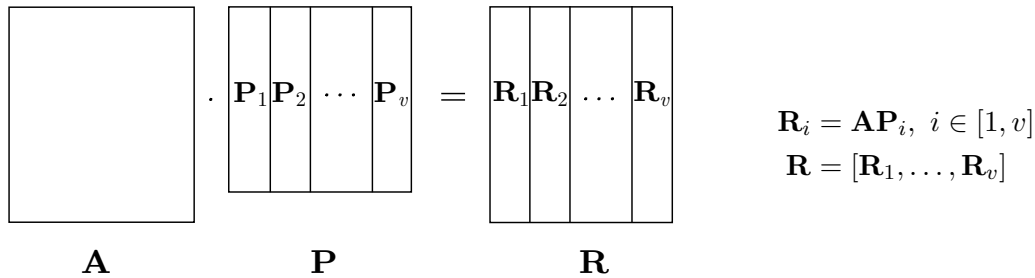


Figure 4.12: Random projection procedure with columnwise slicing of the projection matrix. \mathbf{A} is the dataset matrix, \mathbf{P} is the projection matrix and \mathbf{R} is the result matrix. The number of projection matrix slices is v . $[\mathbf{X}, \mathbf{Y}]$ operation denotes the columnwise concatenation of matrices \mathbf{X} and \mathbf{Y} .

We employ slicing of \mathbf{P} for the Gaussian, Achlioptas', Li's and SRHT RP matrices. Slicing of the Count Sketch matrix \mathbf{P}_{CS} is not necessary since even for high dataset dimensionality d and projection dimensionality k it only contains d non-zero elements. Therefore, it takes just up to a few hundred megabytes of memory. Columnwise slices of Gaussian, Achlioptas' and Li's projection matrices can be generated using the same random number distributions as the one that is used to create their respective unsliced projection matrices. Of course, when creating slices \mathbf{P}_i we must appropriately scale the non-zero elements depending on the number of slices v . Slices of the SRHT matrix \mathbf{P}_{SRHT} can also be easily generated. \mathbf{P}_{SRHT} construction starts with a sparse matrix whose generation uses a random number distribution similar to Li's matrix. This matrix is then deterministically transformed with the Walsh-Hadamard transform and has a random half of its rows multiplied by -1 (see Section 3.2). Therefore, \mathbf{P}_{SRHT} slices are defined by the initial Li's-like matrix slices, which, as discussed above, can be easily

generated.

When the data matrix \mathbf{A} takes a significant amount of RAM or does not fit into the memory, it may also be necessary to split it rowwise into smaller parts \mathbf{A}_i . This is the case, for example, for the `webspam` dataset. In Figure 4.13 we illustrate how to perform dataset slicing in addition to the projection matrix slicing. Both the number of projection matrix slices v and the number of dataset slices h can be adjusted to control the amount of required memory.

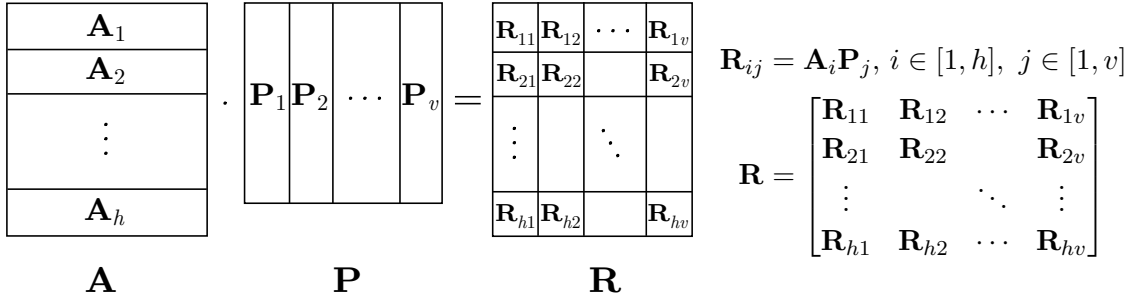


Figure 4.13: Random projection procedure with rowwise slicing of the data matrix and columnwise slicing of the projection matrix. \mathbf{A} is the dataset matrix, \mathbf{P} is the projection matrix and \mathbf{R} is the result matrix. v and h are the numbers of projection and dataset matrix slices, respectively.

Algorithm 2 Pseudocode for the random projection procedure with dataset and projection matrix slicing. \mathbf{A} is the dataset matrix, \mathbf{P} is the projection matrix, and \mathbf{R} is the result matrix. v and h are the numbers of projection and dataset matrix slices, respectively.

- 1: split \mathbf{A} rowwise into h slices, so that $\mathbf{A} = [\mathbf{A}_1, \dots, \mathbf{A}_h]^T$
 - 2: split \mathbf{P} columnwise into v slices, so that $\mathbf{P} = [\mathbf{P}_1, \dots, \mathbf{P}_v]$
 - 3: **for** $j = 1$ **to** v **do**
 - 4: **for** $i = 1$ **to** h **do**
 - 5: $\mathbf{R}_{ij} = \mathbf{A}_i \mathbf{P}_j$
 - 6: save \mathbf{R}_{ij}
 - 7: **end for**
 - 8: read \mathbf{R}_{kj} , for $k \in [1, h]$
 - 9: $\mathbf{R}_{\bullet j} = [\mathbf{R}_{1j}, \dots, \mathbf{R}_{hj}]^T$
 - 10: save $\mathbf{R}_{\bullet j}$
 - 11: **end for**
 - 12: read $\mathbf{R}_{\bullet k}$, for $k \in [1, v]$
 - 13: **return** $\mathbf{R} = [\mathbf{R}_{\bullet 1}, \dots, \mathbf{R}_{\bullet v}]$
-

The pseudocode for RP with matrix slicing is presented in Algorithm 2. Since the partial projection results $\mathbf{R}_{\bullet j}$ and the final result \mathbf{R} are small compared to the projection and dataset matrices, the most memory-demanding part of Algorithm 2 is the projection phase (line 5). During this operation, the procedure needs to store only a single dataset slice \mathbf{A}_i , one projection matrix slice \mathbf{P}_j and the projection result \mathbf{R}_{ij} .

Dimensionality reduction methods

For the PCA, Chi-square and F-score dimensionality reduction procedures we used the implementations from the `scikit-learn` Python library¹³. `scikit-learn` natively supports sparse matrices, is computationally efficient and has a small memory footprint. To compute PCA, we employed the truncated SVD algorithm with the randomized solver by Halko et al. [2011]. Importantly, in addition to being computationally efficient, it can also work directly on sparse data. Since truncated SVD does not center features in the input data, we normalized each feature in the MNIST dataset. Normalization was not necessary for the synthetic dataset variants, as their construction ensures that each feature is centered around zero. To select features in the synthetic datasets with the Chi-square method we used data matrices with absolute feature values. This is because the Chi-square implementation requires the entries of the data matrix to be non-negative. A common practice is to rescale every feature to the $[0, 1]$ interval. However, this operation is impossible for the synthetic datasets as it would destroy their sparse structure and raise the memory footprint to almost 4TB for each dataset (assuming a 4-byte representation of the floating-point numbers). We implemented the IG feature selection by creating a custom score function for the `SelectKBest` class¹⁴ in the `scikit-learn` package.

4.4 Conclusions

In this chapter, we studied the viability of training DNNs with the RP layer with the goal of creating models that can efficiently learn from sparse, high-dimensional data. Our results demonstrate that networks with RP layer can match or improve over the state-of-the-art classification results on data with millions of dimensions and no spatial structure. This opens a path to applying neural networks in tasks where directly learning from the data would be infeasible: experiments on the KDD2010 datasets, for example, involved up to 30,000-fold reduction of the input dimensionality.

We studied two variants of the RP layer: one with weights that are fixed during training and one where they are finetuned with error backpropagation. Our experimental evaluation of DNNs with fixed-weight RP layer shows that Gaussian, Achlioptas', SRHT and Count Sketch projections perform well, while the Li's projection yields worse results. This could be attributed to the sparsity of the projected data – on the MNIST dataset, which is dense, Li's method performed well. Note also that Achlioptas', Count Sketch, Li's and SRHT are fast: the first three do not employ dense projection matrices and the last one can be computed efficiently using a transform similar to the fast Fourier transform. Taking this into account, SRHT and Count Sketch projections combine the best network performance with efficient data projection. We also experimented with using RP for BOW data. Specifically, we experimented with training deep autoencoders similar to the ones described in [Salakhutdinov and Hinton 2009] on randomly projected BOW vectors. While this approach enabled us to train autoencoders on larger dictionaries, it did not achieve performance comparable to the reference networks. This result

¹³<http://scikit-learn.org>

¹⁴http://scikit-learn.org/stable/modules/generated/sklearn.feature_selection.SelectKBest.html

can be a consequence of two facts. First, the autoencoders with projected data require Gaussian input units. The reference networks employ the constrained Poisson model, which is tailored to BOW data. Second, the dictionary used by the reference models already captured most of the word count in the text.

Our experiments with finetuned RP layer suggest that adjusting the non-zero weights in a sparse RP layer can significantly improve the overall network performance. In particular, by using the finetuned Count Sketch RP layer we were able to train networks that achieved more than 30% lower classification error on `webspam` and `url` datasets, compared to the state-of-the-art methods. To make training of the RP layer feasible we employed several architectural optimizations and training regime modifications. First, instead of normalizing the input data we applied batch normalization after the RP layer. Second, we finetuned only these RP weights that were initially non-zero. Finally, we found that applying a nonlinear activation after the batch normalization is viable only when the input data is projected to a high-dimensional space. In practice, the performance gain from this nonlinearity does not justify the additional computational cost introduced by finetuning an RP layer with a high-dimensional output.

CHAPTER 5

INITIALIZING DEEP NETWORKS WITH RANDOM PROJECTION MATRICES

How should we initialize weights in deep neural networks? The answer to this question depends on the network architecture, neuron connectivity and the activation function. Most often it involves a carefully scaled normal or uniform distribution. But what if we used a less trivial random number distribution? In this chapter we investigate the performance of deep neural networks with weights initialized using RP matrices described in Section 3.2. In particular, we study five RP weight initialization schemes: two dense, i.e., Gaussian and SRHT, and three sparse, i.e., Achlioptas', Li's and Count Sketch. We focus mostly on rectifier networks, as the ReLU transfer function is currently the most popular choice for efficient training of deep architectures [LeCun et al. 2015].

We begin by stressing the importance of weight initialization in deep networks. We briefly review the most popular initialization schemes and related techniques. We then motivate the viability of using RP matrices that satisfy the Johnson–Lindenstrauss lemma as the initial weights in deep networks. We follow up by investigating RP initialization in CNNs and in pretrained fully-connected networks. We show that using RP matrices as initial weights is a viable approach in CNNs. Specifically, in our evaluation CNNs initialized with SRHT matrices consistently outperformed the current state-of-the-art initialization scheme on several image classification datasets. Most pretrained networks, however, did not benefit from RP initialization.

Results from this chapter were presented in [Wójcik and Kurdziel 2017]. A Torch7 package implementing our RP initialization for CNNs is available at <https://github.com/piotriwojcik/rpinit>.

5.1 Weight initialization techniques

For typical cost functions training a deep neural network can be viewed as a non-convex optimization problem. As the loss function contains multiple local minima, the optimization process tends to converge to different solutions, depending on the initial conditions. Therefore, initial network parameters, i.e., weights and biases can significantly affect the speed of convergence and the quality of the found solution [Larochelle et al. 2009]. A bad initialization scheme may even prevent the network from learning. The simplest example is an all-zero initialization. It leads to a situation where every hidden unit in

a given layer receives the same input signal ($\sum_i x_i w_i + b = 0$, because $\forall_i w_i = 0$ and $b = 0$), produces the same output and computes the same gradient during backpropagation. Consequently, all neurons receive the same weight updates and learn the same function, wasting the network capacity. To avoid this symmetry, the initial weights should not be equal. Note that the symmetry breaking is not strictly necessary for the output layer, as every output unit receives different gradient signal, and thus learns different weights [Bengio 2012b].

A simple and popular initialization approach is, therefore, to initialize the weight matrix \mathbf{W} with random values drawn from some probability distribution. In fact, a zero-mean normal distribution with a small variance:

$$W_{ij} \sim \mathcal{N}(0, s^2), \quad (5.1)$$

often works surprisingly well. Such initialization scheme with $s = 10^{-2}$ was used, for example, in the influential ImageNet network by Krizhevsky et al. [2012]. One advantage of using small initial weights is particularly clear when training a network with sigmoid or hyperbolic tangent activation functions. The derivative of the sigmoid function is:

$$\sigma'(x) = \sigma(x)(1 - \sigma(x)), \quad (5.2)$$

with maximum for $\sigma(x) = 0.5$. Since the weight updates in backpropagation are proportional to this derivative, sigmoid units will learn the fastest for activations close to 0.5, i.e., when the total unit input is close to zero ($\sigma(0) = 0.5$). When the magnitude of the input rises, the derivative of the activation function quickly becomes very small, making the weight updates inefficient. This leads to units entering a saturated state, which effectively stops their learning. On the other hand, the gradient is proportional to the magnitudes of weights. Therefore, setting the weights too low also leads to small gradient and slow learning process. This becomes an issue especially when backpropagating through deeper networks, where the gradient diminishes exponentially with each layer. This exponential decrease (or explosion, if the initial weights are too large) of the error signal as a function of the distance from the output layer is often referred to as the vanishing (or exploding) gradient problem [Hochreiter et al. 2001].

The issues mentioned above prompted a vigorous research on network initialization. The importance of proper initialization when using first-order optimization methods, such as SGD, was emphasized in [Sutskever et al. 2013]. Therein, Sutskever et al. showed that SGD with momentum and carefully initialized weights can yield results comparable to training with higher-order methods, such as Hessian-free optimization. A parallel line of research focused on making deep networks more robust to the choice of initial weights. For example, ReLU [Nair and Hinton 2010] is a significant step towards alleviating the vanishing gradient problem. Training can also be facilitated with batch normalization [Ioffe and Szegedy 2015], which normalizes the distribution of activations in hidden layers. However, despite these advances, networks employed to obtain current state-of-the-art results still use carefully designed weight initialization schemes [He et al. 2015b].

The topic of weight initialization is vast and includes a number of different approaches ranging from simply drawing the weights from a well-designed probability distribution to more complex approaches, such as transfer learning. Below we briefly review the most common weight initialization techniques.

Pre-deep learning weight initialization. Before the advent of modern deep neural networks, multiple weight initialization techniques were developed to increase the back-propagation convergence rate and quality of solutions. These approaches include, e.g., genetic algorithms, simulated annealing [Masters 1993], linear algebraic methods [Yam and Chow 2000] and other techniques [Drago and Ridella 1992; Martens 1996; Nguyen and Widrow 1990]. However, these methods are usually impractical in modern deep neural networks because of being either computationally too expensive or suitable only for the sigmoid or hyperbolic tangent activation functions.

Sparse initialization. Martens [2010] proposed the Hessian-free optimization method for backpropagation networks. While this algorithm outperforms the standard SGD, it too benefits from a well-designed random initialization scheme. In particular, the best results in [Martens 2010] were obtained with there-proposed sparse initialization (SI) approach. Sparse initialization initializes units with sparse, randomly generated weight vectors. In particular, a fixed number of elements (15 in Martens’ experiments) is randomly chosen in each weight vector. These elements are initialized with random weights, usually drawn from a Gaussian distribution, while the other elements are set to zero. Sparse initialization was designed to fulfill two goals: to prevent the saturation of network units and to make the units initially as different from each other as possible. Sutskever et al. [2013] confirmed the usefulness of SI also in networks trained with SGD.

Random initialization with scaled variance. A significant improvement in weight initialization stemmed from an observation that by simply setting the weights to small random numbers one does not take into account the variance of the layer activations and gradients. A better way to initialize the weights is, therefore, to scale them in a way that normalizes these variances. Without such normalization, the magnitudes of activations of final layers in deeper architectures could either be extremely large or too small to produce a proper training gradient. LeCun et al. [1998b] recommend scaling down the weights of sigmoid units by the square root of the so-called *fan-in*, i.e., the number of unit inputs. The weights were then initialized with:

$$W_{ij} \sim U\left[-\frac{1}{\sqrt{f_{\text{in}}}}, \frac{1}{\sqrt{f_{\text{in}}}}\right], \quad (5.3)$$

where f_{in} is the *fan-in*, and $U[-x, x]$ is the uniform distribution over the $[-x, x]$ interval. Glorot et al. [Glorot and Bengio 2010] in their initialization scheme for sigmoid and hyperbolic tangent units additionally employed the *fan-out*, i.e., the number of outputs:

$$W_{ij}(\text{sigmoid}) \sim U\left[-\sqrt{\frac{6}{f_{\text{in}} + f_{\text{out}}}}, \sqrt{\frac{6}{f_{\text{in}} + f_{\text{out}}}}\right], \quad (5.4)$$

$$W_{ij}(\text{tanh}) \sim U\left[-4\sqrt{\frac{6}{f_{\text{in}} + f_{\text{out}}}}, 4\sqrt{\frac{6}{f_{\text{in}} + f_{\text{out}}}}\right]. \quad (5.5)$$

This initialization scheme, often called the *Xavier* initialization, was one of the factors that made it possible to move away from generative pretraining and successfully train deep networks from scratch [Glorot et al. 2011]. However, Glorot’s initialization was

not primarily designed for rectified linear units. A weight initialization scheme suitable for ReLU and Leaky ReLU, the so called *He's* initialization was proposed in [He et al. 2015b]:

$$W_{ij} \sim \mathcal{N}\left(0, \frac{2}{f_{\text{in}}}\right). \quad (5.6)$$

Using this initialization scheme He et al. reported to have successfully trained 30-layer networks from scratch. He's method is currently the state-of-the-art initialization scheme for practical applications of deep ReLU networks.

Other works employing initialization schemes motivated by controlling the variance of network activations or the variance of the weight gradients include, e.g., [Krähenbühl et al. 2015; Sussillo and Abbott 2014]. Sussillo and Abbott [2014] proposed an initialization scheme, called the random walk initialization that focuses on preventing the vanishing gradient problem by forcing the norms of backpropagated errors to be constant. Krähenbühl et al. [2015] normalized network activations in CNNs by using activation statistics estimated from the training data.

Unsupervised pretraining. In their seminal work Hinton and Salakhutdinov [2006] demonstrated that DNNs can be trained in two phases: layer-by-layer unsupervised pretraining using DBNs, followed by supervised finetuning with error backpropagation. The resultant deep models significantly outperformed the state-of-the-art approaches on multiple machine learning tasks [Hinton et al. 2012; Hinton and Salakhutdinov 2006]. Although the introduction of ReLUs and efficient initialization schemes made the pretraining phase not necessary for most applications, many recommendations indicate that pretraining typically helps [Bengio 2012b; Erhan et al. 2010].

Pretraining can be regarded not only as a type of weight initialization scheme but also as a regularizer that improves generalization [Larochelle et al. 2009]. Another justification for unsupervised pretraining stems from the imbalance between the available labeled and unlabeled data: data acquisition is relatively inexpensive, compared to labeling. Therefore, unsupervised pretraining can often incorporate much bigger training sets than supervised finetuning.

Comparatively less work has been published on initialization of network layers for generative pretraining employed before supervised finetuning. Similarly to feed-forward architectures, weights before pretraining are typically densely initialized with random numbers drawn from a zero-mean normal distribution with a small standard deviation:

$$W_{ij} \sim \mathcal{N}(0, s^2). \quad (5.7)$$

Specifically, Hinton [2012] recommends using $s = 10^{-2}$. An alternative approach is to initialize these weights with Martens' sparse initialization scheme, which was originally proposed for backpropagation networks [Martens 2010]. Specifically, Grzegorzczuk et al. [2015] showed that sparse initialization in DBNs with NReLU hidden layers slightly improves the network performance.

Orthogonal initialization. Saxe et al. [2014] showed that using random orthogonal weights instead of scaled random Gaussian numbers (Eq. 5.3) yields a similar quality of initialization to unsupervised pretraining and makes training deeper models possible.

Although Saxe et al. derived these results for linear networks, they demonstrated that orthogonal initialization leads to better gradient propagation also in deep nonlinear networks. This idea was further extended by Mishkin and Matas [2015] who employed orthonormal initialization combined with batch normalization of layer output similar to [Ioffe and Szegedy 2015] but performed only on the first batch.

Grzegorzczak et al. [2016a] showed that orthogonal initialization can also be achieved with unsupervised pretraining. They proposed to explicitly encourage the orthogonality of features learned by an RBM model during the pretraining phase. Their goal was to increase the diversity of learned features. To this end, Grzegorzczak et al. [2016a] modified the CD algorithm in a way that penalizes parallel components of the weight vectors. They showed that deep networks pretrained in this manner can be finetuned to higher levels of performance, compared to standard pretraining.

Transfer learning. A popular trick to speed up the network training, used especially with modern CNNs, is to employ features that were already trained for a different task or on a different dataset [Bengio 2012a]. This is realized by simply copying (transferring) the weight matrices of several layers of the base network to the layers of the target network. Remaining layers of the target networks are initialized in a standard manner. Then, either the whole target network or only the randomly initialized layers are trained to solve the target task. This approach is motivated by the fact that the initial layers in CNNs usually recognize generic image features, while deeper layers are tuned for a specific task. Therefore, early layers of a trained network should be useful also in other networks trained on similar data. Transfer learning is especially beneficial in situations when the available dataset has a small number of examples.

5.2 Random projection initialization

Feeding data through a Gaussian initialized network with fully-connected layers realizes an operation similar to a series of consecutive RPs that roughly preserves the distances between the observations. To see this, let us consider a single untrained neural network layer with d input and k output units, where the weight matrix $\mathbf{W} \in \mathbb{R}^{d \times k}$ has been initialized, following a common practice, to small random numbers drawn from a Gaussian distribution $\mathcal{N}(0, 10^{-4})$ [Hinton 2012; Krizhevsky et al. 2012] and the biases have been set to zero. In this layout, columns of matrix \mathbf{W} represent latent features learned by the neurons in the hidden layer. The layer receives an input vector $\mathbf{I} \in \mathbb{R}^d$ and computes the output $\mathbf{O} \in \mathbb{R}^k$:

$$\mathbf{O}_{nn} = f(\mathbf{IW}), \quad (5.8)$$

where $f(\mathbf{x})$ denotes application of the activation function to each element of the vector \mathbf{x} . The usual bias term was omitted here, as in this example all biases are equal to zero. Note that the computation realized by this layer is similar to performing an RP of the input vector using a projection matrix \mathbf{R} :

$$\mathbf{O}_{rp} = \mathbf{IR}. \quad (5.9)$$

In fact, matrices \mathbf{W} and \mathbf{R} are constructed in exactly the same manner: they both consist of random numbers drawn from a Gaussian distribution with a small standard

deviation. The only difference between Eq. 5.8 and Eq. 5.9 is the presence of an element-wise activation function f . However, in our settings, application of f does not alter the output vector significantly. This is obviously true for linear units, where the activation function is an identity. For nonlinear activations that are well approximated by an identity function near zero, e.g., hyperbolic tangent, exponential linear [Clevert et al. 2015] or softsign, applying f also has little impact on the result vector. This is because weights in \mathbf{W} have small absolute values, and therefore entries in the vector \mathbf{IW} are also close to zero. For activation functions that are nearly linear and differentiable around zero, application of f results in shifting the entries of \mathbf{IW} by $f(0)$ and scaling them with a constant equal to $f'(0)$. This is the case, for example, for the popular sigmoid activation function, which in our example adds 0.5 to each entry and scales it by a factor 0.25. The rectifier linear activation modifies the input vector in a less trivial way: it zeros-out only the negative entries of \mathbf{IW} . However, the resultant vector \mathbf{O} still contains, on average, half of the elements of \mathbf{O}_{rp} .

Following the above example, a network consisting of l hidden layers performs l consecutive Gaussian RPs, resulting in a k -dimensional data representation, where k is the size of the last hidden layer. Since the Gaussian RP satisfies the Johnson-Lindenstrauss lemma [Dasgupta and Gupta 2003; Indyk and Motwani 1998], unless k is small, feeding data through a Gaussian-initialized network yields an output that roughly preserves the structure in the original data. (For a formal proof of the distance-preserving nature of Gaussian-initialized networks see [Giryes et al. 2015].) This fact is supported by recent findings that random untrained weights can perform surprisingly well in certain network architectures. In particular, in a large-scale evaluation of neural network architectures on multiple object recognition tasks pretrained weights only slightly outperformed completely random filters [Pinto and Cox 2010; Pinto et al. 2009]. Similarly, Saxe et al. [2011] reported surprisingly high performance of CNNs with random weights on NORB and CIFAR-10 datasets. We argue that these results may, to some extent, be attributed to the structure-preserving nature of embeddings realized by untrained neural networks.

The argument used in the above example assumed that weights are initialized with Gaussian RP matrices. However, it also holds for other RP schemes. This motivates us to explore the prospects of initializing the weights in neural networks with more intricate random matrices. In particular, we investigate initialization of deep networks with RP matrices described in Section 3.2, i.e., Achlioptas', Li's, SRHT and Count Sketch. As the Gaussian RP initialization with proper normalization is equivalent to the reference initialization scheme we omit it in this chapter.

Random projection initialization in CNNs

Convolutional neural networks are made from three types of layers: convolutional layers, pooling layers and fully-connected layers. Following [Huang et al. 2016] we only initialize weights in the convolutional layers. In all reported experiments biases are initialized to zeros.

Consider a convolution kernel matrix of size: $c_{\text{out}} \times c_{\text{in}} \times k \times k$, where c_{in} and c_{out} are the number of input and output planes, respectively, and k is the kernel size. In RP-based initialization we use $n = c_{\text{in}} \times k \times k$ as the data dimensionality and c_{out} as the projection dimensionality. Therefore, before training, the convolutional layer can

be seen as performing an RP of the input volume into a c_{out} -dimensional space. We normalize the kernel matrices to the same standard deviation as in He’s initialization, i.e., to $\sqrt{2/n}$. The only exception is the Count Sketch initialization, where we do not normalize the weights to a fixed standard deviation, but instead, multiply them with a scale factor γ chosen with validation experiments. This difference is due to the sparsity of the Count Sketch projection matrix – each of its rows is a randomly chosen standard basis vector multiplied by either 1 or -1 . Normalizing such matrix to a fixed standard deviation alters only its non-zero entries, causing their absolute values to grow to huge numbers. This can impede the learning process or cause the gradients to explode. In SRHT initialization we set the sparsity parameter to $q = n^{-1} \log^2 N$. For the number of projected examples N we use the number of training images that are fed through the network during a single epoch. We have also experimented with using a transposed initialization scheme and not employing weight scaling. However, these tests yielded worse results.

Random projection initialization in pretrained networks

In addition to CNNs, we also investigate initialization in fully-connected networks with generative pretraining. For the pretraining phase we employ stacked RBMs [Hinton and Salakhutdinov 2006]. Random projection initialization is performed before the pretraining phase, and thus serves as the starting point for the CD algorithm. When initializing the RBM weights with an RP matrix we use the number of visible units as the data dimensionality and the number of hidden units as the projection dimensionality. Similarly to CNN initialization, we leave the biases set to zero. A standard advice when training an RBM is to start with small weights [Hinton 2012]. Therefore, after initialization we normalize the weight matrices to zero mean and a small standard deviation $s = 0.01$. The Count Sketch initialization is, again, an exception: because of its sparsity, we scale the weights by a constant factor chosen with validation experiments. In SRHT initialization we set the sparsity parameter q in the same way as in CNN initialization. We also tested the network performance without weight normalization. However, these experiments yielded significantly worse results, and we do not report them here.

5.3 Experiments

We evaluated the RP initialization schemes on several popular image and text datasets, namely MNIST, NORB, CIFAR-10, CIFAR-100, SVHN, TNG and RCV1. For details of these datasets and their preprocessing see Appendix A. We carried out experiments on two important machine learning tasks, namely image classification and document retrieval.

We begin by evaluating RP initialization in deep convolutional neural networks. We then follow up with a similar evaluation for networks pretrained using stacked RBMs.

5.3.1 Image classification with convolutional neural networks

For the evaluation of RP initialization in CNNs, we employed three datasets, namely CIFAR-10, CIFAR-100 and SVHN. The evaluation was carried out using ResNets with stochastic depth [Huang et al. 2016]. Note, however, that RP initialization proposed

herein is not tailored to this specific network architecture, but can be used in any rectifier network. Our goal in this evaluation is not to improve the performance beyond the current state-of-the-art results on CIFAR or SVHN, but instead to find out whether modern CNN architectures can benefit from RP initialization. We use ResNets with stochastic depth as an example of such modern architecture. We used the best-performing architectures and hyperparameter sets from [Huang et al. 2016], i.e., 110-layer ResNet for the CIFAR experiments and a 152-layer ResNet for the SVHN experiments. With the reference He’s initialization [He et al. 2015b] these models achieved state-of-the-art performance on CIFAR-10 and CIFAR-100 with standard data augmentation and the second best published result on SVHN.

To account for the random nature of weight initialization, we trained ten network instances for each initialization method, using different random number generator seeds. Afterward, we carried out statistical tests to assess the confidence of RP initialization schemes outperforming the He’s initialization. Specifically, for each network instance, we averaged the test errors from the last 100 (for CIFAR) or 10 (for SVHN) epochs and compared the averages obtained with the He’s initialization against averages obtained using RP initialization. For this comparison, we employed the Wilcoxon-Mann-Whitney two-sample rank-sum test. Note that comparing neural network performance with a statistical test is not a common practice. However, a simple comparison of the early-stopping errors would be inconclusive in this evaluation. By performing a statistical test we are able to more reliably assess the performance of the evaluated weight initialization schemes. All experiments were carried out using the implementation of ResNets with stochastic depth by Yu Sun¹.

Performance of the evaluated initialization schemes on the CIFAR and SVHN datasets is reported in Fig. 5.1. The plots report median accuracy on the test sets, the significance level of the hypothesis that the evaluated RP initialization outperforms He’s initialization and the value of the U statistic in the Wilcoxon-Mann-Whitney test. Following [Huang et al. 2016], we report the test error in each epoch for CIFAR and after every 200 iterations for the SVHN experiments. We present the test errors after setting the learning rate to the smallest value.

The SRHT initialization outperformed the reference initialization on all datasets. Note that this is the only dense RP initialization scheme among the four evaluated methods; the other three schemes, i.e., Li’s, Achlioptas’ and Count Sketch are sparse. The second best-performing RP initialization scheme, i.e, Achlioptas’, yielded good but not statistically significant results on CIFAR and average results on SVHN. With one-third non-zero entries, it is the second most dense initialization scheme evaluated in this work. Li’s initialization achieved a similar performance level: competitive on CIFAR but slightly worse than the reference on SVHN. The Count Sketch scheme was the best performing RP initialization method on CIFAR-10 while yielding results comparable to reference on SVHN and significantly worse than reference on CIFAR-100. This method proved to be very sensitive to the scaling factor γ , which led to inconsistent performance. Depending on the dataset, it performed best with $\gamma \in \{0.1, 0.3\}$. The values of γ higher than 1.0 caused the network to not converge, while values smaller than 0.1 led to poor performance.

¹ Available at https://github.com/yueatsprograms/Stochastic_Depth

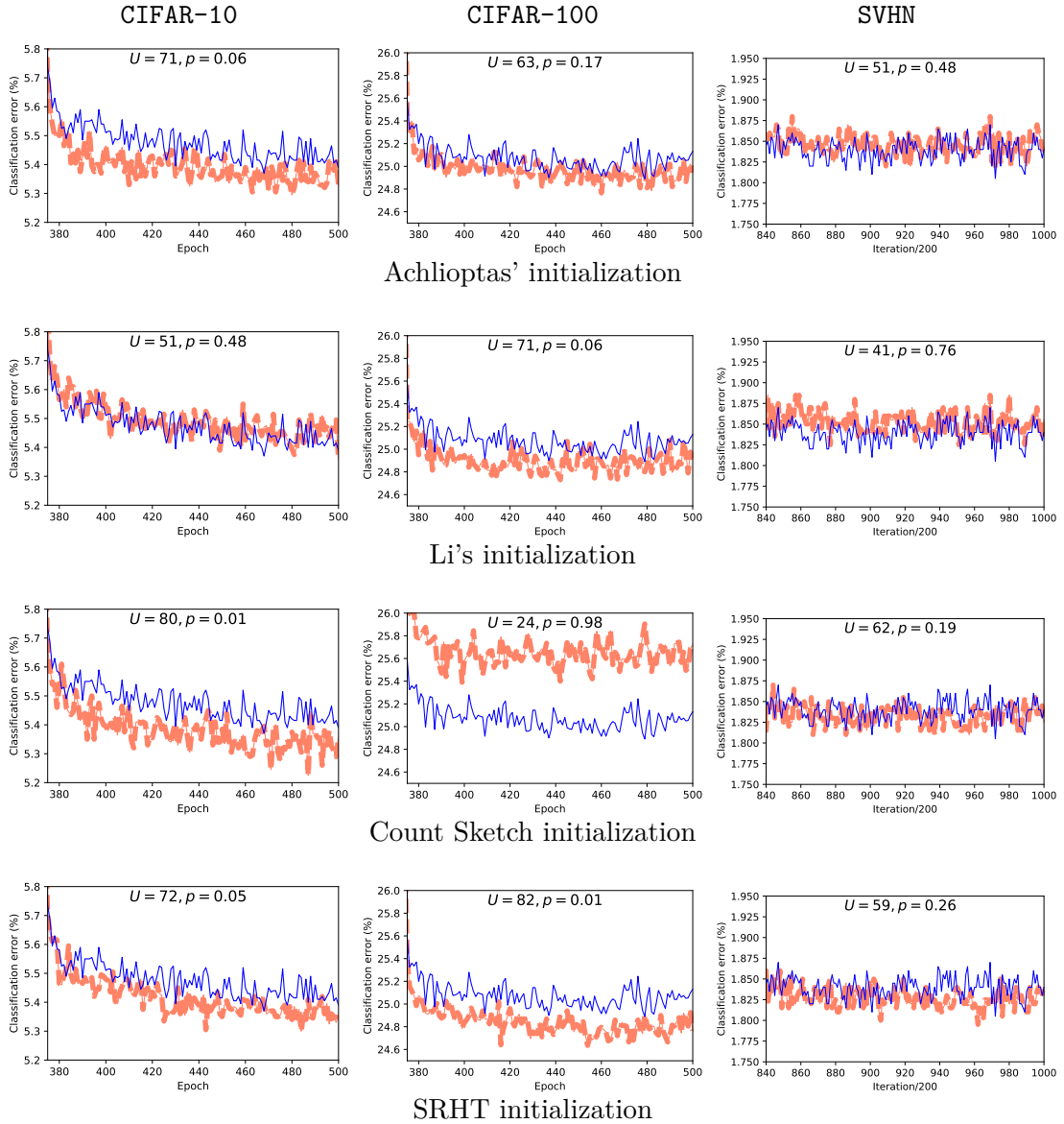


Figure 5.1: RP initialization in convolutional neural networks. Plots show median test error on CIFAR-10, CIFAR-100 and SVHN for different RP initializations (dashed orange line) and the reference He's initialization (solid blue line).

Overall our results suggest that the sparsity of the initialization scheme plays the deciding role in CNNs initialization: CNNs perform best when their weights are densely initialized, as is the case for He's and SRHT initializations. The second important factor is the orthogonality of the initialized weights: the slightly closer to orthogonal SRHT initialization performs better than He's initialization. This finding is also supported by experiments with orthogonal initialization in deep CNNs by Mishkin and Matas [2015].

5.3.2 Image classification with pretrained networks

To evaluate RP initialization in pretrained networks, we experimented on MNIST and Jittered-Cluttered NORB datasets. For the MNIST experiments, we employed one of the network architectures from [Srivastava 2013], namely a binary input layer followed by two hidden layers with 1000 ReLU units and a 10-way softmax. For the NORB experiments, we used the best performing network architecture reported in [Nair and Hinton 2010], i.e., two hidden layers with 4000 and 2000 ReLU units, respectively, followed by a 6-way softmax. Inputs in this network were modeled with Gaussian units. Evaluated networks were pretrained with the CD_1 algorithm and finetuned for 500 epochs with error backpropagation. We trained the networks using mini-batch SGD with momentum. To avoid overfitting during pretraining we used L2 weight decay in all layers. During finetuning we regularized the networks with dropout and decreased the learning rate according to a slow exponential decay while slowly increasing the momentum value. Learning hyperparameters and the scaling factor for the Count Sketch initialization were selected with experiments on the validation sets.

For each dataset and initialization scheme, we trained ten network instances with different random number seeds. Results from these experiments are reported in Fig. 5.2. In each case, we report median test error as a function of the finetuning epoch. The standard Gaussian initialization serves as the baseline result.

Unlike CNNs, image classification with pretrained networks does not benefit from RP initialization. Specifically, Achlioptas’ and SRHT initialization yielded slightly worse results, compared to the reference initialization. Li’s initialization performed better on the NORB dataset but worse on MNIST. The Count Sketch initialization yielded results significantly worse than reference, which can be attributed to its sparsity.

5.3.3 Document retrieval with autoencoders

In the previous sections we presented the results of applying RP initialization in image classification task. In this section we evaluate RP initialization in networks trained for the document retrieval task. In particular, we carry out experiments with RP initialization in deep autoencoders trained on the TNG and RCV1 corpus. As a baseline we use deep autoencoder architectures and training regime from [Grzegorzczak et al. 2016a]. This is the same baseline as in Section 4.1.3. In reference DBNs all layers were initialized with small random numbers from a Gaussian distribution. We compare these baseline networks to DBNs in which weights were initialized with different RP matrices. In this initialization we chose the scaling factor for Count Sketch with experiments on the validation sets ($\gamma = 0.3$). We used the document codes inferred with the autoencoders in a document retrieval task, similarly to the evaluation in Section 4.1.3. We use AUC to compare the performance of the trained networks. Similarly to the previous experiments with RP initialization, for each dataset and RP initialization scheme we trained ten network instances with different random number seeds. In Table 5.1 we report median AUC values for different initialization schemes. In Fig. 5.3 and Fig. 5.4 we present the precision-recall curves for autoencoders with the median value of AUC. Each curve for a RP-initialized autoencoder (plotted in dashed orange line) is juxtaposed with the curve for the reference Gaussian-initialized autoencoder (plotted in solid blue line).

In general, RP initialization had little effect on the document retrieval performance.

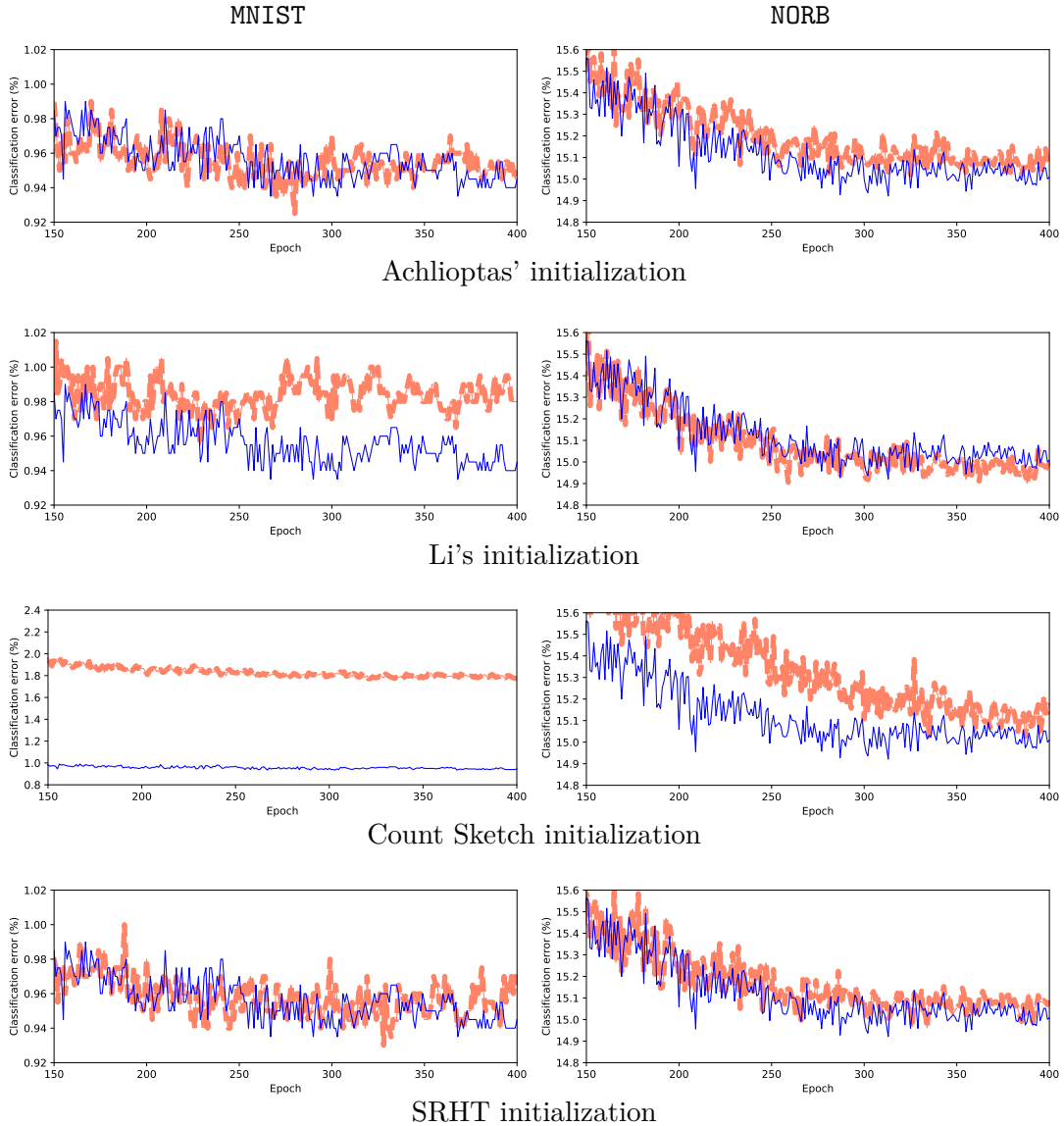


Figure 5.2: RP initialization in pretrained networks. Plots show median test error on MNIST and NORB datasets for different RP initializations (dashed orange line) and the reference Gaussian initialization (solid blue line).

Only for the TNG dataset the Count Sketch initialization yielded slightly better network performance compared to the standard Gaussian initialization.

5.4 Conclusions

In this chapter we explored the viability of initializing deep networks with different RP matrices. We motivated why RP matrices that satisfy the Johnson–Lindenstrauss lemma may serve as good initial weights in deep networks. We then experimentally

Table 5.1: Median area under the precision-recall curve for deep autoencoders initialized with RP matrices.

Weight initialization scheme	Dataset	
	TNG	RCV1
Gaussian (reference)	0.373	0.315
Achlioptas'	0.372	0.314
Li's	0.373	0.311
SRHT	0.372	0.314
Count Sketch	0.381	0.310

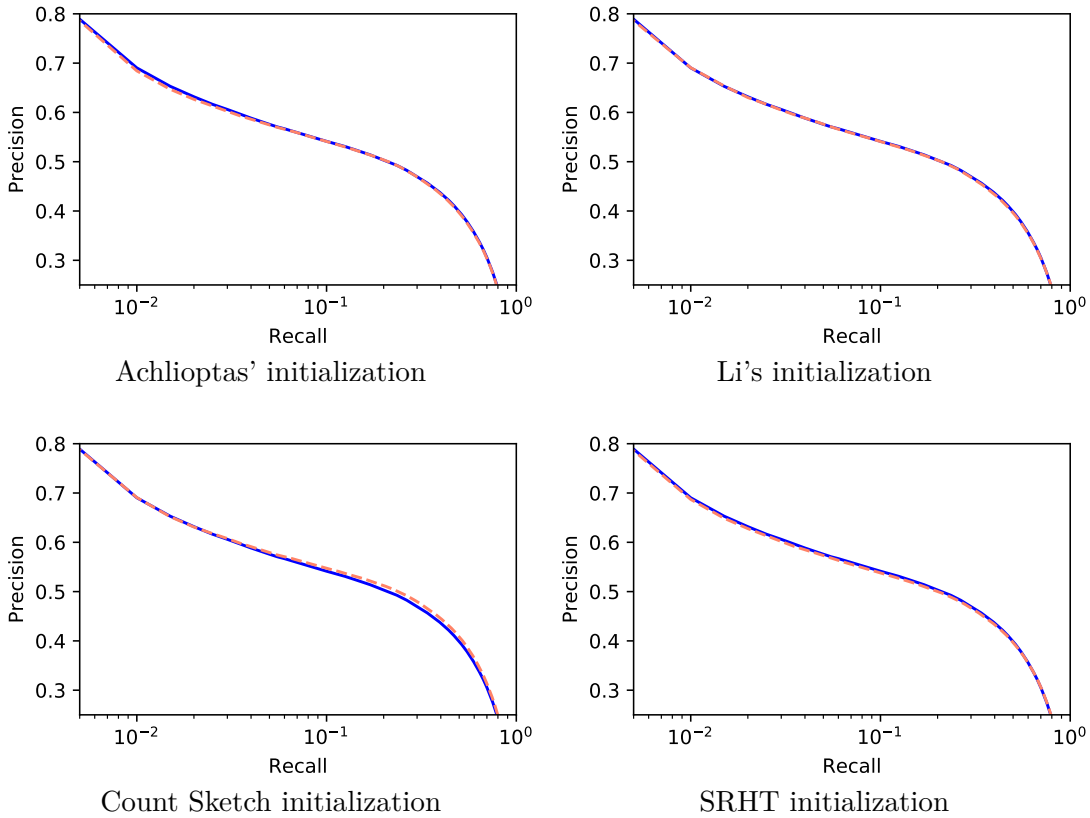


Figure 5.3: RP initialization in autoencoders. Plots show the precision-recall curves for results with median AUC on the TNG dataset for different RP initializations (dashed orange line) and the reference Gaussian initialization (solid blue line).

evaluated the performance of modern networks initialized with RP matrices. Specifically, we experimented with CNNs and with pretrained networks using Achlioptas', Li's, SRHT and Count Sketch RP matrices.

Our results show that dense orthogonal RP initialization schemes can improve the performance of deep convolutional neural networks. In particular, in our evaluation, the

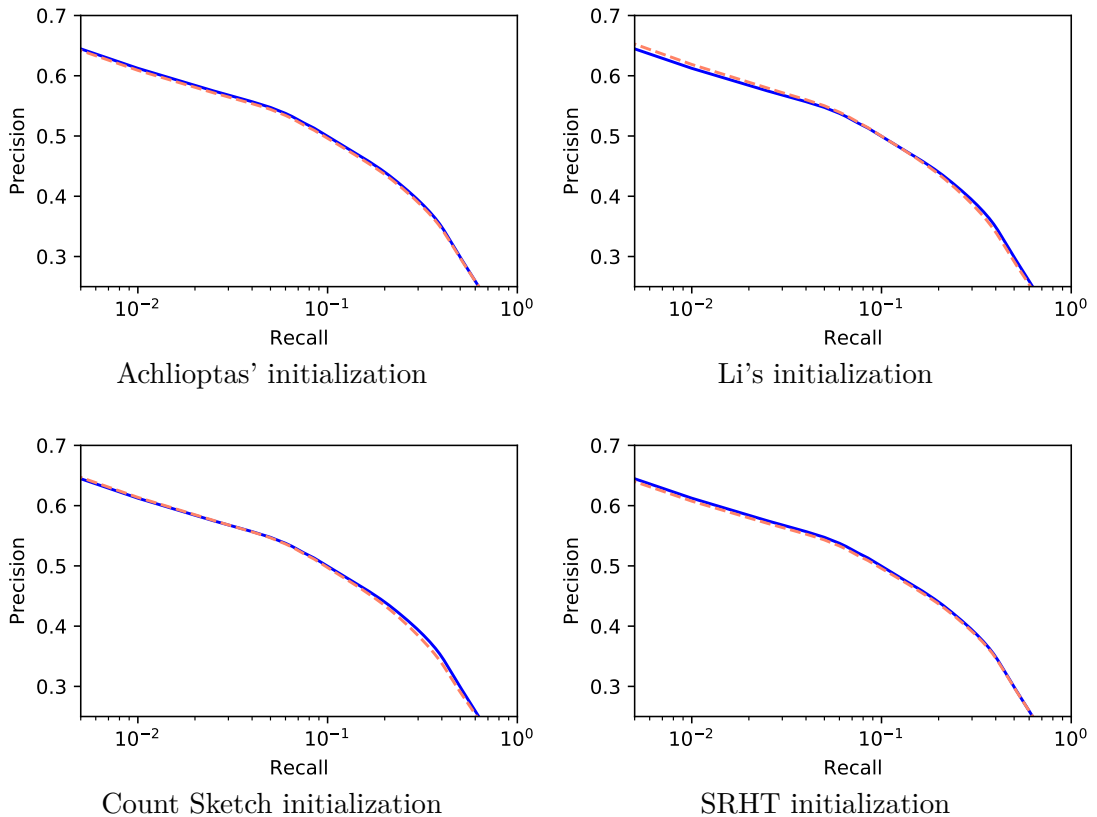


Figure 5.4: RP initialization in autoencoders. Plots show the precision-recall curves for results with median AUC on the RCV1 dataset for different RP initializations (dashed orange line) and the reference Gaussian initialization (solid blue line).

initialization based on SRHT outperformed the reference He’s initialization in state-of-the-art ResNets with stochastic depth. Sparse RP initializations, i.e., Li’s, Achlioptas’ and Count Sketch, yielded results that were inconsistent among different benchmarks.

In pretrained networks RP initialization usually yielded results close to the results obtained with the standard Gaussian initialization. Only the Count Sketch initialization yielded significantly different results: it performed much worse than the reference in image classification networks while in autoencoders used for document retrieval it performed better. We argue that this poor performance in image classification networks is a consequence of too high sparsity of the Count Sketch matrix. When initializing a fully-connected layer that has d inputs and r outputs with Count Sketch, only r elements are set to non-zero values. Therefore, the sparsity of the weight matrix is $\frac{1}{r}$. In our evaluation of image classification networks, depending on the dataset, Count Sketch scheme initialized only 0.1% of all weights to non-zero values. While sparsely initialized pretrained networks have been shown to perform well in [Grzegorzczuk et al. 2015], the Martens’ initialization used therein resulted in approximately 10-times denser initial weight matrices. The autoencoder networks in our experiments were built with much smaller layers compared to the image classification networks. As a result, the weight

matrices in autoencoders were initialized more densely.

CHAPTER 6

CONCLUSIONS

In this work we studied areas in which deep neural networks can benefit from random projection. We started by reviewing the challenges to training machine learning models on extremely high-dimensional data and by discussing the existing approaches. We focused on a particularly difficult type of data – data that is represented by millions of features, is sparse and lacks a structure that could be exploited to simplify the learning model. We discussed why efficiently training DNNs on such type of data is a challenging task and how this challenge can be overcome by incorporating a novel type of layer into the network architecture. Specifically, we propose to extend the network architecture with a layer that incorporates a random projection operation. We consider two variants of the proposed RP layer: one in which its weights are fixed and one where they are learned during training. We found that training the weights in the RP layer, although computationally much more expensive, can significantly improve the overall network performance. We proposed several modifications to the network architecture and the training regime that enabled efficient training DNNs with learnable RP layer on data with as many as tens of millions of input features and examples. Specifically:

- we initialize the RP layer weights with a sparse random projection scheme,
- we finetune only these weights in the RP that were initialized to non-zero values, i.e., we employ sparse connectivity in the RP layer,
- we batch normalize the activations of the RP layer,
- we use linear activation function after the batch normalization,
- we update weights in the RP layer only for a fraction of the training mini-batches.

We conducted an evaluation of DNNs with the RP layer on several large-scale synthetic and real-world datasets. The evaluation showed that our approach is not only viable but also competitive in terms of performance with the state-of-the-art techniques. In particular, incorporating RP into the DNN architecture allowed us to improve the state-of-the-art classification error by over 30% on two real-world benchmarks: **url** and **webspam**. These results open a path to applying neural networks in tasks where directly learning from the data was previously infeasible because of the overly high dimensionality of input examples. The main limitation of our approach is that it is computationally more expensive than classic methods, such as linear SVMs. However, with an already

trained model, the inference time of DNNs with the RP layer is small: feeding a training example through the RP layer can be realized with a single matrix multiplication. By using fast RP schemes, this operation can be performed in linear or nearly linear time. The transformations in subsequent layers can be implemented efficiently on modern hardware, e.g., on GPGPUs. Therefore, despite the high computational cost of training, neural networks with RP layer can be used to solve practical problems. We also found that random projection is useful for initialization of weights in DNNs. Specifically, we propose to initialize the weights in DNNs with scaled RP matrices. This approach yielded deep CNN models that perform better than networks initialized with the current state-of-the-art He’s method. Together, our results fully prove the thesis stated in the introduction: random projection can be beneficial for training deep neural networks by enabling DNNs to learn from sparse, unstructured, high-dimensional data and by improving the network initialization.

In our evaluation, we tested five RP matrix constructions: Gaussian, Achlioptas’, Li’s, SRHT and Count Sketch. Our experiments suggest that in neural network applications the crucial properties of an RP construction are its density and orthogonality. Specifically, in networks with fixed-weight RP layer, orthogonal projection schemes work best. For weight initialization the most successful schemes are the ones that are both orthogonal and dense. Finally, sparse orthogonal schemes yield the best results in finetuned RP layers. Out of the evaluated schemes, the most useful for practical application are therefore the SRHT and Count Sketch constructions. When employed for training DNNs with fixed-weight RP layers, they combine the most efficient projection with the best performance of the final models. Because of its sparsity, Count Sketch projection matrix is also suitable for learnable RP layer. Since networks with finetuned RP layer outperform models with fixed-weight random projection, Count Sketch is the overall best RP construction for deep neural networks. For weight initialization, the best performing RP scheme was SRHT. In our experiments, it improved the performance of the state-of-the-art ResNets on several benchmark datasets. All sparse RP constructions performed poorly when used for weight initialization.

In future work we plan to investigate novel RP schemes proposed during the work on this thesis. In particular, we are eager to explore applications in DNNs of a new family of dense structured random matrices, which extends constructions such as the circulant, Hankel or Toeplitz matrices [Choromanski and Sindhvani 2016]. This family, called random ortho-matrices (ROM) [Choromanski et al. 2017; Felix et al. 2016], provides promising theoretical guarantees on the embedding quality and, as their name suggests, are fully-orthogonal. These two properties should make ROMs a perfect candidate for application in DNNs, especially for weight initialization. We also plan to further investigate training strategies for finetuned RP layers and, especially, the feasibility of changing the connectivity of neurons in the RP layer during finetuning. In other words, we want to update not only the weights that are initially non-zero, but also the weights that are initially set to zero but receive large gradients during training. To prevent the number of learnable parameters from growing uncontrollably, the weights that consistently receive small gradient can be removed from the set of updated weights. We hope that these approaches will further improve performance of DNNs applied to sparse, high-dimensional, unstructured data.

APPENDIX A

DATASETS

In this appendix we list and briefly describe the datasets used in this work. A summary of these datasets is given in Table A.1.

Table A.1: A summary of the datasets used in the conducted experiments. Density is the fraction of non-zero elements in the training set.

Dataset	Training set size	Test set size	Dimensionality	Classes	Density
MNIST	60,000	10,000	784	10	0.191
NORB	291,600	58,320	2,048	6	dense
CIFAR-10	50,000	10,000	3,072	10	dense
CIFAR-100	50,000	10,000	3,072	100	dense
SVHN	604,388	26,032	3,072	10	dense
TNG	11,314	7,532	2,000	20	0.034
RCV1	402,207	402,207	2,000	103	0.035
url	1,976,130	420,000	3,231,961	2	$3.58 \cdot 10^{-5}$
webspam	280,000	70,000	16,609,143	2	$2.24 \cdot 10^{-4}$
KDD2010-a	8,407,752	510,302	20,216,830	2	$1.80 \cdot 10^{-6}$
KDD2010-b	19,264,097	748,401	29,890,095	2	$9.84 \cdot 10^{-7}$
synthetic	1,000,000	250,000	1,000,000	2	from 10^{-6} to $1.7 \cdot 10^{-4}$

MNIST

The MNIST dataset [LeCun et al. 1998a]¹ is a widely used benchmark for machine learning algorithms. It consists of images of handwritten digits (Figure A.1). In the original dataset the images are represented by 256 grey-scale levels, but in this work we use pixel intensities rescaled to the $[0, 1]$ interval. We use the permutation invariant version of the dataset, i.e., we randomly shuffle the pixel order.

¹ Available at <http://yann.lecun.com/exdb/mnist/>

0 1 2 3 4 5 6 7 8 9

Figure A.1: Example MNIST images.

NORB

The Jittered-Cluttered NORB dataset [LeCun et al. 2004]² consists of images depicting one of 50 toys on diverse background captured in stereo mode under variable lighting and viewpoints (Figure A.2). Following Nair and Hinton [2010] we resized original

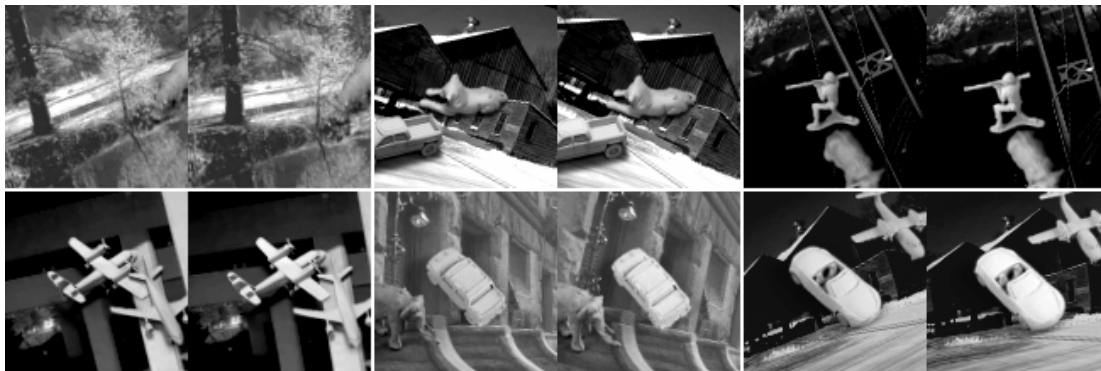


Figure A.2: Example NORB images (one from each of the six classes).

images to 32×64 pixels, subtracted from each image its mean pixel intensity, divided pixel intensities by the standard deviation of pixel intensities in the training set and constructed a validation set consisting of 58,320 cases from the training set.

20-newsgroups (TNG)

The TNG dataset³ is a collection of posts from 20 Usenet newsgroups. Topics in TNG range from religion (e.g., *talk.religion.misc*, *alt.atheism*, *soc.religion.christian*) to computer hardware (e.g., *comp.sys.ibm.pc.hardware*, *comp.sys.mac.hardware*). Following Salakhutdinov and Hinton [2009] we preprocessed the corpus by removing the stop-words, stemming it and constructing a BOW representation using the most common words in the training set. For our experiments we created several dataset variants with different vocabulary sizes, ranging from 2000 to 10,000. For the validation set we use 3,000 documents randomly extracted from the training set.

Reuters Corpus Volume I (RCV1)

Reuters Corpus Volume I [Lewis et al. 2004] is an archive of over 800,000 English newswire stories published between August 1996 and August 1997. We use its corrected version RCV1-v2. Each newswire story in the corpus has been categorized (multi-labeled) into 103 topics from four main groups: Corporate/Industrial, Economics, Government/Social and Markets. Topics from each group form a hierarchical structure,

² Available at <https://cs.nyu.edu/~y1clab/data/norb-v1.0/>

³ Available at <http://qwone.com/~jason/20Newsgroups>

typically with depth three. Following Salakhutdinov and Hinton [2009] we define the relevance of two documents to be the fraction of their agreeing topics. We apply the same train/test split and preprocessing scheme as Salakhutdinov and Hinton [2009]. Similarly to TNG we experiment on BOW dataset variants created over dictionaries with vocabulary sizes ranging from 2000 to 10,000.

Malicious URL (`url`)

`url` [Ma et al. 2009]⁴ is a large binary classification dataset often used for evaluating online learning methods. It consists of 3.2M-dimensional descriptors of 2.4M URL addresses. Descriptors contain lexical features (BOW representations of tokens in the URL) and host-based features (WHOIS information, location, connection, speed, blacklist membership, etc.). The challenge in this dataset is to recognize malicious addresses from benign addresses. Following Wang et al. [2011] we use examples from the first 100 days of data collection as the training set and remaining examples for testing.

KDD2010-a and KDD2010-b

KDD2010-a and KDD2010-b are large student performance prediction datasets from the *KDD Cup 2010* educational data mining competition. We use a preprocessed versions of these datasets made available by the challenge winner [Yu et al. 2010]⁵. For validation we use random subsets of the training set with the same size as the corresponding test sets.

webspam

`webspam` [Webb et al. 2006] is a document dataset consisting of 350,000 descriptors of web pages, which was originally used in Pascal Large Scale Learning Challenge [Sonnenburg et al. 2008]. The challenge in this dataset is to detect examples of the, so called, *Webspam* (or *search spam*), i.e., web pages that are designed to manipulate search engine results. We use the normalized trigram representation available at the LibSVM dataset repository⁶. The original dataset is not split into training and testing set. Therefore, following [Wang et al. 2011] we use a random 80/20 train/test split.

CIFAR-10 and CIFAR-100

CIFAR-10 and CIFAR-100 [Krizhevsky 2009]⁷ are relatively small, widely used benchmarks in machine learning. The task is to classify 32×32 RGB images (Figure A.3) across 10 or 100 categories (for CIFAR-10 and CIFAR-100, respectively). The images are a subset of the 80 million tiny images dataset⁸. We preprocessed the datasets following Huang et al. [2016]. Specifically, we randomly extracted 5000 images from the training sets and used them as the validation sets. We applied standard data augmentation steps, i.e., horizontal flipping and translation by 4 pixels.

⁴ Available at <http://sysnet.ucsd.edu/projects/url/>

⁵ Available at <https://www.csie.ntu.edu.tw/~cjlin/libsvmtools/datasets/>

⁶ Available at <https://www.csie.ntu.edu.tw/~cjlin/libsvmtools/datasets/>

⁷ Available at <https://www.cs.toronto.edu/~kriz/cifar.html>

⁸ <http://people.csail.mit.edu/torralba/tinyimages/>

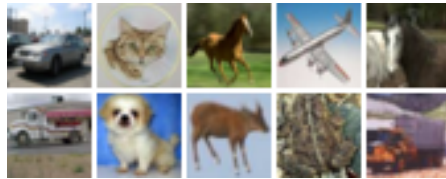


Figure A.3: Example CIFAR images.

Street View House Number (SVHN)

Similarly to MNIST, SVHN⁹ is a digit classification dataset. We use its version that contains 32×32 cropped RGB images extracted from house numbers from Google Street View photographs (Figure A.4). We constructed the validation set and preprocessed the data



Figure A.4: Example SVHN images.

following Huang et al. [2016].

Synthetic datasets

We prepared several 10^6 -dimensional synthetic datasets, each consisting of $1.25 \cdot 10^6$ examples belonging to two balanced classes. Each dataset was constructed by first generating a ρ -dense matrix \mathbf{S} (ρ being the fraction of non-zero elements in \mathbf{S}) and then selecting a fraction of features, ϕ , that would separate examples from the two classes. We refer to these features as the *significant features*. Non-zero elements in \mathbf{S} were drawn randomly from $\mathcal{N}(0,1)$. To separate the classes we picked examples from one class and added a Gaussian noise with non-zero mean to all non-zero elements in significant features. Note that this does not alter the sparsity of \mathbf{S} . We generated two groups of such sparse datasets:

- datasets with fixed fraction of significant features: $\phi = 0.2$ and density ρ ranging from 10^{-6} to 10^{-4} ,
- datasets with fixed density: $\rho = 10^{-4}$ and a fraction of significant features ϕ ranging from 0.01 to 0.2.

The above ranges for ρ and ϕ were chosen so that the most difficult dataset variants had, on average, one or two significant non-zero features per example. We randomly selected 80% rows of \mathbf{S} as the training set and the remaining 20% as the test set.

⁹ Available at <http://ufldl.stanford.edu/housenumbers/>

LIST OF TABLES

3.1	Properties of random projection schemes. \mathbf{A} is a $n \times d$ dataset matrix and k is the projected dimensionality. For sparse matrices \mathbf{A} , $\text{nnz}(\mathbf{A})$ denotes the number of non-zero elements in \mathbf{A} . Embedding quality is the dimensionality for which the oblivious subspace embedding property is satisfied.	31
4.1	Early stopping errors (%) for different dimensionality reduction methods. For each dataset we highlight the best performing dimensionality reduction technique.	44
4.2	Test errors (%) for linear classifiers trained on the unprojected data. For a comparison, we also report the test errors for deep networks trained on data projected with Gaussian random projection.	46
4.3	Average time T_{DR} of performing dimensionality reduction. In parenthesis we report $T_{DR}/T_{\text{total}} = T_{DR}/(T_{DR} + T_{\text{train}})$ – the fraction of time required to reduce the data dimensionality over the total time of training the network.	47
4.4	Average time of training linear classifiers on the original data. For a comparison, we also report training times for deep networks trained on data projected with Gaussian random projection.	48
4.5	Classification errors (%) on large-scale real-world datasets. For each dataset we highlight the result of the best performing method.	50
4.6	Area under the precision-recall curve for deep autoencoders with RP layer trained on different TNG representations. The baseline network trained on 2000-dimensional bag-of-words data achieves AUC of 0.373.	53
4.7	Area under the precision-recall curve for deep autoencoders with RP layer trained on different RCV1 representations. The baseline network trained on 2000-dimensional bag-of-words data achieves AUC of 0.315.	53
4.8	Test errors (%) for networks with Li’s finetuned random projection layer trained using different normalization schemes.	57
4.9	Test errors (%) for networks with Count Sketch finetuned random projection layer trained using different normalization schemes.	57
4.10	Test errors (%) for networks with Li’s finetuned random projection layer using different activation functions.	60
4.11	Test errors (%) for networks with Count Sketch finetuned random projection layer using different activation functions.	60
4.12	Maximum and average number of non-zero elements in rows of the training data matrix for large-scale datasets.	63

4.13	Time complexity of constructing a random projection matrix and performing the projection via matrix multiplication \mathbf{AP} , where \mathbf{A} is a $n \times d$ data matrix and \mathbf{P} is a $d \times k$ projection matrix. $\text{nnz}(\mathbf{A})$ denotes the number of non-zero elements in matrix \mathbf{A} . K is the maximum number of non-zero elements in rows of \mathbf{A} and columns of \mathbf{P}	64
5.1	Median area under the precision-recall curve for deep autoencoders initialized with RP matrices.	80
A.1	A summary of the datasets used in the conducted experiments. Density is the fraction of non-zero elements in the training set.	85

LIST OF FIGURES

2.1	A schematic representation of a multilayer perceptron.	6
4.1	Neural network with fixed-weight random projection layer.	35
4.2	Classification error for different sizes of the random projection input layer (k). Gaussian, Achlioptas' and SRHT yielded almost equal results.	39
4.3	Average time of performing random projection on the million-dimensional synthetic dataset ($\rho = 10^{-5}$, $\psi = 0.2$) for different RP layer size k	40
4.4	Average time of generating an RP matrix and performing the projection by matrix multiplication for the synthetic dataset.	41
4.5	Classification error on the synthetic datasets with fixed significant feature fraction $\psi = 0.2$ and varying density level ρ	42
4.6	Classification error on the synthetic datasets with fixed density $\rho = 10^{-4}$ and varying fraction of significant features ψ	43
4.7	Visualization of features that were chosen by different feature selection methods on the MNIST dataset. Selected and discarded features are represented by white and black pixels, respectively.	45
4.8	Precision-recall curves for deep autoencoders trained on unprojected BOW data (solid red line) and randomly projected BOW representations (dashed lines).	54
4.9	Neural network with finetuned random projection layer. Weights in the finetuned random projection layer are initialized to a sparse RP matrix. Only the weights that are initially non-zero are part of the model. The output of the projection is batch normalized and optionally transformed with a nonlinear activation function.	55
4.10	Influence of η on the performance of networks with finetuned random projection layer. η is the fraction of mini-batches used to train the random projection layer.	59
4.11	Performance of networks with different activation functions in the finetuned random projection layer for varying number of outputs, k , in the RP layer.	61
4.12	Random projection procedure with columnwise slicing of the projection matrix. \mathbf{A} is the dataset matrix, \mathbf{P} is the projection matrix and \mathbf{R} is the result matrix. The number of projection matrix slices is v . $[\mathbf{X}, \mathbf{Y}]$ operation denotes the columnwise concatenation of matrices \mathbf{X} and \mathbf{Y}	64

4.13	Random projection procedure with rowwise slicing of the data matrix and columnwise slicing of the projection matrix. \mathbf{A} is the dataset matrix, \mathbf{P} is the projection matrix and \mathbf{R} is the result matrix. v and h are the numbers of projection and dataset matrix slices, respectively.	65
5.1	RP initialization in convolutional neural networks. Plots show median test error on CIFAR-10, CIFAR-100 and SVHN for different RP initializations (dashed orange line) and the reference He's initialization (solid blue line).	77
5.2	RP initialization in pretrained networks. Plots show median test error on MNIST and NORB datasets for different RP initializations (dashed orange line) and the reference Gaussian initialization (solid blue line).	79
5.3	RP initialization in autoencoders. Plots show the precision-recall curves for results with median AUC on the TNG dataset for different RP initializations (dashed orange line) and the reference Gaussian initialization (solid blue line).	80
5.4	RP initialization in autoencoders. Plots show the precision-recall curves for results with median AUC on the RCV1 dataset for different RP initializations (dashed orange line) and the reference Gaussian initialization (solid blue line).	81
A.1	Example MNIST images.	86
A.2	Example NORB images (one from each of the six classes).	86
A.3	Example CIFAR images.	88
A.4	Example SVHN images.	88

ACRONYMS

ADMM	alternating direction method of multipliers. 49, 50
AMM	adaptive multi-hyperplane machine. 50
AUC	area under the precision-recall curve. 52, 78
BM	block minimization. 49
BN	batch normalization. 10, 11, 56, 58, 67, 70
BOW	bag-of-words. 14–17, 19, 34, 51–53, 66, 67, 86, 87
CCA	canonical correlations analysis. 21, 22
CCIPCA	candid covariance-free incremental principal component analysis. 22
CD	contrastive divergence. 12, 38, 51, 52, 62, 73, 75, 78
CE	cross entropy. 9, 38, 44, 49, 51
CNN	convolutional neural network. 1–3, 5, 13, 14, 17, 69, 72–78, 80, 84
CSR	compressed sparse row. 62
DADM	dual alternating direction method. 49–51
DBN	deep belief network. 5, 11, 12, 35, 45, 51, 52, 61, 72, 78
DNN	deep neural network. 1–3, 5, 8, 10, 14, 34, 36, 37, 40–44, 46, 48, 50, 51, 62, 66, 72, 83, 84
GPGPU	general-purpose computing on graphics processing units. 1, 61, 84
ICA	independent component analysis. 21, 22
IDR/QR	incremental dimension reduction via QR decomposition. 22
IG	information gain. 19, 38, 44, 45, 66

ILDA	incremental linear discriminant analysis. 22
IMMC	incremental maximum margin criterion. 22
IPCA	incremental principal component analysis. 22
JLT	Johnson-Lindenstrauss transform. 26
LDA	linear discriminant analysis. 19–22
LPP	locality preserving projections. 21, 22
LR	logistic regression. 1, 34, 46
LReLU	leaky rectified linear unit. 7, 58
MAF	maximum autocorrelation factors. 21, 22
MDS	multidimensional scaling. 19, 21, 22
MLP	multilayer perceptron. 5–7, 12, 13, 57, 61
MMC	maximum margin criterion. 19, 22
MSE	mean square error. 9
NReLU	noisy rectified linear unit. 12, 72
OSE	oblivious subspace embedding. 25–27, 29
PCA	principal component analysis. 18, 19, 21–23, 38, 44, 46–48, 66
PmSVM	power mean support vector machine. 49, 50
PmSVM-LUT	power mean support vector machine with look-up tables. 50, 51
RBM	restricted Boltzmann machine. 11, 12, 51, 61, 73, 75
ReLU	rectified linear unit. 7, 13, 37, 38, 57–61, 69, 70, 72, 78
ResNet	residual neural network. 14, 75, 76, 81, 84
RP	random projection. 1–3, 19, 23, 25–28, 30, 31, 33–48, 50–67, 69, 73–76, 78–81, 83, 84
RW-FNN	random weight feedforward neural network. 36
SBM	selective block minimization. 49, 50
SDR	sufficient dimensionality reduction. 21
SFA	slow feature analysis. 21, 22
SGD	stochastic gradient descent. 8, 10, 13, 38, 49, 55, 57, 70, 71, 78

SI	sparse initialization. 71
SMMP	sparse matrix multiplication package. 40, 62, 63
SNP	single nucleotide polymorphism. 16
SRDA	spectral regression discriminant analysis. 22
SRHT	subsampled randomized Hadamard transform. 3, 25, 27, 29–31, 34, 36–40, 42, 44, 46, 48, 50, 62, 64, 66, 69, 74–78, 80, 81, 84
SVD	singular value decomposition. 22, 23, 66
SVM	support vector machine. 1, 20, 34, 37, 46, 49, 50, 83
TF-IDF	term frequency–inverse document frequency. 52
URL	uniform resource locator. 16, 17, 51
VW	Vowpal Wabbit. 49, 50

BIBLIOGRAPHY

- Dimitris Achlioptas. 2001. Database-friendly random projections. In *Proceedings of the 20th ACM SIGMOD-SIGACT-SIGART Symposium on Principles of Database Systems*. ACM, 274–281.
- Nir Ailon and Bernard Chazelle. 2006. Approximate nearest neighbors and the fast Johnson-Lindenstrauss transform. In *Proceedings of the 38th Annual ACM Symposium on Theory of Computing*. ACM, 557–563.
- Nir Ailon and Edo Liberty. 2009. Fast dimension reduction using Rademacher series on dual BCH codes. *Discrete & Computational Geometry* 42, 4 (2009), 615–630.
- Noga Alon. 2003. Problems and results in extremal combinatorics-I. *Discrete Mathematics* 273, 1 (2003), 31–53.
- Rosa I Arriaga and Santosh Vempala. 2006. An algorithmic theory of learning: Robust concepts and random projection. *Machine Learning* 63, 2 (2006), 161–182.
- Randolph E Bank and Craig C Douglas. 1993. Sparse matrix multiplication package (SMMP). *Advances in Computational Mathematics* 1, 1 (1993), 127–137.
- Michael R Barnes. 2002. SNP and mutation data on the Web-hidden treasures for uncovering. *Comparative and Functional Genomics* 3, 1 (2002), 67–74.
- Richard E Bellman. 1961. *Adaptive control processes: a guided tour*. Princeton University Press.
- Yoshua Bengio. 2012a. Deep Learning of Representations for Unsupervised and Transfer Learning. In *Proceedings of ICML Workshop on Unsupervised and Transfer Learning*, Vincent Lemaire Graham Taylor Daniel Silver Isabelle Guyon, Gideon Dror (Ed.). PMLR, 17–36.
- Yoshua Bengio. 2012b. Practical Recommendations for Gradient-Based Training of Deep Architectures. In *Neural Networks: Tricks of the Trade*, Grégoire Montavon, Geneviève B. Orr, and Klaus-Robert Müller (Eds.). Lecture Notes in Computer Science, Vol. 7700. Springer Berlin Heidelberg, 437–478.
- Dimitri P Bertsekas. 2010. *Incremental gradient, subgradient, and proximal methods for convex optimization: A survey*. Technical Report LIDS-P-2848. Laboratory for Information and Decision Systems, MIT.

- Ella Bingham and Heikki Mannila. 2001. Random projection in dimensionality reduction: applications to image and text data. In *Proceedings of the 7th ACM SIGKDD International Conference on Knowledge Discovery and Data Mining*. ACM, 245–250.
- Verónica Bolón-Canedo, Noelia Sánchez-Marroño, and Amparo Alonso-Betanzos. 2015. Recent advances and emerging challenges of feature selection in the context of big data. *Knowledge-Based Systems* 86 (2015), 33–45.
- Léon Bottou. 1998. Online algorithms and stochastic approximations. In *Online Learning in Neural Networks*, David Saad (Ed.). Vol. 5. Cambridge Univ. Press, 9–42.
- Hervé Bourlard and Yves Kamp. 1988. Auto-association by multilayer perceptrons and singular value decomposition. *Biological Cybernetics* 59, 4 (1988), 291–294.
- Olivier Bousquet and Léon Bottou. 2008. The tradeoffs of large scale learning. In *Advances in Neural Information Processing Systems 20 (NIPS'07)*, J.C. Platt, D. Koller, Y. Singer, and S.T. Roweis (Eds.). Curran Associates Inc., 161–168.
- Christos Boutsidis, Anastasios Zouzias, and Petros Drineas. 2010. Random projections for k-means clustering. In *Advances in Neural Information Processing Systems 23 (NIPS'10)*, J. Shawe-Taylor R.S. Zemel A. Culotta J.D. Lafferty, C.K.I. Williams (Ed.). Curran Associates Inc., 298–306.
- Leo Breiman. 1996. Bagging predictors. *Machine Learning* 24, 2 (1996), 123–140.
- John S Bridle. 1990. Probabilistic Interpretation of Feedforward Classification Network Outputs, with Relationships to Statistical Pattern Recognition. In *Neurocomputing*, Fogelman Soulié and Jeanny Héroult (Eds.). Springer Berlin Heidelberg, 227–236.
- Deng Cai, Xiaofei He, and Jiawei Han. 2008. SRDA: An efficient algorithm for large-scale discriminant analysis. *IEEE Transactions on Knowledge and Data Engineering* 20, 1 (2008), 1–12.
- Kai-Wei Chang and Dan Roth. 2011. Selective block minimization for faster convergence of limited memory large-scale linear models. In *Proceedings of the 17th ACM SIGKDD International Conference on Knowledge Discovery and Data Mining*. ACM, 699–707.
- Moses Charikar, Kevin Chen, and Martin Farach-Colton. 2004. Finding frequent items in data streams. *Theoretical Computer Science* 312, 1 (2004), 3–15.
- Yi-Wei Chen and Chih-Jen Lin. 2006. Combining SVMs with various feature selection strategies. In *Feature Extraction*, Steve Gunn-Lotfi A. Zadeh Isabelle Guyon, Masoud Nikravesh (Ed.). Springer, 315–324.
- Anna Choromanska, Krzysztof Choromanski, Mariusz Bojarski, Tony Jebara, Sanjiv Kumar, and Yann LeCun. 2016. Binary embeddings with structured hashed projections. In *Proceedings of the 33rd International Conference on Machine Learning (ICML'16)*, Kilian Q. Weinberger Maria Florina Balcan (Ed.). PMLR, 344–353.

- Krzysztof Choromanski and Vikas Sindhwani. 2016. Recycling randomness with structure for sublinear time kernel expansions. In *Proceedings of the 33rd International Conference on Machine Learning (ICML'16)*, Kilian Q. Weinberger Maria Florina Balcan (Ed.). PMLR, 2502–2510.
- Krzysztof M Choromanski, Mark Rowland, and Adrian Weller. 2017. The unreasonable effectiveness of structured random orthogonal embeddings. In *Advances in Neural Information Processing Systems 30 (NIPS'17)*, S. Bengio-H. Wallach R. Fergus S. Vishwanathan R. Garnett I. Guyon, U.V. Luxburg (Ed.). Curran Associates Inc., 218–227.
- Robert Clarke, Habtom W Resson, Antai Wang, Jianhua Xuan, Minetta C Liu, Edmund A Gehan, and Yue Wang. 2008. The properties of high-dimensional data spaces: implications for exploring gene and protein expression data. *Nature Reviews Cancer* 8, 1 (2008), 37–49.
- Kenneth L Clarkson and David P Woodruff. 2013. Low rank approximation and regression in input sparsity time. In *Proceedings of the 45th Annual ACM Symposium on Theory of Computing*. ACM, 81–90.
- Djork-Arné Clevert, Thomas Unterthiner, and Sepp Hochreiter. 2015. Fast and accurate deep network learning by exponential linear units (ELUs). *CoRR* abs/1511.07289 (2015).
- Adam Coates, Brody Huval, Tao Wang, David Wu, Bryan Catanzaro, and Ng Andrew. 2013. Deep learning with COTS HPC systems. In *Proceedings of the 30th International Conference on Machine Learning (ICML'13)*, David McAllester Sanjoy Dasgupta (Ed.). PMLR, 1337–1345.
- Corinna Cortes and Vladimir Vapnik. 1995. Support-vector networks. *Machine Learning* 20, 3 (1995), 273–297.
- John P Cunningham and Zoubin Ghahramani. 2015. Linear dimensionality reduction: Survey, insights, and generalizations. *Journal of Machine Learning Research* 16 (2015), 2859–2900.
- George E Dahl, Jack W Stokes, Li Deng, and Dong Yu. 2013. Large-scale malware classification using random projections and neural networks. In *Proceedings of 2013 IEEE International Conference on Acoustics, Speech and Signal Processing (ICASSP)*. IEEE, 3422–3426.
- Anirban Dasgupta, Ravi Kumar, and Tamás Sarlós. 2010. A sparse Johnson-Lindenstrauss transform. In *Proceedings of the 42nd Annual ACM Symposium on Theory of Computing*. ACM, 341–350.
- Sanjoy Dasgupta and Anupam Gupta. 2003. An elementary proof of a theorem of Johnson and Lindenstrauss. *Random Structures & Algorithms* 22, 1 (2003), 60–65.
- David L Donoho. 2000. High-dimensional data analysis: The curses and blessings of dimensionality. *AMS Math Challenges Lecture* (2000), 1–32.

- David L Donoho. 2006. Compressed sensing. *IEEE Transactions on Information Theory* 52, 4 (2006), 1289–1306.
- Gian Paolo Drago and Sandro Ridella. 1992. Statistically controlled activation weight initialization (SCAWI). *IEEE Transactions on Neural Networks* 3, 4 (1992), 627–631.
- Richard O Duda, Peter E Hart, and David G Stork. 2012. *Pattern classification*. John Wiley & Sons.
- Dumitru Erhan, Yoshua Bengio, Aaron Courville, Pierre-Antoine Manzagol, Pascal Vincent, and Samy Bengio. 2010. Why does unsupervised pre-training help deep learning? *Journal of Machine Learning Research* 11 (2010), 625–660.
- Rong-En Fan, Kai-Wei Chang, Cho-Jui Hsieh, Xiang-Rui Wang, and Chih-Jen Lin. 2008. LIBLINEAR: A library for large linear classification. *Journal of Machine Learning Research* 9 (2008), 1871–1874.
- Usama Fayyad and Keki Irani. 1993. Multi-interval discretization of continuous-valued attributes for classification learning. In *Proceedings of the 13th International Joint Conference on Artificial Intelligence*. Morgan Kaufmann Publishers Inc., 1022–1029.
- Kinnan Yu Felix, Ananda Theertha Suresh, Krzysztof Choromanski, Daniel N Holtmann-Rice, and Sanjiv Kumar. 2016. Orthogonal random features. In *Advances in Neural Information Processing Systems 29 (NIPS'16)*, U.V. Luxburg-I. Guyon R. Garnett D.D. Lee, M. Sugiyama (Ed.). Curran Associates Inc., 1975–1983.
- Xiaoli Z Fern and Carla E Brodley. 2003. Random projection for high dimensional data clustering: A cluster ensemble approach. In *Proceedings of the 20th International Conference on Machine Learning (ICML'03)*, Tom Fawcett and Nina Mishra (Eds.). AAAI Press, 186–193.
- George Forman. 2003. An extensive empirical study of feature selection metrics for text classification. *Journal of Machine Learning Research* 3 (2003), 1289–1305.
- Dmitriy Fradkin and David Madigan. 2003. Experiments with random projections for machine learning. In *Proceedings of the 9th ACM SIGKDD International Conference on Knowledge Discovery and Data Mining*. ACM, 517–522.
- Yoav Freund and David Haussler. 1992. Unsupervised learning of distributions on binary vectors using two layer networks. In *Advances in Neural Information Processing Systems 4 (NIPS 1991)*, J.E. Moody, S.J. Hanson, and R.P. Lippmann (Eds.). Morgan Kaufmann Publishers Inc., 912–919.
- Jerome Friedman, Trevor Hastie, and Robert Tibshirani. 2001. *The elements of statistical learning*. Springer.
- Jerome Friedman, Trevor Hastie, and Robert Tibshirani. 2010. Regularization paths for generalized linear models via coordinate descent. *Journal of Statistical Software* 33, 1 (2010), 1–22.

- Steve Gallant and Donald Smith. 1987. Random cells: an idea whose time has come and gone... and come again. In *Proceeding of the 1987 IEEE International Conference on Neural Networks*. IEEE, 671–678.
- Stoyan Georgiev and Sayan Mukherjee. 2012. Randomized dimension reduction on massive data. *CoRR* abs/1211.1642 (2012).
- Raja Giryes, Guillermo Sapiro, and Alex M Bronstein. 2015. Deep Neural Networks with Random Gaussian Weights: A Universal Classification Strategy? *IEEE Transactions on Signal Processing* 64, 13 (2015), 3444–3457.
- Xavier Glorot and Yoshua Bengio. 2010. Understanding the difficulty of training deep feedforward neural networks. In *Proceedings of the 13th International Conference on Artificial Intelligence and Statistics (AISTATS 2010)*, Mike Titterton Yee Whye Teh (Ed.). PMLR, 249–256.
- Xavier Glorot, Antoine Bordes, and Yoshua Bengio. 2011. Deep Sparse Rectifier Neural Networks. In *Proceedings of the 14th International Conference on Artificial Intelligence and Statistics (AISTATS 2011)*, Miroslav Dudik Geoffrey Gordon, David Dunson (Ed.). PMLR, 315–323.
- Navin Goel, George Bebis, and Ara Nefian. 2005. Face recognition experiments with random projection. In *Proceedings of the Biometric Technology for Human Identification II, Volume 5779*, Anil K. Jain; Nalini K. Ratha (Ed.). SPIE, 426–437.
- Jacob Goldberger, Geoffrey E Hinton, Sam T. Roweis, and Ruslan R Salakhutdinov. 2005. Neighbourhood Components Analysis. In *Advances in Neural Information Processing Systems 17 (NIPS'04)*, L. K. Saul, Y. Weiss, and L. Bottou (Eds.). MIT Press, 513–520.
- Gene H Golub and Charles F Van Loan. 2012. *Matrix computations*. JHU Press.
- Ian Goodfellow, Yoshua Bengio, and Aaron Courville. 2016. *Deep learning*. MIT Press.
- Alan Graves, Abdel-rahman Mohamed, and Geoffrey Hinton. 2013. Speech recognition with deep recurrent neural networks. In *Proceedings of 2013 IEEE International Conference on Acoustics, Speech and Signal Processing (ICASSP)*. IEEE, 6645–6649.
- Gero Greiner. 2012. *Sparse Matrix Computations and their I/O Complexity*. Ph.D. Dissertation. Technische Universität München, München.
- Karol Grzegorzcyk, Marcin Kurdziel, and Piotr Iwo Wójcik. 2015. Effects of sparse initialization in deep belief networks. *Computer Science* 16, 4 (2015), 313–327.
- Karol Grzegorzcyk, Marcin Kurdziel, and Piotr Iwo Wójcik. 2016a. Encouraging orthogonality between weight vectors in pretrained deep neural networks. *Neurocomputing* 202 (2016), 84–90.
- Karol Grzegorzcyk, Marcin Kurdziel, and Piotr Iwo Wójcik. 2016b. Implementing deep learning algorithms on graphics processor units. In *Parallel Processing and Applied Mathematics (PPAM 2015)*. Springer, 473–482.

- Quanquan Gu, Zhenhui Li, and Jiawei Han. 2012. Generalized fisher score for feature selection. *CoRR* abs/1202.3725 (2012).
- Isabelle Guyon and André Elisseeff. 2003. An introduction to variable and feature selection. *Journal of Machine Learning Research* 3 (2003), 1157–1182.
- Isabelle Guyon, Jason Weston, Stephen Barnhill, and Vladimir Vapnik. 2002. Gene selection for cancer classification using support vector machines. *Machine Learning* 46, 1-3 (2002), 389–422.
- Nathan Halko, Per-Gunnar Martinsson, Yoel Shkolnisky, and Mark Tygert. 2011. An algorithm for the principal component analysis of large data sets. *SIAM Journal on Scientific Computing* 33, 5 (2011), 2580–2594.
- Kaiming He, Xiangyu Zhang, Shaoqing Ren, and Jian Sun. 2015a. Deep residual learning for image recognition. In *Proceedings of the 2015 IEEE Conference on Computer Vision and Pattern Recognition (CVPR)*. Conference Publishing Services, 770–778.
- Kaiming He, Xiangyu Zhang, Shaoqing Ren, and Jian Sun. 2015b. Delving deep into rectifiers: Surpassing human-level performance on imagenet classification. In *Proceedings of the IEEE International Conference on Computer Vision*. Conference Publishing Services, 1026–1034.
- Xiaofei He and Partha Niyogi. 2004. Locality preserving projections. In *Advances in Neural Information Processing Systems 16 (NIPS'03)*, S. Thrun, L. K. Saul, and B. Schölkopf (Eds.). MIT Press, 153–160.
- Robert Hecht-Nielsen. 1994. Context vectors: general purpose approximate meaning representations self-organized from raw data. In *World Congress on Computational Intelligence, Neural networks*. IEEE Press, 43–56.
- Chinmay Hegde, Mark A Davenport, Michael B Wakin, and Richard G Baraniuk. 2007. Efficient machine learning using random projections. In *Proceedings of the NIPS Workshop on Efficient Machine Learning*. 1–2.
- Jonathan L Herlocker, Joseph A Konstan, Loren G Terveen, and John T Riedl. 2004. Evaluating collaborative filtering recommender systems. *ACM Transactions on Information Systems (TOIS)* 22, 1 (2004), 5–53.
- Geoffrey E Hinton. 2002. Training products of experts by minimizing contrastive divergence. *Neural Computation* 14, 8 (2002), 1771–1800.
- Geoffrey E Hinton. 2012. A Practical Guide to Training Restricted Boltzmann Machines. In *Neural Networks: Tricks of the Trade*, Grégoire Montavon, Geneviève B Orr, and Klaus-Robert Müller (Eds.). Lecture Notes in Computer Science, Vol. 7700. Springer Berlin Heidelberg, 599–619.
- Geoffrey E Hinton, Li Deng, Dong Yu, George E Dahl, Abdel-rahman Mohamed, Navdeep Jaitly, Andrew Senior, Vincent Vanhoucke, Patrick Nguyen, Tara N Sainath,

- and B Kingsbury. 2012. Deep neural networks for acoustic modeling in speech recognition: The shared views of four research groups. *Signal Processing Magazine* 29, 6 (2012), 82–97.
- Geoffrey E Hinton and Ruslan R Salakhutdinov. 2006. Reducing the dimensionality of data with neural networks. *Science* 313, 5786 (2006), 504–507.
- Sepp Hochreiter, Yoshua Bengio, Paolo Frasconi, and Jürgen Schmidhuber. 2001. Gradient flow in recurrent nets: the difficulty of learning long-term dependencies. In *Field Guide to Dynamical Recurrent Networks*, J. Kolen and S. Kremer (Eds.). IEEE Press, 179–206.
- Chih-Wei Hsu, Chih-Chung Chang, Chih-Jen Lin, et al. 2003. *A practical guide to support vector classification*. Technical Report. Department of Computer Science, National Taiwan University.
- Gao Huang, Yu Sun, Zhuang Liu, Daniel Sedra, and Kilian Q Weinberger. 2016. Deep networks with stochastic depth. In *Proceedings of the European Conference on Computer Vision*. Springer, 646–661.
- Piotr Indyk and Rajeev Motwani. 1998. Approximate nearest neighbors: towards removing the curse of dimensionality. In *Proceedings of the 13th Annual ACM Symposium on Theory of Computing*. ACM, 604–613.
- Sergey Ioffe and Christian Szegedy. 2015. Batch normalization: Accelerating deep network training by reducing internal covariate shift. In *Proceedings of the 32nd International Conference on Machine Learning (ICML'15)*, David Blei Francis Bach (Ed.). PMLR, 448–456.
- Gareth M James and Trevor J Hastie. 2001. Functional linear discriminant analysis for irregularly sampled curves. *Journal of the Royal Statistical Society: Series B (Statistical Methodology)* 63, 3 (2001), 533–550.
- William B Johnson and Joram Lindenstrauss. 1984. Extensions of Lipschitz mappings into a Hilbert space. *Contemp. Math.* 26 (1984), 189–206.
- Ian Jolliffe. 2002. *Principal component analysis*. Wiley Online Library.
- Alan Jović, Karla Brkić, and Nikola Bogunović. 2015. A review of feature selection methods with applications. In *Proceedings of 2015 38th International Convention on Information and Communication Technology, Electronics and Microelectronics (MIPRO)*. IEEE, 1200–1205.
- Ata Kabán. 2014. New bounds on compressive linear least squares regression. In *Proceedings of the 17th International Conference on Artificial Intelligence and Statistics (AISTATS 2014)*, Jukka Corander Samuel Kaski (Ed.). PMLR, 448–456.
- Daniel M Kane and Jelani Nelson. 2014. Sparser Johnson-Lindenstrauss transforms. *Journal of the ACM (JACM)* 61, 1 (2014), 4:1–4:23.

- Tae-Kyun Kim, Shu-Fai Wong, Bjorn Stenger, Josef Kittler, and Roberto Cipolla. 2007. Incremental linear discriminant analysis using sufficient spanning set approximations. In *Proceedings of the 2007 IEEE Conference on Computer Vision and Pattern Recognition (CVPR)*. IEEE, 1–8.
- Ron Kohavi and George H John. 1997. Wrappers for feature subset selection. *Artificial Intelligence* 97, 1 (1997), 273–324.
- Varun Raj Kompella, Matthew Luciw, and Jürgen Schmidhuber. 2012. Incremental slow feature analysis: Adaptive low-complexity slow feature updating from high-dimensional input streams. *Neural Computation* 24, 11 (2012), 2994–3024.
- Philipp Krähenbühl, Carl Doersch, Jeff Donahue, and Trevor Darrell. 2015. Data-dependent initializations of convolutional neural networks. *CoRR* abs/1511.06856 (2015).
- Alexander Kraskov, Harald Stögbauer, and Peter Grassberger. 2004. Estimating mutual information. *Phys. Rev. E* 69, 6 (2004), 066138.
- Alex Krizhevsky. 2009. *Learning multiple layers of features from tiny images*. Master’s thesis. University of Toronto.
- Alex Krizhevsky, Ilya Sutskever, and Geoffrey E Hinton. 2012. Imagenet classification with deep convolutional neural networks. In *Advances in Neural Information Processing Systems 25 (NIPS’12)*, L. Bottou-K.Q. Weinberger F. Pereira, C.J.C. Burges (Ed.). Curran Associates Inc., 1097–1105.
- WJ Krzanowski, Philip Jonathan, WV McCarthy, and MR Thomas. 1995. Discriminant analysis with singular covariance matrices: methods and applications to spectroscopic data. *Journal of the Royal Statistical Society. Series C (Applied Statistics)* 44, 1 (1995), 101–115.
- Vipin Kumar and Sonajharia Minz. 2014. Feature Selection: a literature review. *Smart Computing Review* 4, 3 (2014), 211–229.
- John Langford, Lihong Li, and Alex Strehl. 2007. Vowpal Wabbit online learning project. (2007).
- Hugo Larochelle, Yoshua Bengio, Jérôme Louradour, and Pascal Lamblin. 2009. Exploring strategies for training deep neural networks. *Journal of Machine Learning Research* 10 (2009), 1–40.
- Peter Läuchli. 1961. Jordan-elimination und Ausgleichung nach kleinsten Quadraten. *Numer. Math.* 3, 1 (1961), 226–240.
- François Le Gall. 2014. Powers of tensors and fast matrix multiplication. In *Proceedings of the 39th International Symposium on Symbolic and Algebraic Computation*, Katsusuke Nabeshima (Ed.). ACM, 296–303.
- Yann LeCun. 1987. *Modèles connexionnistes de l’apprentissage*. Ph.D. Dissertation. Universite Paris 6.

- Yann LeCun, Yoshua Bengio, and Geoffrey Hinton. 2015. Deep learning. *Nature* 521, 7553 (2015), 436–444.
- Yann LeCun, Bernhard E Boser, John S Denker, Donnie Henderson, Richard E Howard, Wayne E Hubbard, and Lawrence D Jackel. 1990. Handwritten digit recognition with a back-propagation network. In *Advances in Neural Information Processing Systems 2 (NIPS 1989)*, D.S. Touretzky (Ed.). Morgan Kaufmann Publishers Inc., 396–404.
- Yann LeCun, Léon Bottou, Yoshua Bengio, and Patrick Haffner. 1998a. Gradient-based learning applied to document recognition. *Proc. IEEE* 86, 11 (1998), 2278–2324.
- Yann LeCun, Fu Jie Huang, and Leon Bottou. 2004. Learning methods for generic object recognition with invariance to pose and lighting. In *Proceedings of the 2004 IEEE Conference on Computer Vision and Pattern Recognition (CVPR)*. IEEE, 97–104.
- Yann A LeCun, Léon Bottou, Genevieve B Orr, and Klaus-Robert Müller. 1998b. Efficient backprop. In *Neural networks: Tricks of the Trade*, Geneviève B Orr and Klaus-Robert Müller (Eds.). Lecture Notes in Computer Science, Vol. 1524. Springer Berlin Heidelberg, 9–50.
- Kuang-chih Lee, Burkay Orten, Ali Dasdan, and Wentong Li. 2012. Estimating conversion rate in display advertising from past performance data. In *Proceedings of the 18th ACM SIGKDD International Conference on Knowledge Discovery and Data Mining*. ACM, 768–776.
- David D Lewis, Yiming Yang, Tony G Rose, and Fan Li. 2004. RCV1: A new benchmark collection for text categorization research. *Journal of Machine Learning Research* 5 (2004), 361–397.
- Haifeng Li, Tao Jiang, and Keshu Zhang. 2006b. Efficient and robust feature extraction by maximum margin criterion. *IEEE Transactions on Neural Networks* 17, 1 (2006), 157–165.
- Ping Li, Trevor J Hastie, and Kenneth W Church. 2006a. Very sparse random projections. In *Proceedings of the 12th ACM SIGKDD International Conference on Knowledge Discovery and Data Mining*. ACM, 287–296.
- Yongmin Li, L-Q Xu, Jason Morphet, and Richard Jacobs. 2003. An integrated algorithm of incremental and robust PCA. In *Proceedings of the 2003 International Conference on Image Processing (ICIP 2003)*. IEEE, 245–248.
- Huan Liu and Rudy Setiono. 1995. Chi2: Feature selection and discretization of numeric attributes. In *Proceedings of the 7th International Conference on Tools with Artificial Intelligence*. IEEE, 388–391.
- Huan Liu and Lei Yu. 2005. Toward integrating feature selection algorithms for classification and clustering. *IEEE Transactions on Knowledge and Data Engineering* 17, 4 (2005), 491–502.

- Justin Ma, Lawrence K Saul, Stefan Savage, and Geoffrey M Voelker. 2009. Identifying Suspicious URLs: An Application of Large-Scale Online Learning. In *Proceedings of the 26th International Conference on Machine Learning (ICML'09)*, Léon Bottou and Michael Littman (Eds.). ACM, 681–688.
- Andrew L Maas, Awni Y Hannun, and Andrew Y Ng. 2013. Rectifier nonlinearities improve neural network acoustic models. In *Proceedings of the 30th International Conference on Machine Learning (ICML'13)*, David McAllester Sanjoy Dasgupta (Ed.). PMLR, 3.
- Laurens van der Maaten and Geoffrey Hinton. 2008. Visualizing data using t-SNE. *Journal of Machine Learning Research* 9 (2008), 2579–2605.
- Michael W Mahoney. 2011. Randomized algorithms for matrices and data. *Foundations and Trends in Machine Learning* 3, 2 (2011), 123–224.
- Odalric-Ambrym Maillard and Rémi Munos. 2012. Linear regression with random projections. *Journal of Machine Learning Research* 13 (2012), 2735–2772.
- James Martens. 2010. Deep learning via Hessian-free optimization. In *Proceedings of the 27th International Conference on Machine Learning (ICML'10)*, Johannes Fürnkranz and Thorsten Joachims (Eds.). Omnipress, 735–742.
- Jean-Pierre Martens. 1996. A stochastically motivated random initialization of pattern classifying MLPs. *Neural Processing Letters* 3, 1 (1996), 23–29.
- Timothy Masters. 1993. *Practical neural network recipes in C++*. Morgan Kaufmann.
- Jiří Matoušek. 2008. On variants of the Johnson-Lindenstrauss lemma. *Random Structures & Algorithms* 33, 2 (2008), 142–156.
- Xiangrui Meng and Michael W Mahoney. 2013. Low-distortion subspace embeddings in input-sparsity time and applications to robust linear regression. In *Proceedings of the 45th Annual ACM Symposium on Theory of Computing*. ACM, 91–100.
- Tomas Mikolov, Ilya Sutskever, Kai Chen, Greg S Corrado, and Jeff Dean. 2013. Distributed representations of words and phrases and their compositionality. In *Advances in Neural Information Processing Systems 26 (NIPS'13)*, M. Welling-Z. Ghahramani K.Q. Weinberger C.J.C. Burges, L. Bottou (Ed.). Curran Associates Inc., 3111–3119.
- Dmytro Mishkin and Jiri Matas. 2015. All you need is a good init. *CoRR* abs/1511.06422 (2015).
- Vinod Nair and Geoffrey E Hinton. 2010. Rectified Linear Units Improve Restricted Boltzmann Machines. In *Proceedings of the 27th International Conference on Machine Learning (ICML'10)*, Johannes Fürnkranz and Thorsten Joachims (Eds.). Omnipress, 807–814.
- Jelani Nelson and Huy L Nguyễn. 2014. Lower bounds for oblivious subspace embeddings. In *International Colloquium on Automata, Languages, and Programming*. Springer, 883–894.

- John Nelson and Huy L. Nguyễn. 2013. OSNAP: Faster numerical linear algebra algorithms via sparser subspace embeddings. In *Proceedings of the 54th Annual IEEE Symposium on Foundations of Computer Science*. IEEE, 117–126.
- Derrick Nguyen and Bernard Widrow. 1990. Improving the learning speed of 2-layer neural networks by choosing initial values of the adaptive weights. In *Proceedings of the 1990 International Joint Conference on Neural Networks (IJCNN)*. IEEE, 21–26.
- Erkki Oja. 1982. Simplified neuron model as a principal component analyzer. *Journal of Mathematical Biology* 15, 3 (1982), 267–273.
- Yoh-Han Pao, Gwang-Hoon Park, and Dejan J. Sobajic. 1994. Learning and generalization characteristics of the random vector functional-link net. *Neurocomputing* 6, 2 (1994), 163–180.
- Yoh-Han Pao and Yoshiyasu Takefuji. 1992. Functional-link net computing: theory, system architecture, and functionalities. *Computer* 25, 5 (1992), 76–79.
- Saurabh Paul, Christos Boutsidis, Malik Magdon-Ismail, and Petros Drineas. 2014. Random projections for linear support vector machines. *ACM Transactions on Knowledge Discovery from Data (TKDD)* 8, 4 (2014), 22.
- Karl Pearson. 1901. On lines and planes of closest fit to systems of points in space. *The London, Edinburgh, and Dublin Philosophical Magazine and Journal of Science* 2, 11 (1901), 559–572.
- Nicolas Pinto and David Cox. 2010. An evaluation of the invariance properties of a biologically-inspired system for unconstrained face recognition. In *International Conference on Bio-Inspired Models of Network, Information, and Computing Systems*, Hart E. El-Azouzi-R. Carrera I. Altman E. Hayel, Y. (Ed.). Springer, 505–518.
- Nicolas Pinto, David Doukhan, James J. DiCarlo, and David D. Cox. 2009. A high-throughput screening approach to discovering good forms of biologically inspired visual representation. *PLOS Computational Biology* 5, 11 (2009), 1–12.
- Boris Teodorovich Polyak. 1964. Some methods of speeding up the convergence of iteration methods. *U. S. S. R. Comput. Math. and Math. Phys.* 4, 5 (1964), 1–17.
- J. Ross Quinlan. 1986. Induction of decision trees. *Machine Learning* 1, 1 (1986), 81–106.
- Martin Raab and Angelika Steger. 1998. “Balls into bins” - A simple and tight analysis. *Randomization and Approximation Techniques in Computer Science* (1998), 159–170.
- Ali Rahimi and Benjamin Recht. 2008. Random features for large-scale kernel machines. In *Advances in Neural Information Processing Systems 20 (NIPS’07)*, J.C. Platt, D. Koller, Y. Singer, and S.T. Roweis (Eds.). Curran Associates Inc., 1177–1184.
- Marc’ Aurelio Ranzato, Y-Lan Boureau, and Yann LeCun. 2007. Sparse Feature Learning for Deep Belief Networks. In *Advances in Neural Information Processing Systems 20 (NIPS’07)*, J.C. Platt, D. Koller, Y. Singer, and S.T. Roweis (Eds.). Curran Associates Inc., 1185–1192.

- Matthew Richardson, Ewa Dominowska, and Robert Ragno. 2007. Predicting clicks: estimating the click-through rate for new ads. In *Proceedings of the 16th International Conference on World Wide Web*. ACM, 521–530.
- Salah Rifai, Pascal Vincent, Xavier Muller, Xavier Glorot, and Yoshua Bengio. 2011. Contractive auto-encoders: Explicit invariance during feature extraction. In *Proceedings of the 28th International Conference on Machine Learning (ICML'11)*, Lise Getoor and Tobias Scheffer (Eds.). Omnipress, 833–840.
- Vladimir Rokhlin, Arthur Szlam, and Mark Tygert. 2009. A randomized algorithm for principal component analysis. *SIAM J. Matrix Anal. Appl.* 31, 3 (2009), 1100–1124.
- Sam T Roweis and Lawrence K Saul. 2000. Nonlinear dimensionality reduction by locally linear embedding. *Science* 290, 5500 (2000), 2323–2326.
- David E Rumelhart, Geoffrey E Hinton, and Ronald J Williams. 1986. Learning representations by back-propagating errors. *Nature* 323, 6088 (1986), 533–536.
- Yvan Saeys, Iñaki Inza, and Pedro Larrañaga. 2007. A review of feature selection techniques in bioinformatics. *Bioinformatics* 23, 19 (2007), 2507–2517.
- Ruslan Salakhutdinov. 2009. *Learning deep generative models*. Ph.D. Dissertation. University of Toronto.
- Ruslan Salakhutdinov and Geoffrey E Hinton. 2009. Semantic hashing. *International Journal of Approximate Reasoning* 50, 7 (2009), 969–978.
- Gerard Salton. 1979. Mathematics and information retrieval. *Journal of Documentation* 35, 1 (1979), 1–29.
- Gerard Salton. 1991. Developments in automatic text retrieval. *Science* 253, 5023 (1991), 974–980.
- Gerard Salton and Christopher Buckley. 1988. Term-weighting approaches in automatic text retrieval. *Information Processing & Management* 24, 5 (1988), 513–523.
- John W Sammon. 1969. A nonlinear mapping for data structure analysis. *IEEE Trans. Comput.* 100, 5 (1969), 401–409.
- Tamas Sarlos. 2006. Improved approximation algorithms for large matrices via random projections. In *Proceedings of the 47th Annual IEEE Symposium on Foundations of Computer Science*. IEEE, 143–152.
- Andrew Saxe, Pang W Koh, Zhenghao Chen, Maneesh Bhand, Bipin Suresh, and Andrew Y Ng. 2011. On random weights and unsupervised feature learning. In *Proceedings of the 28th International Conference on Machine Learning (ICML'11)*, Lise Getoor and Tobias Scheffer (Eds.). Omnipress, 1089–1096.
- Andrew M Saxe, James L McClelland, and Surya Ganguli. 2014. Exact solutions to the nonlinear dynamics of learning in deep linear neural networks. In *International Conference on Learning Representations (ICLR)*.

- Simone Scardapane and Dianhui Wang. 2017. Randomness in neural networks: an overview. *Wiley Interdisciplinary Reviews: Data Mining and Knowledge Discovery* 7, 2 (2017).
- Wouter F Schmidt, Martin A Kraaijveld, and Robert PW Duin. 1992. Feedforward neural networks with random weights. In *Proceedings of the 11th IAPR International Conference on Pattern Recognition (IAPR)*. IEEE, 1–4.
- Tom Sercu, Christian Puhersch, Brian Kingsbury, and Yann LeCun. 2016. Very deep multilingual convolutional neural networks for LVCSR. In *Proceedings of the 41st IEEE International Conference on Acoustics, Speech and Signal Processing (ICASSP 2016)*. IEEE, 4955–4959.
- Shai Shalev-Shwartz, Yoram Singer, Nathan Srebro, and Andrew Cotter. 2011. Pegasos: primal estimated sub-gradient solver for SVM. *Mathematical Programming* 127, 1 (2011), 3–30.
- Qinfeng Shi, James Petterson, Gideon Dror, John Langford, Alex Smola, and SVN Vishwanathan. 2009. Hash kernels for structured data. *Journal of Machine Learning Research* 10 (2009), 2615–2637.
- Karen Simonyan and Andrew Zisserman. 2014. Very deep convolutional networks for large-scale image recognition. *CoRR* abs/1409.1556 (2014).
- Paul Smolensky. 1986. Information Processing in Dynamical Systems: Foundations of Harmony Theory. In *Parallel Distributed Processing: Explorations in the Microstructure of Cognition, Vol. 1*, David E. Rumelhart, James L. McClelland, and CORPORATE PDP Research Group (Eds.). MIT Press, 194–281.
- Soeren Sonnenburg, Vojtech Franc, Elad Yom-Tov, and Michele Sebag. 2008. Pascal large scale learning challenge. In *Proceedings of the 25th International Conference on Machine Learning (ICML’08)*, Andrew McCallum and Sam Roweis (Eds.). Omnipress, 1937–1953.
- Nitish Srivastava. 2013. *Improving neural networks with dropout*. Master’s thesis. University of Toronto.
- Nitish Srivastava, Geoffrey E Hinton, Alex Krizhevsky, Ilya Sutskever, and Ruslan Salakhutdinov. 2014. Dropout: A simple way to prevent neural networks from overfitting. *Journal of Machine Learning Research* 15, 1 (2014), 1929–1958.
- Dmitry Storcheus, Afshin Rostamizadeh, and Sanjiv Kumar. 2015. A survey of modern questions and challenges in feature extraction. In *Proceedings of the 1st International Workshop on Feature Extraction: Modern Questions and Challenges at NIPS 2015*, Sanjiv Kumar Dmitry Storcheus, Afshin Rostamizadeh (Ed.). PMLR.
- David Sussillo and LF Abbott. 2014. Random walk initialization for training very deep feedforward networks. *CoRR* abs/1412.6558 (2014).

- Ilya Sutskever, James Martens, George Dahl, and Geoffrey E Hinton. 2013. On the importance of initialization and momentum in deep learning. In *Proceedings of the 30th International Conference on Machine Learning (ICML'13)*, Sanjoy Dasgupta and David Mcallester (Eds.). PMLR, 1139–1147.
- Ilya Sutskever, James Martens, and Geoffrey E Hinton. 2011. Generating text with recurrent neural networks. In *Proceedings of the 28th International Conference on Machine Learning (ICML'11)*, Lise Getoor and Tobias Scheffer (Eds.). Omnipress, 1017–1024.
- Ilya Sutskever, Oriol Vinyals, and Quoc V Le. 2014. Sequence to sequence learning with neural networks. In *Advances in Neural Information Processing Systems 27 (NIPS'14)*, C. Cortes-N.D. Lawrence K.Q. Weinberger Z. Ghahramani, M. Welling (Ed.). Curran Associates Inc., 3104–3112.
- Joshua B Tenenbaum, Vin De Silva, and John C Langford. 2000. A global geometric framework for nonlinear dimensionality reduction. *Science* 290, 5500 (2000), 2319–2323.
- Warren S Torgerson. 1952. Multidimensional scaling: I. Theory and method. *Psychometrika* 17, 4 (1952), 401–419.
- Laurens Van Der Maaten, Eric Postma, and Jaap Van den Herik. 2009. Dimensionality reduction: a comparative review. *Journal of Machine Learning Research* 10 (2009), 66–71.
- Santosh S Vempala. 2005. *The random projection method*. American Mathematical Soc.
- Suleyman Vural, Xiaosheng Wang, and Chittibabu Guda. 2016. Classification of breast cancer patients using somatic mutation profiles and machine learning approaches. *BMC Systems Biology* 10, 3 (2016), 62.
- Jingdong Wang, Ting Zhang, Nicu Sebe, Heng Tao Shen, et al. 2018. A survey on learning to hash. *IEEE Transactions on Pattern Analysis and Machine Intelligence* PP, 99 (2018).
- Zhuang Wang, Nemanja Djuric, Koby Crammer, and Slobodan Vucetic. 2011. Trading representability for scalability: adaptive multi-hyperplane machine for nonlinear classification. In *Proceedings of the 17th ACM SIGKDD International Conference on Knowledge Discovery and Data Mining*. ACM, 24–32.
- David Warde-Farley, Ian J Goodfellow, Aaron Courville, and Yoshua Bengio. 2013. An empirical analysis of dropout in piecewise linear networks. *CoRR* abs/1312.6197 (2013).
- Steve Webb, James Caverlee, and Calton Pu. 2006. Introducing the Webb Spam Corpus: Using Email Spam to Identify Web Spam Automatically. In *Proceedings of the 3rd Conference on Email and Anti-Spam (CEAS 2006)*.

- Kilian Weinberger, Anirban Dasgupta, John Langford, Alex Smola, and Josh Attenberg. 2009. Feature hashing for large scale multitask learning. In *Proceedings of the 26th International Conference on Machine Learning (ICML'09)*, Léon Bottou and Michael Littman (Eds.). ACM, 1113–1120.
- Max Welling, Michal Rosen-Zvi, and Geoffrey E Hinton. 2005. Exponential family harmoniums with an application to information retrieval. In *Advances in Neural Information Processing Systems 17 (NIPS'04)*, L. K. Saul, Y. Weiss, and L. Bottou (Eds.). MIT Press, 1481–1488.
- Juyang Weng, Yilu Zhang, and Wey-Shiuan Hwang. 2003. Candid covariance-free incremental principal component analysis. *IEEE Transactions on Pattern Analysis and Machine Intelligence* 25, 8 (2003), 1034–1040.
- Piotr Iwo Wójcik and Marcin Kurdziel. 2017. Random projection initialization for deep neural networks. In *25th European Symposium on Artificial Neural Networks, Computational Intelligence and Machine Learning (ESANN'2017)*. i6doc.com, 111–116.
- Piotr Iwo Wójcik and Marcin Kurdziel. 2018. Training neural networks on high-dimensional data using random projection. *Pattern Analysis and Applications* (2018). <https://doi.org/10.1007/s10044-018-0697-0>
- David P Woodruff. 2014. Sketching as a tool for numerical linear algebra. *Foundations and Trends in Theoretical Computer Science* 10, 1–2 (2014), 1–157.
- Jianxin Wu. 2012. Power mean SVM for large scale visual classification. In *Proceedings of the 2012 IEEE Conference on Computer Vision and Pattern Recognition (CVPR)*. IEEE, 2344–2351.
- Jim YF Yam and Tommy WS Chow. 2000. A weight initialization method for improving training speed in feedforward neural network. *Neurocomputing* 30, 1 (2000), 219–232.
- Jun Yan, Benyu Zhang, Shuicheng Yan, Qiang Yang, Hua Li, Zheng Chen, Wensi Xi, Weiguo Fan, Wei-Ying Ma, and Qiansheng Cheng. 2004. IMMC: Incremental Maximum Margin Criterion. In *Proceedings of the 10th ACM SIGKDD International Conference on Knowledge Discovery and Data Mining*. ACM, 725–730.
- Hao Yang and Jianxin Wu. 2012. Practical Large Scale Classification with Additive Kernels. In *Proceedings of 4th Asian Conference on Machine Learning*, Wray Buntine Steven C. H. Hoi (Ed.). PMLR, 523–538.
- Jieping Ye, Qi Li, Hui Xiong, Haesun Park, Ravi Janardan, and Vipin Kumar. 2005. IDR/QR: An incremental dimension reduction algorithm via QR decomposition. *IEEE Transactions on Knowledge and Data Engineering* 17, 9 (2005), 1208–1222.
- Hsiang-Fu Yu, Cho-Jui Hsieh, Kai-Wei Chang, and Chih-Jen Lin. 2012. Large linear classification when data cannot fit in memory. *ACM Transactions on Knowledge Discovery from Data (TKDD)* 5, 4 (2012), 23.

- Hsiang-Fu Yu, Hung-Yi Lo, Hsun-Ping Hsieh, Jing-Kai Lou, Todd G McKenzie, Jung-Wei Chou, Po-Han Chung, Chia-Hua Ho, Chun-Fu Chang, Yin-Hsuan Wei, et al. 2010. Feature engineering and classifier ensemble for KDD Cup 2010. In *In JMLR Workshop and Conference Proceedings*. 1–16.
- Guo-Xun Yuan, Kai-Wei Chang, Cho-Jui Hsieh, and Chih-Jen Lin. 2010. A comparison of optimization methods and software for large-scale L1-regularized linear classification. *Journal of Machine Learning Research* 11 (2010), 3183–3234.
- Guo-Xun Yuan, Chia-Hua Ho, and Chih-Jen Lin. 2012a. An improved GLMNET for L1-regularized logistic regression. *Journal of Machine Learning Research* 13, 1 (2012), 1999–2030.
- Guo-Xun Yuan, Chia-Hua Ho, and Chih-Jen Lin. 2012b. Recent advances of large-scale linear classification. *Proc. IEEE* 100, 9 (2012), 2584–2603.
- Guo-Xun Yuan and Kwan-Liu Ma. 2012. Scalable training of sparse linear SVMs. In *Proceedings of 2012 IEEE 12th International Conference on Data Mining (ICDM)*. IEEE, 775–784.
- Raphael Yuster and Uri Zwick. 2005. Fast sparse matrix multiplication. *ACM Transactions on Algorithms (TALG)* 1, 1 (2005), 2–13.
- Caoxie Zhang, Honglak Lee, and Kang G Shin. 2012. Efficient distributed linear classification algorithms via the alternating direction method of multipliers. In *Proceedings of the 15th International Conference on Artificial Intelligence and Statistics (AISTATS 2012)*, Mark Girolami Neil D. Lawrence (Ed.). PMLR, 1398–1406.
- Y. T. Zhou and Rama Chellappa. 1988. Computation of optical flow using a neural network. In *Proceeding of the 1998 IEEE International Conference on Neural Networks*. IEEE, 71–78.

PHD CANDIDATE PUBLICATIONS LIST

Below we list publications co-authored by the author of this thesis along with their MNiSW (Polish Ministry of Science and Higher Education) classification. IF stands for Impact Factor as indexed on the Thomson Journal Citation Reports list.

1. Karol Grzegorzczak, Marcin Kurdziel, Piotr Iwo Wójcik. 2016. Encouraging orthogonality between weight vectors in pretrained deep neural networks. *Neuro-computing*, 202 (2016), 84–90.
IF: 3.317, MNiSW: 30pts (List A)
2. Maciej Malawski, Maciej Kuźniar, Piotr Wójcik, Marian Bubak. 2013. How to use Google App Engine for free computing. *IEEE Internet Computing*, 17, 1 (2013), 50–59.
IF: 1.521, MNiSW: 40pts (List A)
3. Piotr Iwo Wójcik, Marcin Kurdziel. 2018. Training neural networks on high-dimensional data using random projection. *Pattern Analysis and Applications*, doi: 10.1007/s10044-018-0697-0.
IF: 1.352, MNiSW: 20pts (List A)
4. Piotr Iwo Wójcik, Thérèse Ouellet, Margaret Balcerzak, Witold Dzwinel. 2015. Identification of biomarker genes for resistance to a pathogen by a novel method for meta-analysis of single-channel microarray datasets. *Journal of Bioinformatics and Computational Biology*, 13, 4 (2015), 1550013.
IF: 0.8, MNiSW: 15pts (List A)
5. Karol Grzegorzczak, Marcin Kurdziel, Piotr Iwo Wójcik. 2016. Implementing deep learning algorithms on graphics processor units. *Parallel Processing and Applied Mathematics. PPAM 2015. Lecture Notes in Computer Science*, vol. 9573, 473–482.
MNiSW: 15pts (Web of Science)
6. Karol Grzegorzczak, Marcin Kurdziel, Piotr Iwo Wójcik. 2015. Effects of sparse initialization in deep belief networks. *Computer Science*, 16, 4 (2015), 313–327.
MNiSW: 12pts (List B)
7. Chwastowski et al. 2012. The CC1 project – system for Private Cloud Computing. *Computer Science*, 13, 2 (2012), 103–111.
MNiSW: 12pts (List B)

8. Piotr Iwo Wójcik, Marcin Kurdziel. 2017. Random projection initialization for deep neural networks. *25th European Symposium on Artificial Neural Networks, Computational Intelligence and Machine Learning (ESANN'2017)*, April 26–28, 2017, Bruges, Belgium.

MNiSW: 10pts (Web of Science)

9. Joanna Kocot, Tomasz Szepieniec, Piotr Wójcik, Michał Trzeciak, Maciej Golik, Tomasz Grabarczyk, Hubert Siejkowski, Mariusz Sterzel. 2014. A framework for domain-specific science gateways. *eScience on Distributed Computing Infrastructure. Lecture Notes in Computer Science*, vol 8500, 130–146.

MNiSW: 5pts

10. Joanna Kocot, Tomasz Szepieniec, Mariusz Sterzel, Daniel Haręźlak, Maciej Golik, Tomasz Twaróg, Piotr Wójcik. 2012. InSilicoLab: a domain-specific science gateway. *Cracow'12 Grid Workshop*, October 22–24, 2012, Krakow, Poland.